MEMBRANE PROTEINS AS DRUG TARGETS: THE CAAX PROTEASES AND HMBR

by

DAVID ZACHARY MOKRY

(Under the Direction of William N. Lanzilotta and Walter K. Schmidt)

ABSTRACT

To date, half of all pharmaceutical drugs target membrane proteins, which are encoded by 30% of a typical genome. However, less than 0.3% of unique entries in protein structure databases are membrane proteins. Two protein groups pertinent to this dissertation that are promising drug targets are the *CaaX* proteases (Ste24 and Rce1), and the Hemoglobin Receptor (HmbR). The former are involved in the maturation of certain eukaryotic isoprenylated proteins bearing a C-terminal *CaaX* motif (C, cysteine; a, aliphatic amino acid; and X, one of several amino acids), and have been identified in several organisms, including the disease causing agent, *Trypanosoma brucei.* HmbR and related proteins are found in gram negative bacteria, and is involved in the acquisition of heme from the host.

In the first study, the *CaaX* proteases from *Trypanosoma brucei* were heterologously expressed in *Saccharomyces cerevisiae.* The results suggest the conserved presence of two *CaaX* protease activities in trypanosomatids, dispelling a previous notion of only one. This study also identified a trypanosomal Hsp40 chaperone as a substrate of both *Tb CaaX* proteases; the first

substrate outside of yeast that is known to be cleaved by both *CaaX* proteases, and provides evidence that the target specificity of the *Tb CaaX* proteases is influenced by protein context. Finally, our findings support the potential use of small molecule *CaaX* protease inhibitors as general tools for cell biological studies on the trafficking of *CaaX* proteins.

The second study spectroscopically evaluated HmbR heterologously expressed and purified from *Escherichia coli.* The results indicate an overall β-fold structure, and the presence of a 5-coordinate high-spin ferric heme with an axial negatively charged oxygen ligand. We also identified four amino acid residues involved in maintaining heme binding properties. Our study is the first spectroscopic characterization of any heme transporter in *Neisseria meningitidis*, and expands the variety of ways outer membrane heme transporters can coordinate heme.

In summary, these projects showcase the multitude of approaches that can be applied toward the understanding of membrane protein function, even in the absence of purified components, and provides a rational starting point for the development of novel pharmaceuticals.

INDEX WORDS: Rce1, Ste24, *CaaX*, Ras, post-translational modification, isoprenylation, Hemoglobin receptor, Iron transport, ShuA, membrane protein

MEMBRANE PROTEINS AS DRUG TARGETS: THE CAAX PROTEASES AND HMBR

by

DAVID ZACHARY MOKRY

Bachelor of Science, University of Wisconsin-Madison, 2004

A Dissertation Submitted to the Graduate Faculty of The University of Georgia in Partial Fulfillment of the Requirements for the Degree

DOCTOR OF PHILOSOPHY

ATHENS, GEORGIA

2010

© 2010

DAVID ZACHARY MOKRY

All Rights Reserved

MEMBRANE PROTEINS AS DRUG TARGETS: THE CAAX PROTEASES AND HMBR

by

DAVID ZACHARY MOKRY

Major Professors:	William N. Lanzilotta Walter K. Schmidt
Committee:	Harry A. Dailey Zachary A. Wood

Electronic Version Approved:

Maureen Grasso
Dean of the Graduate School
The University of Georgia
July, 2010

DEDICATION

I dedicate this thesis to my oldest sister, Sharon Marie Mokry, who passed away on July 11th, 2002, for teaching me that life has no limitations, and that all things are possible.

ACKNOWLEDGEMENTS

I am indebted to the many people who have made this work possible: I thank my friends, both in academia and elsewhere, for the experiences we have shared together over the course of many years. I thank my family, for always believing in me. Most importantly, I thank my major advisors, Dr. Walter K. Schmidt and Dr. William Lanzilotta, for their instruction, encouragement, and support over the years within their laboratories, and to the members of those laboratories, for all of the countless aid and insight given to me throughout my graduate career.

TABLE OF CONTENTS

Page

LIST OF TABLES

Page

LIST OF FIGURES

Page

CHAPTER 1

INTRODUCTION AND LITERATURE REVIEW

BACKGROUND

Biomedical importance of membrane proteins

The rational design of drugs often impinges upon an understanding of biological protein mechanisms and structures [1-5]. While the number of protein structures available in the Protein Data Bank (PDB) now numbers over 60,000, this figure is not representative of the total diversity of proteins that exist throughout biology. The vast majority of structures available were solved by X-ray crystallography (85%), with some minor contributions from nuclear magnetic resonance (NMR) spectroscopy (15%), as well as electron microscopy (0.5%) [6, 7]. As a result, proteins that do not readily crystallize or are too large to solve by NMR are inadequately represented. The most notable of these proteins are those with multi-spanning transmembrane domains. For example, only 0.3% of the structures within the Protein Data Bank are of unique membrane proteins, yet 30% of a typical genome encodes for membrane proteins [6-10]. Since half of all pharmaceutically-relevant drug targets are membrane proteins, a wealth of medicinal potential exists in understanding this class of biomolecules [11-14].

As a whole, characterization of membrane proteins provides unique challenges relative to that of soluble proteins, namely because of their particular biophysical properties. Considerations must be made to accommodate their hydrophobic character during expression,

purification, crystallization, assay design, and clinical trials [15-19]. Despite these challenges, the targets of many drugs have been identified to be membrane proteins. Well documented examples of drugs that target membrane proteins include aspirin, β-blockers, and L-dopa used to treat, respectively, acute pain, congestive heart failure, and neurological disorders [20-22]. This largely diversified variety of treatments is due mostly in part to the diverse functions membrane proteins mediate within the cell, ranging from signaling, to enzyme catalysis, to transmembrane trafficking [10, 23]. Examples of drugs that target membrane proteins are shown in **Table 1.1**.

On the structural and functional diversity of membrane proteins

The limited structural information on membrane proteins within the PDB has revealed two distinct topologies by which proteins can span a lipid bilayer [24]. For those proteins localized within the phosopholipid bilayers of the plasma membrane, endoplasmic reticulum, Golgi apparatus, and inner mitochondria membrane, numerous α-helices containing predominately hydrophobic amino acid residues are the major structural motif of the membrane embedded regions. These residues are orientated parallel to the plane of the membrane, with a hydrophilic interior stabilized by hydrogen bonds [25-27]. For proteins found within the outer membrane of bacteria, and some residing in the mitochondrial outer membrane, the predominant motif is a series of β-sheets forming an enclosed structure formally referred to as a β-barrel. This tertiary element of structure can be formed from both monomeric or multimeric protein subunits. Like the transmembrane α helices, the β-barrels are also stabilized by hydrogen bonds arranged in a circular pattern, but do not require that individual amino acids be hydrophobic, although there is a propensity for large aromatic amino acids to be found within the center of the β-sheet structure [28-30]. Whether a membrane protein adopts an α-helical or β-barrel fold is

completely dependent on the amino acid sequence [31]. The two archetypical topologies of membrane proteins are shown in **Figure 1.2** using, respectively, bacteriorhodopsin, from *Halobacterium halobium,* and ShuA from *Shigella dysenteriae* as representative members.

The two types of membrane spanning folds are structured specifically for their respective functions. The α-helical transmembrane domains are typically associated with proteins that act as receptors, ion channels, transporters, regulatory proteins, and enzymes, among others [10, 23, 25]. The β-barrel structure is generally associated with porins for the transport of water, nutrients, or metabolites into and out of the cell, but can also be found in proteins with other functions, such as the pore-forming cytotoxins of certain bacteria [28, 32].

Intramembrane cleaving proteases

The hydrophobic character of biological membranes naturally occludes the presence of water within the bilayer. Hence, it is rational to conclude that certain processes that require the presence of water, such as proteolysis, occur in regions outside of the lipid bilayer. However, an interesting class of proteins facilitates peptide bond hydrolysis through the use of residues embedded within the plane of the membrane. These proteins are referred to as intramembrane cleaving proteases (i-CliPs), and can be segregated into four to seven major families, depending on the criteria upon which they are grouped [33-36]. For the purposes of this dissertation, seven distinct classes will be reviewed.

Despite the large differences in the substrates and precise mechanisms of each class, many of the i-CliPs, have important biomedical relevance. Arguably the most biomedically relevant i-CliP is the presenilin family. Presenilins are the active component of the γ-secretase complex, which is involved in the cleavage of several proteins, including the amyloid precursor

protein (APP), and the signaling molecule Notch. Processing of APP has implications in the development and progression of Alzheimer's disease, while Notch has an important role in determining cell fates during development [37, 38]. The presenilin family is unified by an aspartic acid proteolytic mechanism, and this is shared by two other i-CliP families. One is the signal peptide peptidase family (SPP), which are sometimes classified as a type of presenilin due to their common catalytic mechanism. However, unlike presenilins, SPPs have an opposite catalytic topology and a preference for cleaving type II membrane proteins [39, 40]. SPPs are inferred to participate in proper immunological surveillance and development [41]. A single crystal structure of a bacterial SPP suggests that peptide bond hydrolysis is facilitated by a hydrated microenvironment immersed below the surface of the membrane interface, and this is supported by crystal structures of other i-CliPs, namely, that of the rhomboid proteases, which are described below [42]. The remaining i-CliP with an aspartic acid mechanism are the type four prepilins (TFPPs)[43, 44]. TFPPs are the least characterized of all the i-CliPs, and are found predominately in bacteria. They are mainly involved in the cleavage of secreted proteins that serve a range of functions, including genetic transfer, competence, and biofilm formation [44].

Another i-Clip found in bacterial are the rhomboid proteases, but they are also common in eukaryotic organisms [45]. Rhomboids utilize a serine protease mechanism and process substrates responsible for maintaining mitochondrial integrity and cellular differentiation, and at least one is known to be up-regulated in a type of optic atrophy [45]. Many rhomboid structures have been crystallized, and are consistent with the SPP structure that supports the hypothesis of a hydrated microenvironment [46].

Several metalloproteases with membrane embedded active sites have also been identified, and these represent the remaining three classes of i-CliPs. The Site 2 Protease family facilitates processing of proteins that signal the unfolded protein response (UPR), as well as regulation of sterol biosynthesis mediated through the sterol response element binding protein (SREBP) [47, 48]. The last two metalloprotease families are the *CaaX* proteases, which are responsible for the proteolytic step during the maturation of certain proteins bearing a C-terminal *CaaX* motif (defined below). While seemingly functionally redundant, the CaaX proteases are evolutionarily unrelated enzymes with limited overlapping target specificity. The CaaX proteases are termed the Ras converting enzyme (Rce1) or sterile mutant 24 (Ste24). Ste24 is recognized as a zinc dependent protease and has a classic zinc binding motif (HExxH) [49]. The mechanism of Rce1 remains undefined, but a combination of bioinformatic, mutational, and inhibitor data strongly suggests a metalloprotease mechanism [50-53]. Examples of proteins processed by the *CaaX* proteases include fungal mating pheromones, mammalian prelaminA, the Hsp40 family of chaperones, and the Ras and Rho GTPases. A summary of the seven major classes of i-CliPs is shown in **Table 1.2**.

The CaaX processing pathway and novel drug discovery efforts

The C-terminal *CaaX* motif (C, cysteine; a, aliphatic amino acid; and X, one of several amino acids) is found on the precursors to many eukaryotic isoprenylated proteins (i.e. CaaX proteins) and typically directs a tripartite series of sequential posttranslational modifications. The first involves covalent attachment of an isoprenoid lipid (farnesyl or geranylgeranyl) to the cysteine residue by one of two prenyl transferases (FTase, GGTI), the type of which is influenced by the amino acid identity in the *X* position of the *CaaX* motif [54-56]. The second

modification is proteolytic cleavage of the *aaX* sequence by either Rce1 or Ste24, determined in part by the sequence of the *CaaX* motif itself, as well as relatively uncharacterized upstream sequences within the protein backbone [57-60]. Two functionally redundant proteases may be required in order to accommodate the variety of *CaaX* motifs that exist throughout biology [60]. The third modification is carboxy methyl esterification by an isoprenylcysteine carboxyl methyltransferase (Icmt); Ste14p in yeast. The sole recognition determinant of this step is a prenylated cysteine residue with a free carboxyl [61, 62]. A diagram of the activities associated with *CaaX* processing enzymes is summarized in **Figure 1.2**.

Biomedical interest in the *CaaX* processing pathway was initially facilitated by the prominent role of hyperactive Ras isoforms in the oncogenesis of certain types of cancers. Generally, hyperactive Ras is correlated with 30% of all cancers, with higher incidences in specific types of tumors (50% of all solid tumors, 90% pancreatic) [63, 64]. Early drug discovery efforts focused on inhibiting the first step in the Ras processing pathway facilitated by farnesyl transferase [65, 66].

The most interesting farnesyl transferase inhibitors (FTIs) showed promising potential up to late stage clinical trials, but their effectiveness when administered as the sole anti-cancer agent was realized to be less than anticipated, presumably due to the activity of geranylgeranyl transferase on Ras [67]. As a result, a combination of FTIs, geranylgeranyl transfersase inhibitors (GGTIs), and dual prenylation inhibitors (DPIs) have been investigated in clinical trials, with varying degrees of success [68, 69]. Despite the early setback with FTIs, these agents are gaining popularity as a means to reduce the toxicity of accumulated prelamin A, the isoprenylated protein precursor of lamin A [70]. Improper processing of the lamin A precursor results in a number of progeria like diseases collectively referred to as laminopathies.

FTIs also appear to have an effect on the virulence of certain parasitic protozoans, namely, *Plasmodium falciparum* and *Trypanosoma cruzi* [71-73]. *In vitro* inhibitors of the proteolytic enzymes Rce1 and Ste24 have also been identified [53]. The potential of these inhibitors as therapeutics, however, remains to be established. Since RNAi mediated reduction in Rce1 expression has been correlated with decreased viability of bloodstream form *T. brucei*, it is anticipated that Rce1 inhibitors may have use against *Trypansosoma brucei* infections [60, 74].

The last step in the *CaaX* processing pathway, mediated by isoprenylcysteine carboxylmethyltransferase, is also being targeted for drug development as a means to treat cancer, although progress is less advanced relative to FTIs [75, 76]. The effectiveness of Icmt inhibitors in clinical trials will likely represent an exciting area of research in the near future.

Outer membrane receptors and transporters

While many classes of drugs are being developed that target membrane proteins like the *CaaX* proteases, research is also ongoing to identify drugs that target bacterial membrane proteins. Specifically, the emergence of several antibiotic resistant strains of pathogenic bacteria has prompted an interest in designing new antimicrobial agents [77-79]. The relative effectiveness of a given antibiotic is usually contingent on the type of bacteria causing disease due to differences in their membrane structures [80]. In general, bacteria can have two types of membranes, classified according to the ability to retain a Gram stain [81]. In Gram-positive bacteria, a single plasma membrane exists surrounded by a peptidoglycan cell wall. In Gram-negative bacteria, an additional outer membrane surrounds the cell wall. The outer membrane proteins of Gram-negative bacteria are attractive drug targets for three main reasons. First, some

function as drug efflux pumps that transport drugs outside of the cell. Many bacteria have acquired drug resistance by up-regulating the amount of these proteins [82, 83]. Second, many outer membrane proteins mediate the transport of essential vitamins and nutrients into the cell [84]. An understanding of how these systems function could aid in the development of novel drugs that interfere with proper transport, either by rendering the pathogen susceptible to current antibiotics, or less virulent to its host. Last, these prospective targets reside within the outer membrane, and thus are in direct contact with the extracellular environment. As a result of their surface accessibility, complications associated with drug permeability into the cell and enhanced efflux from the cell are significantly reduced. Many drugs that target proteins involved in cell wall biosynthesis, including penicillin, have this advantage [85].

To date, the high-resolution structures of several transporters have been elucidated, most of which are involved in transporting essential components into the cell. Examples include sucrose transporters, nucleoside receptors, fatty acid transporters, and heavy metal transporters [6, 7]. Most of these have been solved using X-ray crystallography, arguably the most useful technique for high-resolution structure determination. However, crystal structures are static in nature, and predicting the protein dynamics involved in transport is contingent on either predictive models, or acquiring a series of structures with trapped intermediates. Hence, a holistic description of a particular transport mechanism should incorporate the use of other methods to augment the information obtained from X-ray crystallography.

Iron acquisition strategies in bacteria

The presence of iron is a requirement for most organisms due to its role in a number of biochemical processes throughout biology [86]. These include oxygen transport, redox

reactions, detoxification of various compounds, and regulation of gene expression. Bacteria have evolved rather sophisticated mechanisms to abstract iron from the environment. Specifically, several pathogenic Gram-negative bacteria have acquired strategies to scavenge the abundant stores of iron in their hosts. These iron uptake systems fall into two broad categories and are not mutually exclusive. First, an iron-chelating compound, referred to as a siderophore, is synthesized and secreted by the bacteria into the extracellular environment. This compound binds to free ferric iron and then undergoes receptor-mediated transport into the periplasm of the bacteria. Examples of bacteria with this acquisition system include *Vibrio cholerae*, *Yersinia pestis*, and *Pseudomonas aeruginosa,* among others [87-89].

The second strategy involves receptor-mediated binding of an iron containing (transferrin or lactoferrin) or heme-iron containing (hemopexin, haptoglobin, or hemoglobin) host protein from which the iron moiety is hijacked at the cell surface by the receptor and transported into the periplasm of the bacteria. Examples of bacteria with this acquisition system include *Haemophilus influenzae, Shigella dysenteriae,* and *Neisseria meniingitidis* [90-92]. Precisely how the receptor is capable of abstracting the heme remains undefined, but the mechanism likely depends on interrupting the coordination of the heme in the host protein and subsequently presenting it with an alternate binding site in the receptor. In either case, the transport of heme-iron into the periplasmic space is coupled to the proton motive force of the accessory protein TonB, demonstrating a thermodynamic requirement for the process to occur [93]. Such proteins are formally referred to as TonB dependent transporters (TBDTs). Once the pathogen has transported the heme-iron into the periplasm, a periplasmic binding protein shuttles it to an inner membrane receptor, where it is transported into the cytoplasm. Upon cytosolic delivery, the iron can be used directly, or in the case of heme, cytosolic enzymes called heme oxygenases degrade

the molecule to liberate free iron (Fe^{3+}), carbon monoxide, and biliverdin [94]. A heme-based iron acquisition system is summarized in **Figure 1.3**.

HmbR as a prospective drug target

The bacterial pathogen *Neisseria meningitidis* is the causative agent of two human diseases, pyogenic meningitis, and meningococcal septicemia. Like all pathogenic organisms, the virulence of this bacterium is strongly dependent upon its ability to obtain iron from the host. To date, the secretion of siderophore compounds in *Neisseria meningitidis* is believed to be completely absent, thereby suggesting that other mechanisms of iron acquisition are the exclusive means through which iron requirements are maintained [95, 96]. Outer membrane receptors that recognize heme containing proteins have been identified in *Neisseria meningitidis*. The four varieties identified to date include a transferrin, lactoferrin, hemoglobin, and a dual specificity hemoglobin/haptoglobin receptor [92]. Since suppression of one of these receptors would reduce the variety of ways the pathogen could obtain iron from the environment, and possibly mitigate the progression of an infection, all of them represent potential drug targets. However, certain transporters appear to be more promising targets for drug development, specifically, the transferrin and hemoglobin receptors. First, both of these transporters have been identified with high frequencies in invasive strains [97, 98]. Second, they have a more specific binding profile for their respective host proteins. For example, HmbR can distinguish between different isoforms of hemoglobin, and preferentially utilizes human hemoglobin over other variants, a feature absent in the haptoglobin/hemoglobin dual receptor [99]. Distinct substrate preferences may indicate the ability to identify more specific inhibitors of these receptors over their less discriminatory counterparts. Third, both the transferrin and hemoglobin receptors are

composed of a single peptide that is believed to function as a monomer. Multimeric protein transporters potentially complicate the degree in which a transport mechanism needs to be characterized for the purpose of drug development. Last, differential expression of iron transport proteins is coupled to different stages of colonization and infection, as the source of iron in the local environment changes. When hemoglobin is the sole source of iron, HmbR is highly expressed and *Neisseria meningitidis* is capable of unrestricted growth [100]. This would likely occur as a result of hemolysis through either a pathological condition, or a hemolytic factor secreted by the invading pathogen. This suggests that when in the bloodstream, HmbR is a major iron delivery protein that contributes to the aggressive nature of meningococcal septicemia.

ShuA: A functional homolog of HmbR

Although there is no crystal structure of the hemoglobin and transferrin receptors from *Neisseria meningitidis*, the structure of a functional homologue found in *Shigella dysenteriae*, named ShuA, has recently been solved [101]. Although ShuA shares only 15% sequence identity to HmbR, it is also an outer membrane, TonB dependent heme/hemoglobin receptor. The crystal structure reveals a canonical β-barrel structure composed of 22 transmembrane antiparallel β- strands, and the same topology is predicted for HmbR [102]. Additional studies on ShuA have revealed a preference for binding heme derived from hemoglobin in the ferric state (methemoglobin) as a tetramer over other hemoglobin or myoglobin variants, and the copurification ferric heme bound to purified ShuA [91]. It is unknown what source of heme HmbR utilizes, but evidence exists suggesting it is also from methemoglobin (Chapter 3). In the structure of ShuA, no transmembrane pore was observed in the crystal structure, and the TonB

interaction box was buried [101]. This suggests that heme abstraction and transport require elaborate conformational changes, consistent with an induced fit mechanism. Like all TBDTs, the extracellular regions of ShuA are highly variable, and believed to be responsible for recognition of specific substrates. Thus, key differences in this region direct the substrate specificity of many TBDTs, including HmbR, and are therefore important regions that must be evaluated individually during the rational design of future drugs.

SUMMARY AND HYPOTHESIS

The characterization of membrane proteins represents exciting prospects in the development of novel pharmaceutical agents, namely because of the implications these proteins have in a number of pathologies. The *CaaX* proteases and HmbR represent promising new therapeutic targets. In the current studies, we have evaluated the *CaaX* proteases from *Trypanosoma brucei* and the hemoglobin receptor from *Neisseria meningitidis*. The two principal goals of this study are as follows. First, experiments were designed to establish the presence of distinct *Tb CaaX* proteolytic activities, to determine potential targets of each, and to identify small molecule inhibitors of the underlying enzymes responsible for these activities. Second, experiments were designed to spectroscopically and biochemically characterize the heme binding site within HmbR. These efforts have contributed to our understanding of the function, mechanisms, and activities of both the *Tb CaaX* proteases and HmbR, and may prove to be of significant utility within the development of therapies to treat *T. brucei* and *N. meningitidis* infections.

REFERENCES

1 Whittle, P. J., Blundell, T. L. (1994) Protein structure-based drug design. Annual Review of Biophysics and Biomolecular Structure. **23**, 349-375

2 Powers, R. (2002) Applications of NMR to structure-based drug design in structural genomics. Journal of structural and functional genomics. **2**, 113-123

3 Kuhn, P., Wilson, K., Patch, M. G., Stevens, R. C. . (2002) The genesis of high-throughput structure-based drug discovery using protein crystallography. Current Opinion in Chemical Biology. **6**, 704-710

4 Blundell, T. L., Patel, S. (2004) High-throughput X-ray crystallography for drug discovery. Current Opinion in Pharmacology. **4**, 490-496

5 Williams, W. P., Kuyper, L. F., Pearce, K. H. (2005) Recent applications of protein crystallography and structure-guided drug design. Current Opinion in Chemical Biology. **9**, 371-380

6 Berman, H. M., Westbrook, J., Feng, Z., Gilligand, G., Bhat, T. N., Weissig, H., Shindyalov, I. N., Bourne, P. E. (2000) The Protein Data Bank. Nucleic Acids Research. **28**, 235-242

7 Berman, H. M., Henrick, K. and Nakamura, H. (2003) Announcing the worldwide Protein Data Bank. Nature Structural Biology. **10**, 980

8 Wallin, E. and von Heijne, G. (1998) Genome-wide analysis of integral membrane proteins from eubacterial, archaen, and eukaryotic organisms. Protein Science. **7**, 1029-1038

9 Stevens, T. J. and Arkin, I. T. (2000) Do more complex organisms have a greater proportion of membrane proteins in their genomes? Proteins: Structure, Function, and Genetics. **1**, 417-420

10 White, S. H. (2009) Biophysical dissection of membrane proteins. Nature. **459**, 344-346

11 Terstappen, G. C., Reggiani, A. (2001) In silico research in drug discovery. Trends in pharmacological sciences. **22**, 23-26

12 Zheng, C. J., Han, L. Y., Yap, C. W., Ji, Z. L., Cao, Z. W., Chen, Y. Z. . (2006) Therapeutic Targets: Progress of Their Exploration and Investigation of Their Characteristics. Pharmacological Reviews. **58**, 259-279

13 Singh, S., Malik, B. K., Sharma, D. K. (2006) Molecular drug targets and structure based drug design: A holistic approach. Bioinformation. **1**, 314-320

14 Arinaminpathy, Y., Khurana, E., Engelman, D. M. and Gerstein, M. B. (2009) Computational analysis of membrane proteins: the largest class of drug targets. Drug Discovery Today. **14**, 1130-1135

15 Caffrey, M. (2003) membrane protein crystallization. Journal of Structural Biology. **142**, 108-132

16 Link, J. A., Georgiou, G. (2007) Advances and Challenges in Membrane Protein Expression. American Institute of Chemical Engineers. **53**, 752-756

17 Loll, P. J. (2003) Membrane protein structural biology: the high throughput challenge. Journal of Structural Biology. **142**, 144-153

18 Carpenter, E. P., Beis, K., Cameron, A. D., Iwata, S. (2008) Overcoming the Challenges of membrane protein crystallography. Current Opinion in Structural Biology. **18**, 581-586

19 Trimpin, S., Brizzard, B. (2009) Analysis of insoluble proteins. BioTechniques. **46**, 409-419

20 Bunimov, N., Laneuville, O. (2008) Cyclooxygenase Inhibitors: Instrumental Drugs to Understand Cardiovascular Homeostasis and Arterial Thrombosis. Cardiovascular & Hematological Disorders-Drug Targets. **8**, 268-277

21 Foody, J. M., Farrell, M. H., Krumholz, H. M. (2002) β-Blocker Therapy in Heart Failure. The Journal of the American Medical Association. **287**, 883-889

22 Mena, M. A., Casarejos, M. J., Solano, R. M., Yebenes, J. G. (2009) Half a Century of l-DOPA. Current Topics in Medicinal Chemistry. **9**, 880-893

23 Walian, P. J., Jap, B. K. (1996) Structure and Functional Mechanism of Porins. Physiological Reviews. **76**, 1073-1088

24 Minetti, C., Remeta, D. P. (2006) Energetics of membrane protein folding and stability. Archives of Biochemistry and Biophysics. **453**, 32-53

25 Lehnert, U., Xia, Y., Royce, T. E., Goh, C., Liu, Y., Senes, A., Yu, H., Zang, Z. L., Engelman, D. M., Gerstein, M. . (2004) Computational analysis of membrane proteins: genomic occurence, structure prediction and helix interactions. Quarterly Reviews of Biophysics. **37**, 121-146

26 MacKenzie, K. R. (2006) Folding and Stability of α-helical Integral Membrane Proteins. Chemical Reviews. **106**, 1931-1977

27 Langosch, D., Arkin, I. T. (2009) Interaction and conformational dynamics of membrane-spanning protein helices. Protein Science. **18**, 1343-1358

28 Schulz, G. E. (2002) The Structure of bacterial outer membrane proteins. Biochemica et Biophysica Acta. **1565**, 308-317

29 Wimley, W. C. (2003) The Versatile β-Barrel membrane protein. Current Opinion in Structural Biology. **13**, 404-411

30 Walian, P., Cross, T.A., Jap, B. K. (2004) Structural genomics of membrane proteins. Genome Biology. **5**, 215

31 Chou, K., Elrod, D. W. (1999) Prediction of Membrane Protein Types and Subcellular Localizations. Proteins: Structure, Function, and Genetics. **34**, 137-153

32 Geny, B., Popoff, M. R. (2006) Bacterial protein toxins and lipids: pore formation or toxin entry into cells. Biology of the Cell. **98**, 667-678

33 Wolfe, M. S. and Selkoe, D. J. (2002) Biochemistry. Intramembrane proteases-mixing oil and water. Science. **296**, 2156-2157

34 Weihofen, A., Martoglio, B. (2003) Intramembrane-cleaving proteases: controlled liberation of proteins and bioactive peptides. Trends in Cell Biology. **13**, 71-78

35 Ha, Y. (2007) Structural principals of intramembrane proteases. Current Opinion in Structural Biology. **17**, 405-411

36 Wolfe, M. S. (2009) Intramembrane-cleaving Proteases. Biological Chemistry. **284**, 13969-13973

37 Hardy, J. and Selkoe, D. J. (2002) The amyloid hypothesis of Alzheimer's disease: progress and problems on the road to therapeutics. Science. **297**, 353-356

38 Woo, H., Park, J., Gwon, A., Arumugan, T. V., Jo, D. (2009) Alzheimer's disease and Notch signaling. BBRC. **390**, 1093-1097

39 Friedmann, E., Lemberg, M. K., Weihofen, A., Dev, K. K., Dengler, U., Rovelli, G., Martoglio, B. (2004) Consensus Analysis of Signal Peptide Peptidase and Homologous

Human Aspartic Proteases Reveals Opposite Topology of Catalytic Domains Compared with Presenilins The Journal of Biological Chemistry. **279**, 50790-50798

40 Fluhrer, R., Steiner, H., Haas, C. (2009) Intramembrane Proteolysis by Signal Peptide Peptidases: A Comparative Discussion of GXGD-type Aspartyl Proteases The Journal of Biological Chemistry. **284**, 13975

41 Golde, T. E., Wolfe, M. S., Greenbaum, D. C. (2009) Signal peptide peptidases: A family of intramembrane-cleaving proteases that cleave type 2 transmembrane proteins. Seminars in Cell & Developmental Biology. **20**, 225-230

42 Kim, A., Oliver, D. C., Paetzel, M. (2007) Crystal Structure of a Bacterial Signal Peptide Peptidase. JMB. **376**, 352-366

43 Wolfe, M. S. and Selkoe, D. J. (2002) Intramembrane proteases--mixing oil and water. Science. **296**, 2156-2157

44 LaPointe, C. F., Taylors, R. K. (2000) The Type 4 Prepilin Peptidases Comprise a Novel Family of Aspartic Acid Proteases. The Journal of Biological Chemistry. **275**, 1502-1510

45 Freeman, M. (2009) Rhomboids: 7 years of a new protease family. Seminars in Cell & Developmental Biology. **20**, 231-239

46 Urban, S. (2010) Taking the plunge: integrating structural, enzymatic and computational insights into a unified model for membrane-immersed rhomboid proteolysis. Biochemical Journal. **425**, 501-512

47 Brown, M. S., Goldstein, J. L. (1999) A proteolytic pathway that controls the cholesterol content of membranes, cells, and blood. Proceedings of the National Academy of Sciences U S A. **96**, 11041-11048

48 Zhang, K., Kaufman, R. J. (2006) The unfolded protein response: a stress signaling pathway critical for health and disease. Neurology. **66**, S102-109

49 Schmidt, W. K., Tam, A. and Michaelis, S. (2000) Reconstitution of the Ste24p-dependent N-terminal proteolytic step in yeast **a**-factor biogenesis. JBC. **275**, 6227-6233

50 Tam, A., Schmidt, W. K. and Michaelis, S. (2001) The multispanning membrane protein Ste24p catalyzes CAAX proteolysis and NH2-terminal processing of the yeast a-factor precursor. J Biol Chem. **276**, 46798-46806

51 Pei, J. and Grishin, N. V. (2001) Type II CAAX prenyl endopeptidases belong to a novel superfamily of putative membrane-bound metalloproteases. Trends Biochem Sci. **26**, 275-277

52 Plummer, L. J., Hildebrandt, E. R., Porter, S. B., Rogers, V. A., McCracken, J. and Schmidt, W. K. (2006) Mutational analysis of the ras converting enzyme reveals a requirement for glutamate and histidine residues. J Biol Chem. **281**, 4596-4605

53 Manandhar, S. P., Hildebrandt, E. R. and Schmidt, W. K. (2007) Small-molecule inhibitors of the Rce1p CaaX protease. J Biomol Screen. **12**, 983-993

54 Caplin, B. E., Hettich, L. A. and Marshall, M. S. (1994) Substrate characterization of the Saccharomyces cerevisiae protein farnesyltransferase and type-I protein geranylgeranyltransferase. Biochim Biophys Acta. **1205**, 39-48

55 Lane, K. T. and Beese, L. S. (2006) Thematic review series: lipid posttranslational modifications. Structural biology of protein farnesyltransferase and geranylgeranyltransferase type I. J Lipid Res. **47**, 681-699

56 Moores, S. L., Schaber, M. D., Mosser, S. D., Rands, E., O'Hara, M. B., Garsky, V. M., Marshall, M. S., Pompliano, D. L. and Gibbs, J. B. (1991) Sequence dependence of protein isoprenylation. JBC. **266**, 14603-14610

57 Boyartchuk, V. L., Ashby, M. N. and Rine, J. (1997) Modulation of Ras and **a**-factor function by carboxyl-terminal proteolysis. Science. **275**, 1796-1800

58 Schmidt, W. K., Tam, A., Fujimura-Kamada, K. and Michaelis, S. (1998) Endoplasmic reticulum membrane localization of Rce1p and Ste24p, yeast proteases involved in carboxyl-terminal CAAX protein processing and amino-terminal **a**-factor cleavage. Proc Natl Acad Sci USA. **95**, 11175-11180

59 Tam, A., Nouvet, F., Fujimura-Kamada, K., Slunt, H., Sisodia, S. S. and Michaelis, S. (1998) Dual roles for Ste24p in yeast **a**-factor maturation: NH_2-terminal proteolysis and COOH-terminal CAAX processing. JCB. **142**, 635-649

60 Mokry, D. Z., Manandhar, S. P., Chicola, K. A., Santangelo, G. M. and Schmidt, W. K. (2009) Heterologous expression studies of Saccharomyces cerevisiae reveal two distinct trypanosomatid CaaX protease activities and identify their potential targets. Eukaryot Cell. **8**, 1891-1900

61 Young, S. G., Ambroziak, P., Kim, E. and Clarke, S. (2001) Postisoprenylation protein processing: CXXX (CaaX) endoproteases and isoprenylcysteine carboxyl methyltransferase. In The Enzymes (Tamanoi, F. and Sigman, D. S., eds.). pp. 155-213, Academic Press, New York, NY

62 Hrycyna, C. A., Sapperstein, S. K., Clarke, S. and Michaelis, S. (1991) The *Saccharomyces cerevisiae STE14* gene encodes a methyltransferase that mediates C-terminal methylation of **a**-factor and RAS proteins. EMBO. **10**, 1699-1709

63 Flanders, T. Y. and Foulkes, W. D. (1996) Pancreatic adenocarcinoma: epidemiology and genetics. J Med Genet. **33**, 889-898

64 Andreyev, H. J., Norman, A. R., Cunningham, D., Oates, J. R. and Clarke, P. A. (1998) Kirsten ras mutations in patients with colorectal cancer: the multicenter "RASCAL" study. J Natl Cancer Inst. **90**, 675-684

65 Cox, A. and Der, C. (2002) Farnesyltransferase inhibitors: promises and realities. Current Opinion in Pharmacology. **2**, 388-393

66 Zhu, K., Hamilton, A. D. and Sebti, S. M. (2003) Farnesyltransferase inhibitors as anticancer agents: current status. Curr Opin Investig Drugs. **4**, 1428-1435

67 Brunner, T. B., Hahn, S. M., Gupta, A. K., Muschel, R. J., McKenna, W. G., Bernhard, E. J. (2003) Farnesyltransferase Inhibitors: An Overview of the Results of Preclinical and Clinical Investigations Cancer Research. **63**, 5656-5668

68 Lobell, R. B., Omer, C. A., Abrams, M. T., Bhimnathwala, H. G., Brucker, M. J., Buser, C. A., Davide, J. P., deSolms, S. J., Dinsmore, C. J., Ellis-Hutchings, M. S., Kral, A. M., Liu, D., Lumma, W. C., Machotka, S. V., Rands, E., Williams, T. M., Graham, S. L., Hartman, G. D., Oliff, A. I., Heimbrook, D. C., Kohl, N. E. (2001) Evaluation of farnesyl:protein transferase and geranylgeranyl:protein transferase inhibitor combinations in preclinical models. American Association for Cancer Research. **61**, 8758-8768

69 deSolms, S. J., Ciccarone, T. M., MacTough, S. C., Shaw, A. W., Buser, C. A., Ellis-Hutchings, M., Fernandes, C., Hamilton, K. A., Huber, H. E., Kohl, N. E., Lobell, R. B., Robinson, R. G., Tsou, N. N., Walsh, E. S., Graham, S. L., Beese, L. S. and Taylor, J. S. (2003) Dual protein farnesyltransferase-geranylgeranyltransferase-I inhibitors as potential cancer chemotherapeutic agents. J Med Chem. **46**, 2973-2984

70 Young, S. G., Meta, M., Yang, S. H. and Fong, L. G. (2006) Prelamin A farnesylation and progeroid syndromes. J Biol Chem. **281**, 39741-39745

71 Ohkanda, J., Lockman, J. W., Yokoyama, K., Gelb, M. H., Croft, S. L., Kendrick, H., Harrell, M. I., Feagin, J. E., Blaskovich, M. A., Sebti, S. M. and Hamilton, A. D. (2001) Peptidomimetic inhibitors of protein farnesyltransferase show potent antimalarial activity. Bioorg Med Chem Lett. **11**, 761-764

72 Esteva, M. I., Kettler, K., Maidana, C., Fichera, L., Ruiz, A. M., Bontempi, E. J., Andersson, B., Dahse, H. M., Haebel, P., Ortmann, R., Klebe, G. and Schlitzer, M. (2005) Benzophenone-based farnesyltransferase inhibitors with high activity against Trypanosoma cruzi. J Med Chem. **48**, 7186-7191

73 Eastman, R. T., Buckner, F. S., Yokoyama, K., Gelb, M. H. and Van Voorhis, W. C. (2006) Thematic review series: lipid posttranslational modifications. Fighting parasitic disease by blocking protein farnesylation. J Lipid Res. **47**, 233-240

74 Gillespie, J. R., Yokoyama, K., Lu, K., Eastman, R. T., Bollinger, J. G., Van Voorhis, W. C., Gelb, M. H. and Buckner, F. S. (2007) C-terminal proteolysis of prenylated proteins in trypanosomatids and RNA interference of enzymes required for the post-translational processing pathway of farnesylated proteins. Mol Biochem Parasitol. **153(2)**, 115-124

75 Wang, M., Tan, W., Zhou, J., Leow, J., Go, M., Lee, H. S. and Casey, P. J. (2008) A small molecule inhibitor of isoprenylcysteine carboxymethyltransferase induces autophagic cell death in PC3 prostate cancer cells. J Biol Chem. **283**, 18678-18684

76 Winter-Vann, A. M., Baron, R. A., Wong, W., dela Cruz, J., York, J. D., Gooden, D. M., Bergo, M. O., Young, S. G., Toone, E. J. and Casey, P. J. (2005) A small-molecule

inhibitor of isoprenylcysteine carboxyl methyltransferase with antitumor activity in cancer cells. Proc Natl Acad Sci U S A. **102**, 4336-4341

77 Woodford, N., Livermore, D. M. (2009) Infections caused by Gram-positive bacteria: a review of the global challenge. Journal of Infection. **59**, S4-S16

78 Giamarellou, H., Poulakou, G. (2009) Multidrug resistant Gram-negative infections: what are the treatment options? Drugs. **69**, 1879-1901

79 Rasko, D. A., Sperandio, V. (2010) Anti-virulence strategies to combat bacteria-mediated disease. Nature Reviews Drug Discovery. **9**, 117-128

80 Salton, M. R. (1953) Studies of the Bacterial Cell Wall. Biochim et Biophysica Acta. **10**, 512-523

81 Gregersen, T. (1978) Rapid Method for Distinction of Gram-Negative from Gram-Positive Bacteria. European Journal of Applied Microbiology and Biotechnology. **5**, 123-127

82 Pietras, Z., Bavro, V. N., Furnham, N., Pellegrini-Calace, M., Milner-White, E. J. and Luisi, B. F. (2008) Structure and Mechanism of Drug Efflux Machinery in Gram Negative Bacteria. Current Drug Targets. **9**, 719-728

83 Pages, J., Masi, M. and Barbe, J. (2005) Inhibitors of efflux pumps in Gram-negative bacteria. Trends in Molecular Medicine. **11**, 382-389

84 Koebnik, R., Locher, K. and Gelder, P. V. (2000) Structure and function of bacterial outer membrane proteins: barrels in a nutshell. Molecular Microbiology. **37**, 239-253

85 Su, Z. and Honek, J. F. (2007) Emerging bacterial enzyme targets. Current opinion in Investigational Drugs. **8**, 140-149

86 Posey, J. E. and Gherardini, F. C. (2000) Lack of a Role for Iron in the Lyme Disease Pathogen. Science. **288**, 1651-1653

87 Wyckoff, E. E., Mey, A. R. and Payne, S. M. (2007) Iron acquisition in Vibrio cholerae. Biometals. **20**, 405-416

88 Fetherston, J. D., Kirillina, O., Bobrov, A. G., Paulley, J. T. and Perry, R. D. (2010) The yersiniabactin transport system is critical for the pathogenesis of bubonic and pneumonic plague. Infection and Immunity. **In press**

89 Poole, K. and McKay, G. A. (2003) Iron acquisition and its control in Pseudomonas aeruginosa: many roads lead to Rome. Frontiers in Bioscience. **1**, d661-d686

90 Schryvers, A. B. and Gray-Owen, S. (1992) Iron acquisition in Haemophilus influenzae: receptors for human transferrin. journal of Infectious Diseases. **165 Supplemental**, S103-S104

91 Burkhard, K., Wilks, A. (2007) Characterization of the Outer Membrane Receptor ShuA from the Heme Uptake System of Shigella dysenteriae The Journal of Biological Chemistry **282**, 15126-15136

92 Perkins-Balding, D., Ratliff-Griffin, M., Stojiljkovic, I. (2004) Iron Transport Systems in Neisseria meningitidis. Microbiology and Molecular Biology Reviews. **68**, 154-171

93 Fergusen, A. D., Deisenhofer, J. (2002) TonB-dependent receptors-structural perspectives. Biochimica et Biophysica Acta. **1565**, 318-332

94 Frankenberg-Dinkel, N. (2004) Bacterial heme oxygenases. Antioxidants & Redox Signaling. **6**, 825-834

95 Archibald, F. S. and DeVoe, I. W. (1980) Iron acqusition by Neisseria meningitidis in vitro. Infection and Immunity. **27**, 322-334

96 West, S. E. and Sparling, P. F. (1985) Response of Neisseria gonorrhoeae to iron limitation: alterations in expression of membrane proteins without apparent siderophore production. Infection and Immunity. **47**, 388-394

97 Cornelissen, C. N., Kelley, M., Hobbs, M. M., Anderson, J. E., Cannon, J. G., Cohen, M. S. and Sparling, P. F. (1998) The transferrin receptor expressed by gonococcal strain FA1090 is required for the experimental infection of human male volunteers. Molecular Microbiology. **27**

98 Harrison, O. B., Evans, N. J., Blair, J. M., Grimes, H. S., Tinsley, C. R., Nassif, X., Kriz, P., Ure, R., Gray, S. J., Derrick, J. P., Maiden, M. C. J. and Feavers, I. M. (2009) Epidemiological evidence for the role of the haemoglobin receptor, HmbR, in meningococcal virulence. The Journal of Infectious Diseases. **200**, 94-98

99 Stojiljkovic, I., Larson, J., Hwa, V., Anic, S., So, M. (1996) HmbR Outer Membrane Receptors of Pathogenic Neisseria spp.: Iron-regulated, Hemoglobin-Binding Proteins with a High Level of Primary Structure Conservation. American Society for Microbiology. **178**, 4670-4678

100 Stojiljkovic, I., Hwa, V., de Saint Martin, L., O'Gaora, P., Nassif, X., Heffron, F. and So, M. (1995) The Neisseria meningitidis haemoglobin receptor: its role in iron utilization and virulence. Molecular Microbiology. **15**, 531-541

101 Cobessi, D., Meksem, A., Brillet, K. (2009) Structure of the heme/hemoglobin outer membrane receptor ShuA from Shigella dysenteriae: Heme binding by an induced fit mechansim. Proteins. **78**, 286-294

102 Perkins-Balding, D., Baer, M., T., Stojiljkovic. (2003) Identification of functionally important regions of a haemoglobin receptor from neisseria meningitidis. Microbiology. **149**, 3423-3435

103 Wishart, D. S., Knox, C., Guo, A. C., Shrivastava, S., Hassanali, M., Stothard, P., Chang, Z., Woolsey, J. (2006) DrugBank: a comprehensive resource for in silico drug discovery and exploration. Nucleic Acids Research. **34**, D668-672

104 Wishart, D. S., Knox, C., Guo, A. C., Cheng, D., Shrivastava, S., Tzur, D., Gautam, B., Hassanali, M. (2008) DrugBank: a knowledgebase for drugs, drug actions and drug targets. Nucleic Acids Research. **36**, D901-906

105 Edman, K., Nollert, P., Royant, A., Belrhali, H., Pebay-Peyroula, E., Hadju, J., Neutze, R., Landau, E. M. (1999) High-resolution X-ray structure of an early intermediate in the bacteriorhodopsin photocycle. Nature. **401**, 822-826

Table 1.1 Examples of drugs that target membrane proteins[1]

DRUG	TARGET	TREATMENT
Aspirin	Cox-1 and Cox-2	Acute pain, anti-inflammatory
Vioxx/celebrex	Cox-2	Acute pain, anti-inflammatory
Amlexanox	Cysteinyl leukotriene receptor	Anti-inflammatory
Cimetidine	Histamine H2 Receptor	Acid reflux
Hydroxyzine	H1-receptor	Anxiety
Digoxin	Sodium/potassium APase	Congestive heart failure
Betaxolol	β-adrenergic receptor	Congestive heart failure
Picrotoxin	$GABA_A$ receptor	Respiratory distress
Phenobarbital	$GABA_A$ receptor	Epilepsy
Zaleplon	$GABA_Z$ receptor	Insomnia
Etanercept	P75 and p55	Rheumatoid arthritis
Losartan	At1 receptor	Hypertension
Paclitaxel	Bcl-2	Ovarian, breast cancer
Oxybuprocaine	Sodium ion channel	Local anesthetic
Decamethonium	Nicotinic acetylcholine receptor	Anesthetic
Chlorprothixene	D1 and D2 receptors	Psychotic disorders
L-Dopa	β-adrenoceptors	Neurological disorders
Naloxone	μ-opiod receptors	Depression
Zoloft	5HT Transporter	Depression
Etretinate	Retinoic acid receptor	Psoriasis

[1]All information obtained from the drug database [103, 104]

Table 1.2 Summary of the different classes of intramembrane cleaving proteases (i-CliPs)

Family	Protease Type	Substrates
Type four prepilins (TFPPs)	Aspartic acid	Bacterial prepilins
Presenilins	Aspartic acid	Amyloid precursor protein, Notch
Signal peptide peptidase (SPP)	Aspartic acid	Signal peptide remnants
Rhomboid	Serine	TGFα, mitochondrial regulatory proteins
Site 2 Protease (S2P)	Metallo	SREBP, ATF6
Ste24 *CaaX* Protease	Metallo	*CaaX* prenylated proteins
Rce1 *CaaX* Protease	unknown	*CaaX* prenylated proteins

Figure 1.1 *Crystal structures showing the archetypical topologies of inner and outer bacterial membrane proteins*

(A) The cytoplasmic membrane protein bacteriorhodopsin from *Halobacterium halobium.* Seven transmembrane α-helices form a cylindrical global structure. (B) The heme/hemoglobin outer membrane receptor, ShuA, from *Shigella dysenteriae*. Twenty-two antiparallel β-sheets form a closed β-barrel structure. Images were generated from the RCSB PDB coordinate files 1QKO, and 3FHH, respectively using PyMOL molecular visualization software [101, 105].

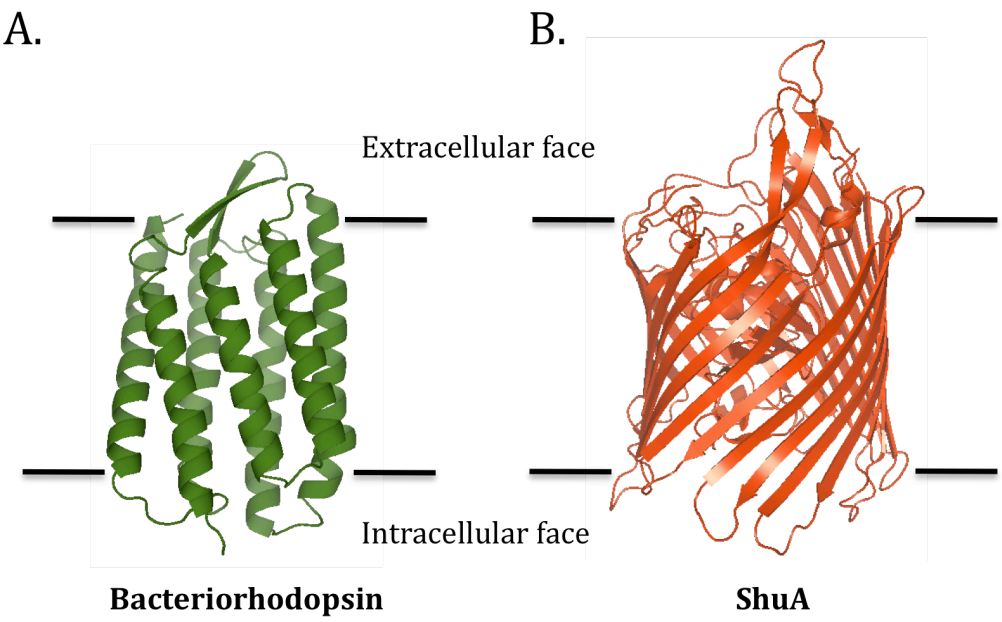
A.
B.
Extracellular face
Intracellular face
Bacteriorhodopsin
ShuA

Figure 1.2 *The CaaX processing pathway*

The processing of *CaaX* (C, cysteine; a, aliphatic amino acid; and X, one of several amino acids) proteins involves three sequential post-translational events. (1) The precursor protein is isoprenylated by either a farnesyl or gernylgeranyl transferase. (2) The protein is further modified by C-terminal proteolysis facilitated by Rce1 or Ste24. (3) The final processing step is carboxymethylation by a Ictm (3). The modified peptide is usually the mature or active form of the protein.

1. Isoprenylation

2. Proteolysis

3. Carboxymethylation

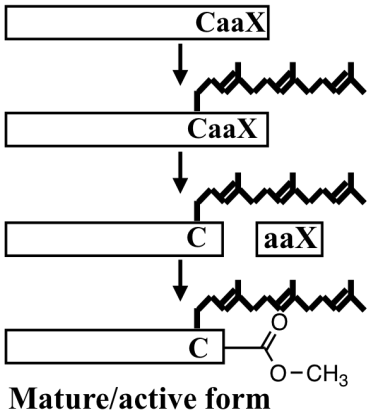

Mature/active form

Figure 1.3 *Proposed HmbR dependent iron acquisition mechanism of Neisseria meningitidis*

Heme abstraction, transport, and iron acquisition from hemoglobin are represented in four steps. 1) Hemoglobin binds to HmbR, initiating abstraction and transport of the heme moiety in a TonB dependent manner into the periplasm. 2) A periplasmic heme binding protein (PBP) transports the heme to an inner membrane transporter (IMT). 3) The inner membrane transporter facilitates the transfer of heme from the periplasm to the cytosol. 4) A heme oxygenase (HO) catalyzes the breakdown of heme into CO, Fe^{+3}, and biliverdin. Adapted from Perkins-Balding, D., et alius [92].

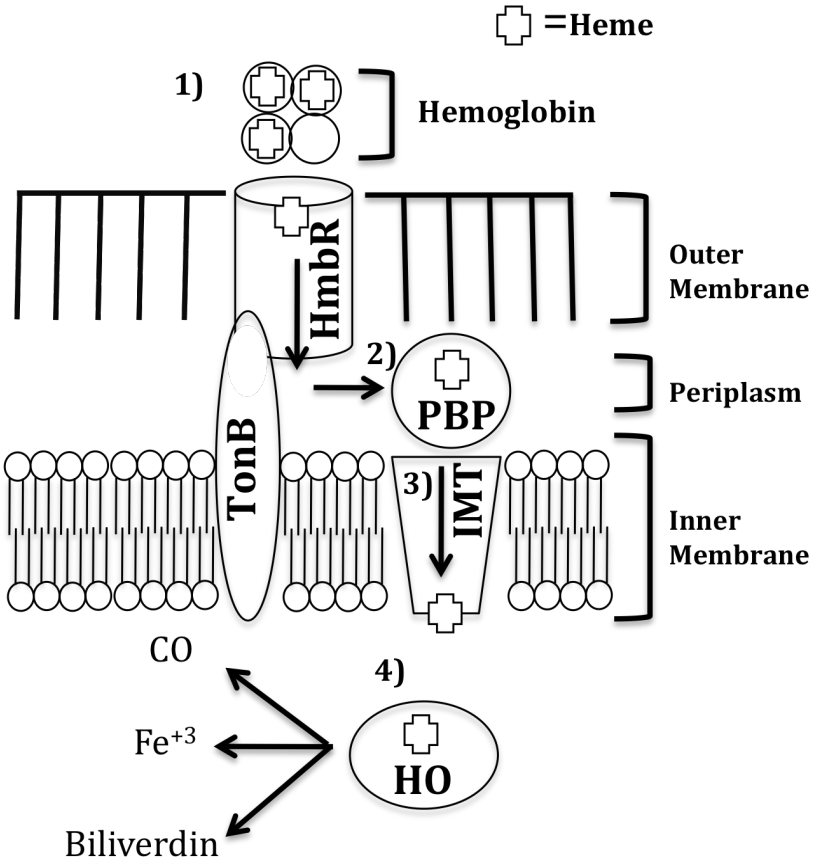
=Heme
1)
Hemoglobin
HmbR
Outer
Membrane
2)
PBP
Periplasm
TonB
3)
IMT
Inner
Membrane
CO
4)
Fe+3
HO
Biliverdin

CHAPTER 2

HETEROLOGOUS EXPRESSION STUDIES IN YEAST REVEAL TWO DISTINCT TRYPANOSOMATID *CAAX* PROTEASE ACTIVITIES AND IDENTIFIES THEIR POTENTIAL TARGETS[1]

[1] David Z. Mokry, Surya P. Manandhar, Kristen A. Chicola, George M. Santangelo, and Walter K. Schmidt. 2009. *Eukaryotic Cell*. 8(12) 1891-1900

Reprinted here with permission of publisher

SYNOPSIS

The *CaaX* tetrapeptide motif typically directs three sequential post-translational modifications: namely, isoprenylation, proteolysis, and carboxyl methylation. In all eukaryotic systems evaluated to date, two *CaaX* proteases (Rce1 and Ste24/Afc1) have been identified. While the *Trypanosoma brucei* genome also encodes two putative *CaaX* proteases, the lack of detectable *Tb* Ste24 activity in trypanosome cell extracts has suggested that *CaaX* proteolytic activity within this organism is solely attributed to *Tb* Rce1 (20). In this study, we demonstrate that both *Tb* Rce1 and *Tb* Ste24 are enzymatically active when heterologously expressed in yeast. Using **a**-factor and GTPase reporters, we demonstrate that *Tb* Rce1 and *Tb* Ste24 possess partially overlapping specificities much like, but not identical to, their fungal and human counterparts. Of interest, a *CaaX* motif found on a trypanosomal Hsp40 protein was not cleaved by either *Tb* CaaX protease when examined in the context of the yeast **a**-factor reporter, but was cleaved by both in the context of the Hsp40 protein itself when evaluated using an *in vitro* radiolabeling assay. We further demonstrate that *Tb* Rce1 is sensitive to small molecules previously identified as inhibitors of the yeast and human *CaaX* proteases, and that a subset of these compounds disrupt *Tb* Rce1-dependent localization of our GTPase reporter in yeast. Together, our results suggest the conserved presence of two *CaaX* proteases in trypanosomatids, identify an Hsp40 protein as a substrate of both *Tb CaaX* proteases, support the potential use of small molecule *CaaX* protease inhibitors as tools for cell biological studies on the trafficking of *CaaX* proteins, and provide evidence that protein context influences *Tb CaaX* protease specificity.

INTRODUCTION

Certain isoprenylated proteins are synthesized as precursors having a highly degenerate C-terminal tetrapeptide *CaaX* motif (C = cysteine; a = aliphatic amino acid; X = one of several amino acids). This motif typically directs three post-translational modifications that include covalent attachment of an isoprenoid lipid to the cysteine residue, followed by endoproteolytic removal of the terminal three residues (*i.e.,* aaX), and lastly, carboxyl methyl esterification of the farnesylated cysteine (50, 51). Relevant examples of proteins subject to the above modifications, also referred to as *CaaX* proteins, include the Ras and Ras-related GTPases, Gγ subunits, prelamin A, members of the Hsp40 family of chaperones, and fungal mating pheromones.

Isoprenylation of *CaaX* proteins is performed by either the farnesyltransferase (FTase) or the geranylgeranyl transferase I (GGTase I). The particular isoprenoid attached, C15 farnesyl or C20 geranylgeranyl, respectively, depends in part on the sequence of the *CaaX* motif (8, 26, 32). Proteolysis of isoprenylated intermediates is carried out by the otherwise unrelated Rce1p and Ste24p (sterile mutant 24) enzymes, collectively referred to as *CaaX* proteases, which are integral membrane proteins residing within the ER (3, 41, 46). Studies to elucidate the specificities of the *CaaX* proteases have often involved reporters designed from biological substrates (e.g. Ras GTPases), (2, 3, 16, 21, 22, 24, 35). While these studies suggest that isoprenylated *CaaX* tetrapeptides alone are sufficient for recognition as a substrate, insufficient evidence exists to assert whether this sequence contains all the necessary information for substrate specificity. Reporters are typically cleaved by either Rce1p or Ste24p. The *Saccharomyces cerevisiae* **a**-factor mating pheromone is a rather unusual biological reporter as it is cleaved by both yeast *CaaX* proteases. Orthologs of the *CaaX* proteases from human, worm, and plant can also cleave **a**-factor when heterologously expressed in yeast, thereby making **a**-

factor a convenient reporter for comparative analyses of *CaaX* protease activities (3, 5, 6, 37). Where evaluated using the **a**-factor reporter, Rce1p and Ste24p display partially overlapping target specificity, and this is an expected property of *CaaX* proteases in all eukaryotic systems (5, 6, 37, 48). Unlike the isoprenylation and proteolysis steps, carboxyl methyl esterification exclusively relies on a single enzyme, the isoprenylcysteine carboxyl methyltransferase (ICMT) (23, 51). A farnesylated cysteine appears to be the sole recognition determinant of the ER-localized ICMT (10, 23, 39).

Disruption of the post-translational modifications associated with *CaaX* proteins is often perceived as an anti-cancer strategy because of the prominent role of *CaaX* proteins in cellular transformation (*i.e.,* the Ras GTPases) (50). To date, the most advanced drug discovery efforts have focused on farnesyltransferase inhibitors (FTIs) (9, 54). Inhibitors of the *CaaX* proteases and ICMT are also being developed (1, 11, 29, 38, 40, 49). Disrupting *CaaX* protein modifications has therapeutic application to other diseases as well. The relief of prelamin A toxicity by FTIs is a well-documented example (52). Accumulation of the farnesylated but unproteolyzed precursor of lamin A results in a progeroid phenotype in individuals lacking ZmpSte24 proteolytic activity. The treatment of parasitic disease is another area under investigation (13). A number of FTIs have been developed that inhibit protozoan FTases, and *in vivo* testing is a continued effort (15, 33). While research is less advanced with respect to *CaaX* protease and ICMT inhibitors, RNAi experiments on the bloodstream form of *Trypanosoma. brucei* indicate that *CaaX* processing enzymes are required for viability and proliferation of the parasite (20).

In the present study, we have evaluated the enzymatic properties of the trypanosomal *CaaX* proteases. We establish through use of a variety of *in vivo* and *in vitro* assays that *Tb* Rce1 and

Tb Ste24 are active when heterologously expressed in *S. cerevisiae*, and have partially overlapping substrate specificities. The assays rely on various reporters, specifically the yeast **a**-factor mating pheromone, a K-Ras4B-based fluorogenic peptide, a GFP-GTPase fusion, and a *Tb* Hsp40 protein. All but the GTPase reporter could be effectively cleaved by both *Tb CaaX* proteases. We also demonstrate that the trypanosomal *CaaX* proteases can be targeted for inhibition by small molecules both *in vitro* and when heterologously expressed in yeast, suggesting that the trypanosomal *CaaX* proteases may be attractive drug targets for pharmacological inhibition.

MATERIALS AND METHODS

Yeast Strains and Media – The yeast strains used in this study are listed in **Table 2.1**. To assess *in vivo Tb CaaX* protease function, strains EG123 (ATCC#204278*; MAT***a** *trp1 leu2 ura3 his4 can1*), IH1793 (ATCC#204279; *MAT*α *lys1*), and yWS164 (*MAT***a** *trp1 leu2 ura3 his4 can1 mfa1*-Δ*1 mfa2*-Δ*1 rce1::TRP1 ste24::KAN*^{R}) were transformed with appropriate plasmids (37). For isolation of membranes enriched for *Tb CaaX* proteases, the strain used was SM3614 (*MAT***a** *trp1 leu2 ura3 his4 can1 rce1::TRP1 ste24::LEU2*) transformed with the appropriate plasmid (46). This strain was also used for purification of heterologously expressed GST-Tbj1. To assess *Tb* Hsp40 function *in vivo,* strains BY4741 (*MAT***a** *his3 leu2 met15 ura3*) and a BY4741 derivative (*MAT***a** *his3 leu2 met15 ura3 ydj1*Δ) were obtained from the yeast haploid knockout collection (Research Genetics, Inc.) (19).

Plasmid-transformed strains were created according to published methods (14). Unless otherwise noted, strains were routinely cultured at 30 °C using YEPD or synthetic complete dropout (SC-) medium as previously described (25). Where temperature sensitivity was

evaluated, yeast were simultaneously grown at 25 °C and 35.5 °C for three and two days, respectively, on YEPD solid media. Experiments involving galactose induced GFP-Ras2p and GST-Tbj1 expression used synthetic media lacking glucose and uracil but containing 2% galactose, 1% glycerol, and 1% ethanol (SGal-ura).

Plasmids – The plasmids used in this study are listed in **Table 2.2**. Yeast expression plasmids encoding *Tb* Rce1 (pWS766) and *Tb* Ste24 (pWS767) were created by PCR-directed recombination-mediated plasmid construction (34). In brief, the open reading frames (ORFs) of *Tb* Rce1 and *Tb* Ste24 (accession # XP_843748 and # XP_827211, respectively) were used to replace the ORFs of yeast *RCE1* and *STE24* encoded in pWS479 and pWS154, respectively (37, 46). The trypanosomal ORFs were amplified by PCR from *Trypanosoma brucei brucei* genomic DNA (TREU 927). The appropriate PCR product was co-transformed into yeast with pWS479 or pWS154 that had been linearized with SphI and BglII/NotI, respectively, within the *CaaX* protease ORF. To facilitate recombination between PCR products and linearized plasmids, the PCR products were engineered to contain 39 basepair extensions homologous to sequences immediately 5′ and 3′ of the yeast ORFs encoded in pWS479 and pWS154. The transformed yeast were plated on selective media (SC-ura) to allow for growth of cells that had formed a circularized plasmid; a linearized plasmid is inefficiently propagated and does not support colony growth on selective media. Independent plasmids were isolated from yeast colonies, reamplified in *E. coli*, and subjected to restriction digest analysis and sequencing to verify the presence and sequence of the trypanosomal ORF.

The above process was used to create site-directed mutants of *Tb* Rce1 and *Tb* Ste24. For creating the *Tb* Rce1 mutants, pWS766 was linearized with either AatII or BglII, as appropriate. Creation of *Tb* Ste24 mutants relied on a SacI digest of pWS767. To facilitate identification of

plasmid candidates for sequencing, the oligonucleotides used for PCR were engineered to contain the intended mutation and a silent restriction site near the mutational site.

Yeast expression plasmids encoding **a**-factor *CaaX* variants were also created by recombination-based plasmid construction. In most instances, PstI and MluI gapped pWS654 was used as the recipient vector for PCR products amplified from pWS438 (6). The PCR products contained regions of 5′ and 3′ homology for recombination, the desired mutation, and a silent restriction site that was used to facilitate identification of the appropriate recombinant clone for confirmatory DNA sequencing. The **a**-factor variants containing CAMQ and CTVM motifs were constructed in two steps. First, intermediate plasmids were created by recombination of MluI gapped pSM1605 with PCR products amplified from pSM1605 using mutagenic oligonucleotides. The resultant plasmids were then modified by standard methods to replace the existing *URA3* marker with *LEU2*.

Constructs encoding GST-Tbj1 (pWS782) and GST-Tbj1(C401S) (pWS783) behind the constitutive *CUP1* promoter were created by replacement of *YDJ1* with Tbj1 using recombination within a GST-*YDJ1* expression construct (pWS338) recovered from a GST-fusion library (30). To facilitate recombination, pWS338 was linearized with NarI and Bsu36I. The construct encoding GST-Tbj1 behind the inducible *GAL* promoter (pWS900) was created similarly but used a GST-*YDJ1* expression vector (pWS523) obtained from a different GST fusion library (45). pWS523 was linearized with NarI and PstI. The constructs encoding other *Tb* Hsp40 proteins (Tbj2-4) behind the constitutive phosphoglycerate kinase (*PGK*) promoter were also created by recombination using pWS28 linearized with XmaI as the recipient vector. PCR products for the above constructs were derived from TREU 927 genomic DNA. Candidate

clones identified by restriction digest were sequenced to confirm the presence of the appropriate Hsp40 gene.

Mating Assay – The serial dilution yeast mating assay was performed as previously described (37). In brief, *MAT***a** yeast expressing the indicated *CaaX* protease were cultured for 36 hrs at 30 °C in selective media. The cultures were normalized to A_{600} 1.0 ± 0.05 by the addition of sterile media. The *MAT*α mating partner was cultured in YEPD and normalized in parallel using YEPD. In wells of a 96-well microtiter plate, individual *MAT***a** strains were mixed with *MAT*α yeast using 10 and 90 µl volumes, respectively, of each normalized culture. The mating suspensions were serially diluted by repeatedly transferring 10 µl of each mixture into a new well containing 90 µl of *MAT*α cells until 5 dilutions were prepared. All mixtures were subsequently spotted (5 µl volumes) onto an SD plate, and the plates incubated for 72-96 hours before recording results using a flatbed scanner. The cell suspensions were also spotted onto SC-lysine solid media, which is selective for *MAT***a** and diploid growth, to confirm that *MAT***a** cell dilutions were appropriately prepared.

GFP-Ras2p Localization Assay – An inducible GFP-Ras2p reporter (pWS750) was used to determine the ability of yeast, human, and trypanosomal Rce1 (pWS479, pWS335, and pWS766, respectively) to promote proper localization of GFP-Ras2p in yeast and to evaluate the effect of chemical agents on Ras2p localization (29). Where yeast and trypanosomal Ste24 were evaluated, pSM1282 and pWS767 were used, respectively. In brief, mid-log yeast cells were harvested, washed twice with sterile H_2O, and incubated in SGal-ura for 6-7 hrs at 30 °C to induce expression of GFP-Ras2p. Where applicable, cells were incubated with compounds that were sonicated prior to use with a Fisher Scientific Model 100 Sonic Dismembrator (10 minutes, maximum setting) at predetermined concentrations (0.6 to 55.6 µM) for 1 hr at 30 °C. In

general, the compounds were used at doses where minimal cellular toxicity was observed (i.e. EC_{10}; 90% cell survival). The doses were based on previously reported dose-response toxicity profiles (28). Evaluation of compound **3** required the addition of a non-toxic amount of SDS (0.003%) during the incubation period to maximize effectiveness. The induced cells were mounted on a microscope slide, and the expression pattern of the GFP fusion was visualized using a Zeiss Axioskop 2 Mot Plus microscope equipped with fluorescence optics and a 100x Plan Apochromat objective (numerical aperture 1.4). Images were captured using an ORCA-AG digital camera (Hamamatsu, Japan) and IPLab Spectrum Software. At least five cell fields were taken from which representative images were selected. Using the above protocol, ca. 80% of the cells examined had GFP fluorescence.

To quantify the degree of GFP-Ras2p plasma membrane localization conferred by *CaaX* proteases, a confocal laser scanning microscopy protocol was implemented as previously described (28). In brief, yeast were cultured and induced to express GFP-Ras2p as described above and images collected using a Zeiss LSM510 META microscope with a 100x alpha Plan Fluar 1.45 NA oil objective lens at a resolution of 0.04 μm per pixel. GFP excitation was performed with a 488 nm laser, and the light emitted was captured through a 505-530 nm BP filter. The relative association of GFP-Ras2p with the plasma membrane was determined with Zeiss LSM imaging software from a minimum of 5 pictures, and is reported relative to the total fluorescence associated with the image. Delocalized fluorescence was defined as fluoresence 0.75 μm or more from the peak boundaries. The error of the associated bar graphs was calculated as the standard error of the mean for each value.

In Vitro CaaX Proteolysis Fluorescence Assay – Cleavage of a synthetic quenched fluorogenic farnesylated peptide was used to monitor the *in vitro* activity of the yeast, human, and

trypanosomal *CaaX* proteases (21, 38). In brief, a yeast strain devoid of endogenous *CaaX* protease activity (yWS164) was transformed with a heterologous expression vector encoding a particular *CaaX* protease (as defined in figure or table legends). The resulting transformants were lysed and subjected to a differential centrifugation protocol optimized for the recovery of *CaaX* protease enriched membranes as described below. The membranes (0.5 mg/ml) were incubated with a fluorogenic substrate (20 μM) and relative fluorescence was monitored over a 90 min timecourse using a BioTek Synergy™ HT microtiter plate fluorometer equipped with a 320/420 nm excitation/emission filter set. The substrates used were all internally quenched fluorogenic peptides based on K-Ras4B (21).

Inhibitory compounds were evaluated using two methods. To determine values for percent inhibition of *Tb* Rce1 and *Tb* Ste24 using fixed concentrations of compounds, membranes prepared as described below were pretreated with compounds at 200 μM (FKBK, TPCK, EDTA, EGTA) or 100 μM (all others) for 10 minutes at 30 °C prior to substrate addition and activity analysis. Compounds were typically prepared as 10 mM stocks in water (EDTA and EGTA) or DMSO (all others). Collected data was graphed (change in fluorescence vs. time) and initial velocities determined using Microsoft Excel. These values were used to calculate percent activities relative to an untreated DMSO control. To determine IC_{50} values, the above method was modified such that each condition contained 2.8 mg/ml BSA, and compound stocks were prepared at 100 mM in DMSO. Initial velocities were determined at various inhibitor concentrations ranging from 0.46 μM to 471 μM (11 points minimum). The NSC compounds were provided by the NCI Developmental Therapeutics Program.

Isolation of Yeast Membranes – Yeast membranes were essentially isolated as previously described using two slightly modified protocols to lyse cells (38). In general, membranes used

for determination of IC_{50} values and *in vitro* coupled proteolysis methylation assays were isolated directly from cells by bead beating. In brief, mid-log cells were incubated in pretreatment buffer (100 mM Tris, pH 9.4, 10 mM NaN_3 10 mM DTT; 10 A_{600}/ml) for 10 minutes, resuspended in lysis buffer (50 mM Tris, pH 7.5, 0.2 M sorbitol, 1 mM EDTA, 1 mM phenylmethylsulfonyl fluoride, 2 μg/ml aprotinin, 3 μg/ml each leupeptin, chymostatin, and pepstatin; 500 A_{600}/ml), and lysed using a Biospec mini-beadbeater and silica beads (5000 rpm; three 20-second bursts; 3-min intervals on ice). For all other *in vitro* assays, membranes were isolated from spheroplasts. In brief, cells were pretreated as described above, and spheroplasts generated by treatment with Zymolyase (4 μg /A_{600}; Cape Cod Inc.) for 30 min at 30 °C in spheroplasting buffer (50 mM potassium phosphate, pH 7.5, 1.4 M sorbitol, 10 mM NaN_3; 25 A_{600}/ml), followed by 10 minutes on ice. Spheroplasts were harvested (3,000 x *g*, 10 min, 4 °C), washed in spheroplasting buffer, resuspended in cold lysis buffer, and lysed by vortexing in the presence of silica beads (four 4-min vortex bursts at 4 °C; 2-min intervals on ice). Independent of the method used for cell lysis, crude lysates were clarified twice (500 x *g,* 10 min, 4 °C) and membranes recovered (16,000 x *g*, 15 min, 4 °C) from the clarified lysate. The membranes were resuspended in lysis buffer, reisolated by centrifugation, resuspended in lysis buffer to the original sample volume, adjusted to 1 mg/ml total protein by dilution with lysis buffer, and frozen as aliquots at -80 °C.

In Vitro Tbj1 Proteolysis Assay – TbJ1 (accession # XP_951689) was heterologously expressed as a GST fusion protein (pWS900) in SM3614 (*rce1*Δ *ste24*Δ) and used for coupled proteolysis-methylation radiolabeling assays. In brief, cells from a four liter culture of yeast grown to A_{600} ~1.0 in SGal-ura were harvested (3000 x g for 10 min), incubated with pretreatment buffer, and cells lysed directly as described above with the exception that lysis buffer was supplemented

with 20 μg/ml each leupeptin, pepstatin, chymostatin, aprotinin, and trypsin inhibitor. The resulting lysate was clarified (16,000 x g, 15 minutes) and incubated with a slurry of glutathione Sepharose 4B resin (10 min, 25 °C, 0.675 ml resin/liter of starting culture). The unbound fraction was decanted after centrifugation of the mixture in a standard 15 ml conical tube.

Resin-bound GST-Tbj1 was used directly for *in vitro* assays. In brief, the resin was supplemented with approximately 800 μl of lysis buffer, and the mixture apportioned into nine 300 μl aliquots. Individual aliquots were supplemented with membranes lacking *CaaX* protease activity (yWS164/pRS316) or enriched for a specific trypanosomal *CaaX* protease (yWS164/pWS766 or yWS164/pWS767), and further supplemented with membranes enriched for the yeast ICMT (yWS164/pSM1317). The final sample was 550 μl and contained 0.54 mg/ml of control and *CaaX* protease-enriched membranes, and 0.11 mg/ml of ICMT-enriched membranes. The membranes were isolated from cells lysed directly as described above. The samples also contained 13.9 μM S-adenosylmethionine (SAM; 19.6 mCi ^{14}C/mmol) derived by mixing appropriate amounts of SAM (Sigma) and [^{14}C]-SAM (GE Healthcare; 56 mCi/mmol). After constant mixing for 12 hours at 30 °C, the samples were transferred to individual spin columns (GE Healthcare), centrifuged (1 min, 4000 x g), washed three times with lysis buffer supplemented with 1% N-octyl-β-D-glucopyranoside (OG), and the recovered resin quantitatively transferred to scintillation vials containing 10 ml of Bio-safe II scintillation counting cocktail. Decays per minute (dpm) were determined for each sample using a Fisher/GP-200 Wallac 1409 scintillation counter.

RESULTS

Both of the trypanosomal CaaX proteases are functional enzymes. The yeast *CaaX* proteases promote yeast mating, ostensibly through their ability to proteolyze the isoprenylated yeast **a**-factor precursor (3). *CaaX* proteases from distinct species can do the same when heterologously expressed in yeast (4-6, 37). Since a previous study had concluded that *Tb* Ste24 may be inactive, we first challenged *Tb* Rce1 and *Tb* Ste24 to cleave the CVIA *CaaX* motif present on yeast **a**-factor (20). This analysis revealed that the trypanosomal *CaaX* proteases could both promote yeast mating, as judged by quantitative serial dilution mating tests (**Fig. 2.1A**). This result suggests that the lack of activity previously reported for *Tb* Ste24 may be due to an assay specific or other issue, and not reflective of the intrinsic properties of this enzyme. By our analysis, the trypanosomal *CaaX* proteases performed as well if not better than their respective yeast counterparts in promoting yeast mating. In part, this observation can be explained by the fact that the yeast and *Tb CaaX* proteases were expressed using different plasmid systems. The yeast *CaaX* proteases were encoded on low-copy plasmids behind their respective promoters while the *Tb CaaX* proteases were encoded on high-copy plasmids behind the strong constitutive phosphoglycerate kinase (PGK) promoter. Despite this issue, our result nonetheless indicates an activity for *Tb* Ste24, and suggests that both *Tb* Rce1 and *Tb* Ste24, like their counterparts in other organisms, have the common ability to recognize the **a**-factor precursor as a substrate (3-6, 37).

Mutational analysis of the trypanosomal CaaX proteases. To confirm that the mating observed in our genetic test was indeed dependent on the proteolytic activities of the *Tb CaaX* proteases and not some unrecognized activity, we next evaluated the effect of mutations predicted to

inactivate the enzymes. Despite having a formally unresolved mechanism, a glutamate and two histidine residues are known to be essential for yeast Rce1p activity (12, 37). These residues are conserved in Rce1p orthologs, including *Tb* Rce1, but their functional importance in any ortholog outside of yeast had not been previously addressed (36). Mutation of *Tb* Rce1 at these conserved sites resulted in loss of activity as measured by the yeast mating assay (**Fig. 2.1B**), further supporting a role for histidine and glutamate residues in the Rce1p mechanism. In the instance of yeast Ste24p, histidine and glutamate residues are also required (18). These amino acids are part of a putative HExxH zinc-coordination motif that is common among zinc-dependent metalloproteases. Expectedly, *Tb* Ste24 required this motif for activity (**Fig. 2.1C**). For both *Tb CaaX* proteases, the mutations had no observable effect on protein expression relative to the native proteins, as judged by immunoblots (Mokry and Schmidt, unpublished observation). Our observations as a whole thus support that both *Tb* Rce1 and *Tb* Ste24 have proteolytic activity.

Specificity of the trypanosomal CaaX proteases. To gain additional insight into the enzymatic properties of the trypanosomal *CaaX* proteases, we applied our genetic approach to assess the target specificity of the enzymes by measuring their ability to recognize disparate *CaaX* motifs (**Fig. 2.1D**). Variants of the **a**-factor precursor were created that contained *CaaX* motifs previously documented to be Rce1-specific (*e.g.*, CTLM, CTVM), Ste24-specific (*e.g.*, CASQ), and non-specific (*e.g.*, CVIA, CAMQ) in the context of *CaaX* proteases from other species, namely, yeast and human (37, 48). Consistent with these prior observations, *Tb* Rce1 was observed to be specific for the CTLM and CTVM motifs, *Tb* Ste24 was specific for CASQ, and both were active against the native CVIA motif (see **Fig. 2.1A**). The CAMQ motif was

recognized by both *Tb CaaX* proteases as predicted, but was recognized preferentially by *Tb* Ste24.

We extended our analysis to include an evaluation of motifs associated with predicted trypanosomal *CaaX* proteins. Because trypanosomes do not appear to have a true Ras ortholog, the CTML and CVIM motifs found on the Ras-related proteins *Tb* RLP and *Tb* RHP, respectively, were evaluated as targets for *Tb* Rce1 activity (17). While *Tb* Rce1 recognized both motifs, *Tb* Ste24 also recognized CVIM, indicating that the *Tb CaaX* proteases have overlapping specificity for this motif. Interestingly, CVIM is found on mammalian Ras and is considered to be an Rce1p-specific motif in mammalian systems. We also evaluated *CaaX* motifs found on putative trypanosomal Hsp40 proteins. This family of proteins was targeted because the CASQ motif, which is present on the farnesylated Hsp40 chaperone Ydj1p, is preferentially cleaved by various Ste24 orthologs in our genetic system. None of these motifs (CTQQ, CVHQ, and CTAQ) were cleaved by *Tb* Rce1, and only CVHQ was cleaved by *Tb* Ste24. This pattern was also observed in the context of yeast and human *CaaX* proteases, with the exception of the CTAQ motif, which was readily cleaved by Rce1 from these organisms. The reason for the lack of recognition of the CTQQ (found on two trypanosomal homologs of yeast Ydj1p) and CTAQ motifs by the *Tb CaaX* proteases is unknown, but may relate to the protein context in which they were evaluated (see below and **Discussion**). When considering our results as a whole and in the context of the **a**-factor reporter, the trypanosomal *CaaX* proteases appear to have substantial but not complete conservation of substrate specificity with respect to that observed with *CaaX* proteases from other systems.

Trypanosomal Rce1 can cleave a yeast GTPase. Both yeast and human Rce1p preferentially, if not exclusively, recognize GTPases of the Ras superfamily as substrates. Considering that the

Tb CaaX proteases displayed target specificity profiles by our genetic test that were largely similar to the profiles displayed by the yeast and human *CaaX* proteases, we next evaluated whether *Tb* Rce1 had conserved the ability to recognize Ras GTPases as substrates. Attempts to heterologously express trypanosomal GTPases GFP-RLP and GFP-RHP in yeast did not yield a discernable membrane association for either GTPase, suggesting a potential defect with isoprenylation, so we addressed the ability of *Tb* Rce1 to interact with the yeast Ras2p GTPase. Ras2p normally decorates the cytosolic face of the yeast plasma membrane (**Fig. 2.2A**). This localization pattern is highly dependent on the status of Ras2p post-translational processing (3, 29). In the absence of *CaaX* protease activity (*rce1*Δ *ste24*Δ), subcellular punctate structures are observed with a GFP-Ras2p reporter (**Fig. 2.2B**). As determined through qualitative and quantitative methods, plasmid-based expression of yeast Rce1p, but not Ste24p, can restore proper GFP-Ras2p localization in this genetic background (**Figs. 2.2C** and **D**, respectively, and **Table 2.3**). We took advantage of this observation to investigate whether either of the trypanosomal *CaaX* proteases could properly modify a GTPase. When the trypanosomal *CaaX* proteases were evaluated in the context of GFP-Ras2p, proper localization of the reporter was observed with *Tb* Rce1 but not *Tb* Ste24 (**Figs. 2.2E** and **F**, respectively, and **Table 2.3**).

Trypanosomal Hsp40 protein Tbj1 can substitute for yeast Ydj1p and is cleaved by both Tb CaaX proteases. Primarily through use of **a**-factor as a reporter molecule, the *CaaX* proteases have been demonstrated to possess partially overlapping substrate specificity (48). Yet, the only two established substrates for the Ste24p family of *CaaX* proteases are the precursors of the yeast **a**-factor mating pheromone and mammalian lamin A molecules. Since trypanosomes are not known to express orthologs of either of these molecules, and given the apparent specific ability of *Tb* Ste24 to cleave *CaaX* motifs associated with Hsp40 proteins from different organisms (*i.e.*,

CASQ of yeast Ydj1p and CVHQ of Tbj4), we postulated that isoprenylated Hsp40 proteins are substrates of Ste24p. In obvious conflict with this prediction is our observation that the *Tb* Hsp40-associated *CaaX* motifs CTQQ and CTAQ fail to promote **a**-factor production when co-expressed with either trypanosomal *CaaX* protease (see **Fig. 2.1D**). This leads to one of several possible hypotheses for these motifs – either they are not bona fide *CaaX* motifs (i.e. isoprenylated), they are farnesylated but not proteolyzed, or they require a certain protein context in order to be recognized by Ste24 (*i.e.*, CTQQ and CTAQ are unrecognizable by Ste24 in the context of yeast **a**-factor).

To differentiate between the above possibilities, we first determined whether any *Tb* Hsp40 protein having a *CaaX* motif could be isoprenylated by taking advantage of the observation that yeast are temperature sensitive when yeast Ydj1p is either absent or fails to be isoprenylated (7). A query of the *Trypanosoma brucei* genome database yielded four putative Ydj1 orthologs, herein referred to as Tbj1-4 (accession #XP_951689, #XP_822483, XP_827509, and XP_845830, respectively). The amount of sequence identity relative to yeast Ydj1p for Tbj1, Tbj2, Tbj3, and Tbj4 is 37%, 18%, 13%, and 20%, respectively, as determined through ClustalW2 analysis. Heterologous expression of Tbj1 and Tbj2 rescued growth of a *ydj1*Δ strain at elevated temperature to an extent indistinguishable from wildtype, Tbj3 rescued growth less robustly, and for all practical purposes, Tbj4 failed to rescue growth (**Fig. 2.3A**). Tbj1 and Tbj2 both possess the CTQQ *CaaX* motif, whereas Tbj3 and Tbj4 possess the motifs CVHQ and CTAQ, respectively. The inability of Tbj4 to complement growth was surprising, as it contains more sequence homology to yeast Ydj1p than both Tbj2 and Tbj3. Sequence analysis of this clone, and others isolated independently during construction of the Tbj4 expression plasmid, consistently revealed an 18 nucleotide deletion near the amino terminus. While this may be the

cause for the lack of complementation observed, it is also possible that the sequence for this protein is incorrectly annotated within the *T. brucei* genome database. The sequence we obtained for this clone has been submitted to NCBI (accession #FJ_611958).

To specifically determine the impact of protein farnesylation on Tbj1 function, we mutated its *CaaX* motif cysteine to a serine and evaluated the effect. Tbj1(C401S) could not rescue the temperature sensitivity of the *ydj1*Δ yeast strain (**Fig. 2.3B**), which is the same effect observed for yeast Ydj1p when similarly mutated (7). We interpret this observation to indicate that the function of Tbj1 in trypanosomes has an absolute requirement for the cysteine residue within the CTQQ motif, thereby suggesting that Tbj1 is indeed isoprenylated.

To further test our hypothesis of protein context being important for specificity, we investigated whether *Tb* Rce1 and/or *Tb* Ste24 could cleave the *CaaX* motif of Tbj1 using a coupled proteolysis-carboxylmethylation assay. In this type of assay, the extent of *CaaX* proteolytic activity is indirectly monitored by the extent of ICMT-dependent carboxyl methylation, which is followed using a radioactive tracer. For the purposes of this experiment, the source of the Tbj1 substrate was a cell extract prepared from *CaaX* protease deficient yeast that expressed Tbj1 heterologously. While the use of a purified form of the Tbj1 precursor would have been preferred, attempts to purify an adequate quantity of Tbj1 from yeast cell extracts were unsuccessful due to instability of the precursor during purification. Use of the cell extract revealed that both *Tb CaaX* proteases can cleave the CTQQ motif of GST-TbJ1 (**Table 2.4**). This observation stands in contrast to that observed for the cleavage of the CTQQ motif in the context of the yeast **a**-factor reporter (see **Fig. 2.1D**), which is not recognized by either *Tb CaaX* protease. Hence, we propose that contextual information exists outside the *CaaX* motif that aids in directing *CaaX* processing.

The trypanosomal CaaX proteases can be pharmacologically inhibited. Protein isoprenylation is considered a target for anti-parasitic drug discovery (13). Post-isoprenylation enzymes appear to hold similar potential as drug discovery targets as evidenced by the observation that RNAi-mediated gene silencing of *Tb* Rce1 or *Tb* ICMT impairs growth of trypanosomes (20). Hence, we decided to determine the inhibitor profiles of the trypanosomal *CaaX* proteases using *in vitro* and *in vivo* approaches with small molecules known to inhibit *CaaX* proteases from other species (11, 12, 29).

For our *in vitro* approach, we first determined the utility of K-Ras4B-based, internally quenched, fluorogenic peptide substrates previously used to assess the function of the yeast and human *CaaX* proteases (21, 29, 38). Our previous studies indicated that quencher position within the *CaaX* motif can specify cleavage by Rce1 or Ste24, which prefer quencher placement at the a_1 and *X* position, respectively (38). We predicted a similar result for the trypanosomal *CaaX* proteases in part because of their differential ability to recognize a GTPase *CaaX* motif (see **Fig. 2.2**) and our observation that yeast and human orthologs have similar quencher position preferences (38; Porter and Schmidt, unpublished observation). Surprisingly, this prediction was not supported by our findings. Unlike the profiles of yeast Rce1p and Ste24p, the trypanosomal *CaaX* proteases had largely overlapping profiles, with both proteases preferring the quencher at the *X* position (**Fig. 2.4**).

Using the optimized fluorogenic reporter ($CVIQ_L$), we evaluated the relative *in vitro* sensitivities of the trypanosomal *CaaX* proteases to TPCK, a dipeptidyl (acyloxy)methyl ketone (FKBK), EDTA, EGTA, and a set of small molecule compounds previously demonstrated to inhibit yeast and human Rce1p (29, 38). This analysis revealed that *Tb* Rce1 was inhibited by all of the compounds, with the exception of EDTA and EGTA (**Table 2.5**). The observed inhibitor

profile of *Tb* Rce1 was similar if not identical to that of yeast and human Rce1p (29). Unlike its yeast and human counterparts, *Tb* Ste24 was sensitive to TPCK. Otherwise, *Tb* Ste24 behaved as predicted, being relatively insensitive to the effects of EDTA, EGTA, weakly inhibited by compound **1**, and strongly inhibited by the other compounds evaluated. To gain a more detailed understanding of the observed inhibitor effects on *Tb* Rce1, we determined IC_{50} values for the small molecule compound set (**Table 2.6**). The compounds largely had IC_{50} values below 10 μM, with the exception of three compounds (**2**, **4**, and **5**) having IC_{50} values greater than 80 μM.

We have observed that the small molecule inhibitors described above can induce delocalization of GFP-Ras2p *in vivo* when applied to yeast cultures expressing yeast Rce1p, and that this phenotype is similar to that observed in the absence of *CaaX* protease activity (29). Thus, we predicted that chemical treatment of yeast heterologously expressing trypanosomal Rce1 as the only *CaaX* protease would result in a similar phenotype. Indeed, six compounds induced delocalization (**Fig. 2.5A**). Compounds **4** and **9** strongly induced delocalization, with 91%, and 79% of the cell population responding, respectively. Compounds **3**, **6**, **7**, and **8** also induced delocalization, but less dramatically, with 48%, 47%, 62% and 59% of the cell population responding, respectively. Examples of the delocalized patterns, regardless of being the majority or minority phenotype, are shown in the respective panels of the figure. Compounds **1**, **2**, and **5** had no effect on GFP-Ras2p localization at the concentrations evaluated, which may represent a lack of cell permeability by these compounds.

We were intrigued by the observation that compounds **7** and **8** could induce GFP-Ras2p delocalization, even if only in a minority of the population, because of evidence suggesting that that human Rce1 was less sensitive to these compounds (29). To further investigate the relative effects of these compounds on trypanosomal and human Rce1, we performed both *in vivo* and *in*

vitro dose response studies. Consistent with expectations, *Tb* Rce1 was more sensitive to compounds **7** and **8** than *Hs* Rce1 when evaluated using our GFP-Ras2p localization assay (**Fig. 2.5B**). We observed that 5.3 μM of compound **7** was sufficient to induce delocalization of GFP-Ras2p in the context of *Tb* Rce1, but this concentration had no apparent effect on *Hs* Rce1. In fact, 11.2 μM of compound was required to delocalize the reporter to the same extent in the context of *Hs* Rce1. Similarly, a lower concentration of compound **8** was needed to comparably delocalize GFP-Ras2p in the context of *Tb* Rce1 by comparison to *Hs* Rce1 (10.8 and 25 μM, respectively). Consistent with our *in vivo* results, *in vitro* IC_{50} determinations revealed that compound **7** was nearly 10-fold more selective for *Tb* Rce1 over its human counterpart (**Table 2.7**). The opposite, however, was true for compound **8**, which was approximately 2-fold less potent against *Tb* Rce1. The reason for the lack of correlation with this compound is unknown. Together, our observations indicate that GFP-Ras2p is an effective reporter for *Tb* Rce1 activity, that the subcellular distribution of GFP-Ras2p can be used as an indicator for determining the effectiveness of compounds for disrupting *Tb* Rce1 activity *in vivo*, and that the reporter can be used to demonstrate differential targeting specificity by Rce1 inhibitors (i.e. human vs. trypanosomal Rce1).

DISCUSSION

The results of this study are consistent with the conclusion that two separate *CaaX* protease activities are present in *T. brucei* corresponding with genes encoding orthologs of Rce1p and Ste24p found in other eukaryotic systems. This observation can be contrasted with that of a previous investigation into the enzymatic properties of these proteins that revealed a

proteolytic activity in association with *Tb* Rce1 but not *Tb* Ste24 (20). We propose that the lack of activity observed in the earlier study for *Tb* Ste24 may be a direct consequence of an inappropriate reporter for the enzyme. By our own evidence, we find that *Tb* Ste24 is active against several *CaaX* motifs when it is evaluated in the context of the yeast **a**-factor reporter, including the CVIM motif present on the substrate used in the prior trypanosomal study (**Fig. 2.1**). From these observations, we hypothesize that contextual information is present within the non-*CaaX* portion of reporters that helps specify *Tb CaaX* protease specificity. The idea of contextual information being required by the *CaaX* proteases has been previously proposed (48) and is further supported by our observation that CTQQ is suitable as a *CaaX* motif in the context of Tbj1, but not yeast **a**-factor (**Fig. 2.1D** and **Table 2.4**). Moreover, it has been demonstrated that yeast Ste24p cannot cleave the CIIS motif in its natural protein context (i.e. Ras2p), but can when appended to the **a**-factor precursor (3, 48). Collectively, these observations challenge the predictive utility of the **a**-factor reporter system, or any single reporter background for that matter, as a means by which to assess *CaaX* protease specificity.

Our most contextually correct data set for the *Tb CaaX* proteases establishes that both can mediate maturation of the *Tb* Hsp40-family protein Tbj1 (**Table 2.4**). However, it would be inappropriate to extrapolate that Tbj2, Tbj3, and Tbj4 are also processed in this manner because their *CaaX* motifs have not been assessed in their proper protein context. We also cannot infer that *Tb* Rce1 specifically mediates maturation of the *Tb* RLP GTPase, despite an obvious preference for cleavage of its *CaaX* motif (CTML) by *Tb* Rce1 in our **a**-factor assay. Likewise, *Tb* Rce1 might specifically cleave *Tb* RHP despite its motif (CVIM) being cleaved by both *Tb CaaX* proteases in our yeast assay. It appears that determination of specific *CaaX* protease processing preferences must be experimentally addressed on an individual basis within their

native context using methods similar to those applied in this and other studies (4, 27, 35). This will certainly be a challenging task given that inspection of the *Trypanosome brucei brucei* genome using the TriTrypDB server reveals over 200 proteins having a canonical *CaaX* motif, which can be reduced to 61 by applying filters that eliminate pseudogenes, hypothetical proteins, and those with putative signal sequences that would not be expected to be associated with isoprenylated *CaaX* proteins (**Table 2.8**). It remains to be determined which among these presumptive *CaaX* proteins undergoes isoprenylation, let alone *CaaX* proteolysis. Among the *Tb* GTPases previously identified, only a few have *CaaX* motifs (17). These include the Ras-like GTPase *Tb* RLP (CTML), the Rho-like GTPase *Tb* RHP (CVIM), the Rab-like GTPase *Tb* Rab23 (CSVM), and the Rag-like GTPase *Tb* Rab28 (CAVM). All other identified trypanosomal GTPases, including those of the Arf and Ran families, do not contain *CaaX* motifs, while additional members of the Rab family possess canonical dicysteine geranylgeranylation motifs. Future studies may ascertain the role of *Tb* Rce1 and/or *Tb* Ste24 in the maturation of trypanosomal GTPases containing a *CaaX* motif and help elucidate the reported essential role of *Tb* Rce1 (20).

This study cautions the use of a single reporter system to specifically determine which *CaaX* protease cleaves a particular motif. Nonetheless, such reporters still retain value for assessing whether a particular set of *CaaX* protease orthologs has conserved or dissimilar specificity. For example, the observation that yeast and human Rce1p better recognize certain motifs (**Fig. 2.1D**, CAMQ and CTAQ) than does *Tb* Rce1 in the context of the **a**-factor reporter implies that *Tb* Rce1 has an intrinsic specificity difference from its relatives. Similar arguments can be made for *Tb* Ste24 by comparing its specificity profile to that of its orthologs, although the observed differences are less dramatic (**Fig. 2.1D**, CASQ and CAMQ).

The inhibition of *Tb* Rce1 could hold therapeutic potential, as loss of *Tb* Rce1 function appears to be correlated with loss of parasite viability (20); the impact of Ste24 loss of function has not yet been addressed. Should trypanosomal and human Rce1 ultimately have overlapping substrate specificities, substrate-based inactivators of *Tb* Rce1 will likely target the human enzyme, thereby leading to unintended and undesirable side-effects for patients. We have observed some differences, however, in the activities of trypanosomal and human Rce1 that may indicate that specific targeting of the parasitic enzyme may be possible. First, we determined that *Tb* Rce1 does not readily cleave CTAQ and CAMQ motifs in the context of the **a**-factor reporter, and thus does not have the exact specificity profile as its human and yeast counterparts (**Fig. 2.1D**). Second, we observed that *Tb* Rce1 has a distinct preference, by comparison to the yeast and human enzymes, for the optimal placement of a lysine dinitrophenol quenching group on a synthetic fluorogenic peptide reporter (**Fig. 2.4**) (38). Last, we have identified two small molecule agents that inhibit *Tb* Rce1 preferentially over the human enzyme *in vivo* (**Fig. 2.5** and (28)). The specificity and inhibitor profiles of *Tb* Rce1 seem to reflect enzymatic differences between it and human Rce1, suggesting the exciting prospect that trypanosomal-specific agents can be identified and developed. This conclusion is predicated on the observed specificity differences holding true independent of protein context.

In conclusion, our study continues to support the observation that eukaryotic systems generally possess two distinct *CaaX* proteolytic activities. The purpose for this redundancy is not immediately obvious and is likely tied to the need to accommodate the great variety of substrate *CaaX* proteins encoded in eukaryotic genomes. We argue based on our results that these substrates possess information both within their *CaaX* motifs and protein backbones that provides specificity for one or both proteolytic systems.

ACKNOWLEDGEMENTS

We are grateful to Drs. T. Ochsenreiter for providing genomic *Tb* DNA, M.P. Terns for access to a Zeiss Axioskop 2 Mot Plus microscope, and T.M. Dore and members of the Schmidt laboratory (all of the University of Georgia) for critical discussions and technical assistance, and Dr. R.G. Mallon (Wyeth Research) for initial samples of fluorogenic K-Ras4B peptides. This work was supported by an R01 grant (GM067092) from the National Institutes of Health (to WKS) and associated research supplement (for KAC).

REFERENCES

1. **Anderson, J. L., B. S. Henriksen, R. A. Gibbs, and C. A. Hrycyna**. 2005. The isoprenoid substrate specificity of isoprenylcysteine carboxylmethyltransferase: development of novel inhibitors. J Biol Chem **280**:29454-29461.

2. **Ashby, M., D. King, and J. Rine**. 1992. Endoproteolytic processing of a farnesylated peptide *in vitro*. PNAS **89**:4613-4617.

3. **Boyartchuk, V. L., M. N. Ashby, and J. Rine**. 1997. Modulation of Ras and **a**-factor function by carboxyl-terminal proteolysis. Science **275**:1796-1800.

4. **Bracha, K., M. Lavy, and S. Yalovsky**. 2002. The Arabidopsis AtSTE24 is a CAAX protease with broad substrate specificity. J Biol Chem **277**:29856-29864.

5. **Cadiñanos, J., W. K. Schmidt, A. Fueyo, I. Varela, C. Lopez-Otin, and J. M. Freije**. 2003. Identification, functional expression and enzymic analysis of two distinct CaaX proteases from *Caenorhabditis elegans*. Biochem J **370**:1047-1054.

6. **Cadiñanos, J., I. Varela, D. Mandel, W. K. Schmidt, A. Díaz-Perales, C. López-Otín, and F. JMP**. 2003. AtFACE-2, a prenylated-protein protease from *Arabidopsis thaliana* related to Ras converting enzymes. Journal of Biological Chemistry **278**:42091-42097.

7. **Caplan, A. J., J. Tsai, P. J. Casey, and M. G. Douglas**. 1992. Farnesylation of Ydj1p is required for function at elevated growth temperatures in *Saccharomyces cerevisiae*. J Biol Chem **267**:18890-18895.

8. **Caplin, B. E., L. A. Hettich, and M. S. Marshall**. 1994. Substrate characterization of the Saccharomyces cerevisiae protein farnesyltransferase and type-I protein geranylgeranyltransferase. Biochim Biophys Acta **1205**:39-48.

9. **Cox, A., and C. Der**. 2002. Farnesyltransferase inhibitors: promises and realities. Current Opinion in Pharmacology **2**:388-393.

10. **Dai, Q., E. Choy, V. Chiu, J. Romano, S. R. Slivka, S. A. Steitz, S. Michaelis, and M. R. Philips**. 1998. Human prenylcysteine carboxyl methyltransferase is in the endoplasmic reticulum. JBC **273**:15030-15034.

11. **Dolence, E. K., J. M. Dolence, and C. D. Poulter**. 2000. Solid-phase synthesis of a farnesylated CaaX peptide library: inhibitors of the Ras CaaX endoprotease. J Comb Chem **2**:522-536.

12. **Dolence, J. M., L. E. Steward, E. K. Dolence, D. H. Wong, and C. D. Poulter**. 2000. Studies with recombinant *Saccharomyces cerevisiae* CaaX prenyl protease Rce1p. Biochemistry **39**:4096-4104.

13. **Eastman, R. T., F. S. Buckner, K. Yokoyama, M. H. Gelb, and W. C. Van Voorhis**. 2006. Thematic review series: lipid posttranslational modifications. Fighting parasitic disease by blocking protein farnesylation. J Lipid Res **47**:233-240.

14. **Elble, R.** 1992. A simple and efficient procedure for transformation of yeasts. BioTechniques **13**:18-20.

15. **Esteva, M. I., K. Kettler, C. Maidana, L. Fichera, A. M. Ruiz, E. J. Bontempi, B. Andersson, H. M. Dahse, P. Haebel, R. Ortmann, G. Klebe, and M. Schlitzer**. 2005. Benzophenone-based farnesyltransferase inhibitors with high activity against Trypanosoma cruzi. J Med Chem **48**:7186-7191.

16. **Farh, L., D. Mitchell, and R. Deschenes**. 1995. Farnesylation and Proteolysis are sequential, but distinct steps in the CaaX box modifcation pathway. Archives of Biochemistry and Biophysics **318**:113-121.

17. **Field, M. C.** 2005. Signalling the genome: the Ras-like small GTPase family of trypanosomatids. Trends Parasitol **21**:447-450.

18. **Fujimura-Kamada, K., F. J. Nouvet, and S. Michaelis**. 1997. A novel membrane-associated metalloprotease, Ste24p, is required for the first step of NH_2-terminal processing of the yeast **a**-factor precursor. JCB **136**:271-285.

19. **Giaever, G., A. M. Chu, L. Ni, C. Connelly, L. Riles, S. Veronneau, S. Dow, A. Lucau-Danila, K. Anderson, B. Andre, A. P. Arkin, A. Astromoff, M. El-Bakkoury, R. Bangham, R. Benito, S. Brachat, S. Campanaro, M. Curtiss, K. Davis, A. Deutschbauer, K. D. Entian, P. Flaherty, F. Foury, D. J. Garfinkel, M. Gerstein, D. Gotte, U. Guldener, J. H. Hegemann, S. Hempel, Z. Herman, D. F. Jaramillo, D. E. Kelly, S. L. Kelly, P. Kotter, D. LaBonte, D. C. Lamb, N. Lan, H. Liang, H. Liao, L. Liu, C. Luo, M. Lussier, R. Mao, P. Menard, S. L. Ooi, J. L. Revuelta, C. J. Roberts, M. Rose, P. Ross-Macdonald, B. Scherens, G. Schimmack, B. Shafer, D. D. Shoemaker, S. Sookhai-Mahadeo, R. K. Storms, J. N. Strathern, G. Valle, M. Voet, G. Volckaert, C. Y. Wang, T. R. Ward, J. Wilhelmy, E. A. Winzeler, Y. Yang, G. Yen, E. Youngman, K. Yu, H. Bussey, J. D. Boeke, M. Snyder, P. Philippsen, R. W. Davis, and M. Johnston**. 2002. Functional profiling of the Saccharomyces cerevisiae genome. Nature **418**:387-391.

20. **Gillespie, J. R., K. Yokoyama, K. Lu, R. T. Eastman, J. G. Bollinger, W. C. Van Voorhis, M. H. Gelb, and F. S. Buckner**. 2007. C-terminal proteolysis of prenylated proteins in trypanosomatids and RNA interference of enzymes required for the post-translational processing pathway of farnesylated proteins. Mol Biochem Parasitol **153(2)**:115-124.

21. **Hollander, I., E. Frommer, and R. Mallon**. 2000. Human ras-converting enzyme (hRCE1) endoproteolytic activity on K-ras-derived peptides. Anal Biochem **286**:129-137.

22. **Hrycyna, C. A., and S. Clarke**. 1992. Maturation of isoprenylated proteins in *Saccharomyces cerevisiae*. JBC **267**:10457-10464.

23. **Hrycyna, C. A., S. K. Sapperstein, S. Clarke, and S. Michaelis**. 1991. The *Saccharomyces cerevisiae STE14* gene encodes a methyltransferase that mediates C-terminal methylation of **a**-factor and RAS proteins. EMBO **10**:1699-1709.

24. **Jang, G. F., K. Yokoyama, and M. H. Gelb**. 1993. A prenylated protein-specific endoprotease in rat liver microsomes that produces a carboxyl-terminal tripeptide. Biochemistry **32**:9500-9507.

25. **Kim, S., A. Lapham, C. Freedman, T. Reed, and W. Schmidt**. 2005. Yeast as a tractable genetic system for functional studies of the insulin-degrading enzyme. J Biol Chem. **280**:27481-27490.

26. **Lane, K. T., and L. S. Beese**. 2006. Thematic review series: lipid posttranslational modifications. Structural biology of protein farnesyltransferase and geranylgeranyltransferase type I. J Lipid Res **47**:681-699.

27. **Leung, K. F., R. Baron, B. R. Ali, A. I. Magee, and M. C. Seabra**. 2007. Rab GTPases containing a CAAX motif are processed post-geranylgeranylation by proteolysis and methylation. Journal of Biological Chemistry **282**
:1487-1497.

28. **Manandhar, S. P., E. Hildebrandt, W. H. Jacobsen, G. Santangelo, and W. K. Schmidt**. submitted. Chemical inhibition of CaaX protease activity disrupts yeast Ras localization. Yeast.

29. **Manandhar, S. P., E. R. Hildebrandt, and W. K. Schmidt**. 2007. Small-molecule inhibitors of the Rce1p CaaX protease. J Biomol Screen **12**:983-993.

30. **Martzen, M. R., S. M. McCraith, S. L. Spinelli, F. M. Torres, S. Fields, E. J. Grayhack, and E. M. Phizicky**. 1999. A biochemical genomics approach for identifying genes by the activity of their products. Science **286**:1153-1155.

31. **Michaelis, S., and I. Herskowitz**. 1988. The **a**-factor pheromone of *Saccharomyces cerevisiae* is essential for mating. MCB **8**:1309-1318.

32. **Moores, S. L., M. D. Schaber, S. D. Mosser, E. Rands, M. B. O'Hara, V. M. Garsky, M. S. Marshall, D. L. Pompliano, and J. B. Gibbs**. 1991. Sequence dependence of protein isoprenylation. JBC **266**:14603-14610.

33. **Ohkanda, J., J. W. Lockman, K. Yokoyama, M. H. Gelb, S. L. Croft, H. Kendrick, M. I. Harrell, J. E. Feagin, M. A. Blaskovich, S. M. Sebti, and A. D. Hamilton**. 2001. Peptidomimetic inhibitors of protein farnesyltransferase show potent antimalarial activity. Bioorg Med Chem Lett **11**:761-764.

34. **Oldenburg, K. R., K. T. Vo, S. Michaelis, and C. Paddon**. 1997. Recombination-mediated PCR-directed plasmid construction *in vivo* in yeast. Nucleic Acids Res **25**:451-452.

35. **Otto, J. C., E. Kim, S. G. Young, and P. J. Casey**. 1999. Cloning and characterization of a mammalian prenyl protein-specific protease. JBC **274**:8379-8382.

36. **Pei, J., and N. V. Grishin**. 2001. Type II CAAX prenyl endopeptidases belong to a novel superfamily of putative membrane-bound metalloproteases. Trends Biochem Sci **26**:275-277.

37. **Plummer, L. J., E. R. Hildebrandt, S. B. Porter, V. A. Rogers, J. McCracken, and W. K. Schmidt**. 2006. Mutational analysis of the ras converting enzyme reveals a requirement for glutamate and histidine residues. J Biol Chem **281**:4596-4605.

38. **Porter, S. B., E. R. Hildebrandt, S. R. Breevoort, D. Z. Mokry, T. M. Dore, and W. K. Schmidt**. 2007. Inhibition of the CaaX proteases Rce1p and Ste24p by peptidyl (acyloxy)methyl ketones. Biochim Biophys Acta **1773**:853-862.

39. **Romano, J. D., W. K. Schmidt, and S. Michaelis**. 1998. The *Saccharomyces cerevisiae* prenylcysteine carboxyl methltransferase Ste14p is in the endoplasmic reticulum membrane. MBC **9**:2231-2247.

40. **Schlitzer, M., A. Winter-Vann, and P. J. Casey**. 2001. Non-peptidic, non-prenylic inhibitors of the prenyl protein-specific protease Rce1. Bioorg Med Chem Lett **11**:425-427.

41. **Schmidt, W. K., A. Tam, K. Fujimura-Kamada, and S. Michaelis**. 1998. Endoplasmic reticulum membrane localization of Rce1p and Ste24p, yeast proteases involved in carboxyl-terminal CAAX protein processing and amino-terminal **a**-factor cleavage. Proc Natl Acad Sci USA **95**:11175-11180.

42. **Schmidt, W. K., A. Tam, and S. Michaelis**. 2000. Reconstitution of the Ste24p-dependent N-terminal proteolytic step in yeast **a**-factor biogenesis. JBC **275**:6227-6233.

43. **Sikorski, R. S., and P. Hieter**. 1989. A system of shuttle vectors and yeast host strains designed for efficient manipulation of DNA in Saccharomyces cerevisiae. Genetics **122**:19-27.

44. Reference deleted in proofs

45. **Snyder, M.** 1989. The SPA2 protein of yeast localizes to sites of cell growth. J Cell Biol **108**:1419-1429.

46. **Tam, A., F. Nouvet, K. Fujimura-Kamada, H. Slunt, S. S. Sisodia, and S. Michaelis**. 1998. Dual roles for Ste24p in yeast **a**-factor maturation: NH_2-terminal proteolysis and COOH-terminal CAAX processing. JCB **142**:635-649.

47. **Tam, A., W. K. Schmidt, and S. Michaelis**. 2001. The multispanning membrane protein Ste24p catalyzes CAAX proteolysis and NH2-terminal processing of the yeast a-factor precursor. J Biol Chem **276**:46798-46806.

48. **Trueblood, C. E., V. L. Boyartchuk, E. A. Picologlou, D. Rozema, C. D. Poulter, and J. Rine**. 2000. The CaaX proteases, Afc1p and Rce1p, have overlapping but distinct substrate specificities. MCB **20**:4381-4392.

49. **Winter-Vann, A. M., R. A. Baron, W. Wong, J. dela Cruz, J. D. York, D. M. Gooden, M. O. Bergo, S. G. Young, E. J. Toone, and P. J. Casey**. 2005. A small-molecule inhibitor of isoprenylcysteine carboxyl methyltransferase with antitumor activity in cancer cells. Proc Natl Acad Sci U S A **102**:4336-4341.

50. **Winter-Vann, A. M., and P. J. Casey**. 2005. Post-prenylation-processing enzymes as new targets in oncogenesis. Nat Rev Cancer **5**:405-412.

51. **Young, S. G., P. Ambroziak, E. Kim, and S. Clarke**. 2001. Postisoprenylation protein processing: CXXX (CaaX) endoproteases and isoprenylcysteine carboxyl methyltransferase., p. 155-213. *In* F. Tamanoi, and D. S. Sigman (eds.), The Enzymes, vol. XXI. Academic Press, New York, NY.

52. **Young, S. G., M. Meta, S. H. Yang, and L. G. Fong**. 2006. Prelamin A farnesylation and progeroid syndromes. J Biol Chem **281**:39741-39745.

53. **Zhang, Y., G. Nijbroek, M. L. Sullivan, A. A. McCracken, S. C. Watkins, S. Michaelis, and J. L. Brodsky**. 2001. Hsp70 molecular chaperone facilitates endoplasmic reticulum-associated protein degradation of Cystic Fibrosis Transmembrane Conductance Regulator in yeast. Mol Biol Cell **12**:1303-1314.

54. **Zhu, K., A. D. Hamilton, and S. M. Sebti**. 2003. Farnesyltransferase inhibitors as anticancer agents: current status. Curr Opin Investig Drugs **4**:1428-1435.

Table 2.1 Yeast Strains used in this study.

Strain	Genotype[1]	Reference
BY4741	*MAT***a** *his3 leu2 met15 ura3*	(19)
EG123	*MAT***a** *trp1 leu2 ura3 his4 can1*	(43)
IH1793	*MAT*α *lys1*	(31)
SM3614	*MAT***a** *trp1 leu2 ura3 his4 can1 rce1::TRP1 ste24::LEU2*	(46)
yWS164	*MAT***a** *trp1 leu2 ura3 his4 can1 mfa1-*Δ*1 mfa2-*Δ*1 rce1::TRP1 ste24::KAN*^{R}	(6)
yWS304	*MAT***a** *his3 leu2 met15 ura3 ydj1*Δ	(19)

[1]All strains are isogenic with the exception of BY4741 and yWS304 that are a separate isogenic pair.

Table 2.2 Plasmids used in this study.

Plasmid	Genotype	Reference
pRS315	*CEN LEU2*	(43)
pRS316	*CEN URA3*	(43)
pSM1107	*CEN URA3 HA-STE24*	(18)
pSM1282	*2μ URA3* P_{PGK} *10HIS-HA-STE24*	(47)
pSM1314	*CEN URA3 RCE1-HA*	(41)
pSM1317	*2μ URA3 STE14*	(39)
pSM1585	*2μ URA3 Hs HA-STE24*	(37)
pSM1605	*2μ URA3 MFA1*	(42)
pWS28	*2μ URA* P_{PGK}	(53)
pWS335	*2μ URA3* P_{PGK} *HIS-HA-Hs Rce1*Δ*22*	(37)
pWS338	*2μ URA3 leu2-d* P_{CUP1}*GST-YDJ1*	(30)
pWS438	*2μ LEU2 MFA1*	(6)
pWS439	*2μ LEU2 MFA1(CAMQ)*	This study
pWS440	*2μ LEU2 MFA1(CASQ)*	(6)
pWS441	*2μ LEU2 MFA1(CTLM)*	(6)
pWS442	*2μ LEU2 MFA1(CTVM)*	This study
pWS479	*2μ URA3* P_{PGK} *RCE1-HAc*	(37)
pWS523	*CEN URA3* P_{GAL} *GST*-Ydj1	(45)
pWS750	*CEN LEU2* P_{GAL} *GFP-RAS2*	(29)
pWS766	*2μ URA3* P_{PGK} *TbRce1-HA*	This study
pWS767	*2μ URA3* P_{PGK} *His-HA-TbSte24*	This study
pWS773	*2μ LEU2 MFA1(CTML)*	This study
pWS774	*2μ LEU2 MFA1(CVIM)*	This study
pWS775	*2μ LEU2 MFA1(CTQQ)*	This study
pWS776	*2μ LEU2 MFA1(CVHQ)*	This study
pWS782	*2μ URA3 leu2-d* P_{CUP1} *GST-Tbj1*	This study

pWS783	*2μ URA3 leu2-d* P_{CUP1} *GST-Tbj1(C401S)*	This study
pWS798	*2μ URA3* P_{PGK} *TbRce1(E151A)-HA*	This study
pWS838	*2μ URA3* P_{PGK} *TbRce1(H184A)-HA*	This study
pWS800	*2μ URA3* P_{PGK} *TbRce1(H254A)-HA*	This study
pWS801	*2μ URA3* P_{PGK} *His-HA-TbSte24(H286A)*	This study
pWS805	*2μ URA3* P_{PGK} *His-HA-TbSte24(E287A)*	This study
pWS802	*2μ URA3* P_{PGK} *His-HA-TbSte24(H290A)*	This study
pWS880	*2μ LEU2 MFA1(CTAQ)*	This study
pWS888	*2μ URA3* P_{PGK} *Tbj2*	This study
pWS889	*2μ URA3* P_{PGK} *Tbj3*	This study
pWS890	*2μ URA3* P_{PGK} *Tbj4*	This study
pWS900	*CEN URA3* P_{GAL} *GST-Tbj1*	This study

Table 2.3. Quantification of GFP-Ras2p plasma membrane localization.

Background[1]	*CaaX* Protease	% PM localization[2]
WT	vector	93.2 ± 1.5
*rce1*Δ *ste24*Δ	vector	37.6 ± 4.2
*rce1*Δ *ste24*Δ	*Sc* Rce1	80.7 ± 1.2
*rce1*Δ *ste24*Δ	*Tb* Rce1	83.0 ± 1.4
*rce1*Δ *ste24*Δ	*Sc* Ste24	42.3 ± 5.8
*rce1*Δ *ste24*Δ	*Tb* Ste24	38.6 ± 2.0

[1]Strains used were EG123 (WT) or isogenic yWS164 (*rce1*Δ *ste24*Δ) that were co-transformed with plasmids encoding GFP-Ras2p (pWS750) and as indicated, an empty vector (pRS316), or plasmid encoding a *CaaX* protease (pSM1107, pSM1314, pWS766, and pWS767).
[2]Values for plasma membrane (PM) localization are reported ± SEM, which was calculated as $s/\sqrt{n}$, where *s* is sample standard deviation, and *n* is number of observations.

Table 2.4. Coupled proteolysis-carboxyl methylation *in vitro* assay reveals cleavage of Tbj1 by both *Tb CaaX* proteases.

	Vector	*Tb* Rce1	*Tb* Ste24
CPM[1]	345.5	499.2	454.0
SEM[2]	18.8	31.2	35.7
P Value[3]	-	0.002	0.032

[1]Values represent mean of 6 data points derived from 2 independent experiments (3 replicates per experiment).
[2]Standard error of the mean was calculated from the equation $s/\sqrt{n}$, where s is sample standard deviation, and n is number of observations.
[3]P values calculated by ANOVA (single factor) relative to vector condition.

Table 2.5. Inhibitor profiles of trypanosomal *CaaX* proteases.

	% activity[2]	
Compound[1]	*Tb* Rce1	*Tb* Ste24
TPCK	21.6 ± 5.1	24.5 ± 5.0
FKBK	34.4 ± 6.0	30.0 ± 3.5
EDTA	92.0 ± 11.1	79.2 ± 10.2
EGTA	94.6 ± 5.5	75.7 ± 3.2
1	30.7 ± 4.8	59.4 ± 5.9
2	22.1 ± 4.7	24.1 ± 5.3
3	18.6 ± 2.7	14.9 ± 5.8
4	23.9 ± 9.5	31.3 ± 10.9
5	34.2 ± 9.4	35.1 ± 8.6
6	19.3 ± 4.0	28.0 ± 2.4
7	18.4 ± 3.8	28.6 ± 2.2
8	16.1 ± 3.3	14.6 ± 5.4
9	15.4 ± 3.7	20.6 ± 3.8

[1]TPCK, FKBK, EDTA, and EGTA were used at 200 μM. Compounds **1-9** are as previously identified and were used at 100 μM (29).
[2]Values are relative to an appropriate untreated control treated with H_2O (EDTA and EGTA) or DMSO (TPCK, FKBK, compounds **1-9**).

Table 2.6. IC_{50} values of Rce1p inhibitors for *Tb* Rce1.

Compound[1]	IC_{50} (μM)
1	3.24 ± 0.52
2	83.42 ± 7.18
3	8.10 ± 3.21
4	160.75 ± 14.21
5	176.77 ± 34.16
6	1.30 ± 0.07
7	0.25 ± 0.22
8	4.23 ± 1.46
9	0.91 ± 0.13

Table 2.7. Comparison of IC_{50} values of compounds **7** and **8** on trypanosomal and human Rce1.

	IC_{50} (μM)[1]	
Enzyme	**7**	**8**
Tb Rce1	0.25 ± 0.22	4.23 ± 1.46
Hs Rce1	2.38 ± 0.19	2.43 ± 0.77

[1]Compounds were serially diluted from 100 mM stocks in DMSO and evaluated from 0.46-471 μM.

Table 2.8. Trypanosomal proteins possessing a canonical *CaaX* motif.[1]

Gene ID	Annotated Protein Description	Predicted *CaaX* Motif
Tb927.2.1380	leucine-rich repeat protein (LRRP), putative	CSQC
Tb927.2.5160	chaperone protein DnaJ, putative	CTQQ
Tb927.2.5800	sedoheptulose-1,7-bisphosphatase	CSKL
Tb927.3.2310	flagellar component	CIFS
Tb927.3.5230	DNA repair protein, putative	CNDE
Tb927.4.1700	protein kinase, putative	CHCM
Tb927.4.4320	divalent cation tolerance protein, putative	CSCR
Tb927.4.4960	metal-ion transporter, putative	CGTV
Tb927.5.1550	mitochondrial carrier protein, putative	CAPA
Tb927.5.4430	protein kinase, putative	CEEG
Tb927.6.3040	small GTP-binding protein Rab28, putative; Ras- related protein Rab-26 (Rab26), putative	CAVM
Tb927.6.4970	serine/arginine-rich protein specific kinase SRPK, putative	CTND
Tb927.6.5020	cyclin 7, putative	CLYW
Tb927.7.2070	heat shock protein DnaJ, putative	CTAQ
Tb927.7.4770	cyclophilin-type peptidyl-prolyl cis-trans isomerase, putative	CGVL
Tb927.8.980	phosphoacetylglucosamine mutase, putative	CGGA
Tb927.8.2310	(H+)-ATPase G subunit, putative	CQDN
Tb927.8.5780	phosphatase of regenerating liver-type phosphatase, putative	CAIM
Tb927.8.7000	E1-like ubiquitin-activating enzyme, putative	CDSG
Tb927.8.7020	peptidase, putative	CRTF
Tb09.160.2210	glutaredoxin-like protein	CRDL
Tb09.160.4240	nucleosome assembly protein-like protein	CQQQ
Tb09.211.2730	Gim5A protein; glycosomal membrane protein	CEFY
Tb09.211.2740	Gim5B protein; glycosomal membrane protein	CEFY
Tb09.211.3680	chaperone protein DNAJ, putative	CVHQ
Tb09.211.4610	vesicle-associated membrane protein, putative	CTVM
Tb09.244.2070	small GTPase, putative; GTP-binding protein, putative	CCCQ
Tb10.70.6010	syntaxin, putative	CVFS
Tb10.70.5440	chaperone protein DNAJ, putative	CTQQ

Tb10.70.4880	eukaryotic translation initiation factor 5, putative	CVAA
Tb10.70.4300	U2 splicing auxiliary factor, putative; U2AF35	CPLK
Tb10.70.4100	protein kinase, putative	CIIM
Tb10.70.2270	protein phosphatase 2C, putative	CSER
Tb10.70.0820	universal minicircle sequence binding protein (UMSBP), putative; DNA-binding protein HEXBP, putative; zinc finger protein	CPVK
Tb10.70.0800	universal minicircle sequence binding protein (UMSBP), putative; predicted zinc finger protein	CPVK
Tb10.70.0590	small GTPase, putative; ras-like small GTPase, putative	CVIM
Tb10.70.0350	protein phosphatase 2B, putative	CEGA
Tb10.6k15.3370	terminal uridylyltransferase 3, putative	CQKN
Tb10.6k15.2060	phosphatidylinositol 3 kinase, putative	CPFW
Tb10.6k15.1990	small GTPase, putative	CSVM
Tb10.6k15.1790	GTPase activating protein, putative	CQQL
Tb10.389.1800	syntaxin, putative; vesicle-associated membrane protein, putative	CTLM
Tb10.389.1270	kinesin, putative	CVIM
Tb10.61.1330	nucleosome assembly protein, putative	CKHQ
Tb10.61.0730	zinc finger protein, putative	CLKP
Tb11.03.0250	cyclophilin a; cyclophilin type peptidyl-prolyl cis-trans isomerase	CGQL
Tb11.47.0002	phosphatidylinositol (3,5) kinase, putative	CSLA
Tb11.02.1380	actin, putative	CKCQ
Tb11.02.3850	GTP binding protein; ras-related protein, putative	CTML
Tb11.02.3990	S-phase kinase-associated protein, putative; SKP1 family protein, putative; Cyclin A/CDK2-associated protein; SKP1 family protein, putative; Cyclin A/CDK2- associated protein	CEEA
Tb11.02.5060	SNF2 DNA repair protein, putative	CPTV
Tb11.02.5470	vacuolar type H+ ATPase subunit, putative	CDSS
Tb11.02.5700	endonuclease/exonuclease/phosphatase, putative	CLLS
Tb11.02.5810	kinetoplastid-specific dual specificity phosphatase, putative	CSGE
Tb11.01.0420	protein transport protein sec13, putative	CKLP
Tb11.01.1120	phosphonopyruvate decarboxylase-like protein, putative	CLRG
Tb11.01.1160	lipoate-protein ligase, putative; lipoyltransferase, putative	CELE
Tb11.01.1740	2-oxoglutarate dehydrogenase E1 component, putative	CVFS
Tb11.01.2530	kinesin-like protein, putative	CVTM
Tb11.01.3915	RNA-binding protein, putative; RBP5	CITA
Tb11.01.4450	cyclin 1; serine peptidase family S51, peptidase E, putative	CAPR

[1]The Protein Motif Pattern search function of the TriTrypDB server (http://tritrypdb.org) was used to identify proteins having a C-terminal *CaaX* motif using a "C…$" search string. The identified set was reduced by applying filters to remove proteins having the terms "hypothetical" and "pseudogene" associated with the gene product description. The revised set was further reduced by eliminating those containing predicted signal peptides as identified by the database and one protein that did not have a Tb927 designation. The signal peptide filter eliminated Tbj3,

which was manually added back to the set.

Figure 2.1. *The trypanosomal CaaX proteases promote yeast mating*.

A) Yeast wildtype (WT) or lacking Rce1p and Ste24p were evaluated for their ability to mate using the serial dilution mating test. The WT strain (EG123) was co-transformed with the empty vectors marked with *LEU2* (pRS315) and *URA3* (pRS316). The *CaaX* protease deficient strain (yWS164) was co-transformed with an **a**-factor encoding plasmid (pWS438) and a plasmid encoding the indicated *CaaX* protease from trypanosome or yeast. The *CaaX* protease encoding plasmids were pSM1107, pSM1314, pWS766, and pWS767. **B**, **C**) Mutagenized forms of *Tb* Rce1 (B) and *Tb* Ste24 (C) were evaluated by the serial dilution mating test as described in panel A. Only the first row of data from the mating test is shown. The *CaaX* proteases were encoded in pWS766, pWS767, pWS798, pWS800, pWS801, pWS802, pWS805, and pWS838. **D**) Trypanosomal, yeast, and human *CaaX* proteases were evaluated by the serial dilution mating test as in panel A to assess their specificities against a panel of *CaaX* motifs, some of which have previously been evaluated and others that naturally occur on trypanosomal proteins (see text for details). Only the first row of data from the mating test is shown. The *CaaX* proteases were encoded in pSM1107, pSM1314, pSM1585, pWS335, pWS766, and pWS767. The **a**-factor variants were encoded within pWS439, pWS440, pWS441, pWS442, pWS773, pWS774, pWS775, pWS776, and pWS880.

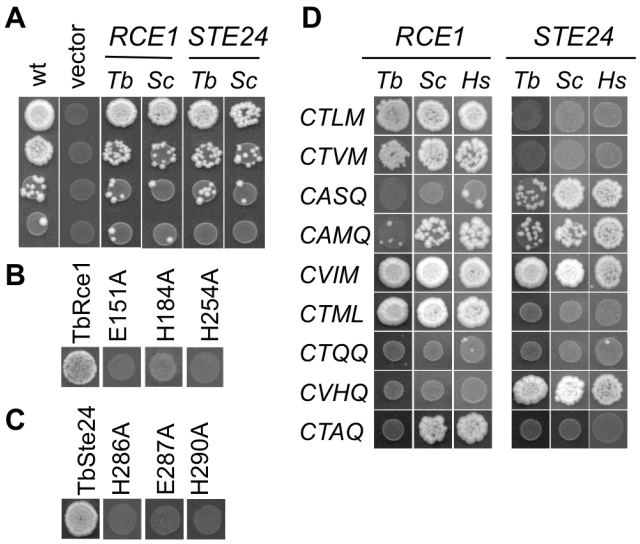
A
wt
vector
RCE1
STE24
Tb
Sc
Tb
Sc
B
TbRce1
E151A
H184A
H254A
C
TbSte24
H286A
E287A
H290A
D
RCE1
STE24
Tb
Sc
Hs
Tb
Sc
Hs
CTLM
CTVM
CASQ
CAMQ
CVIM
CTML
CTQQ
CVHQ
CTAQ

Figure 2.2. *Tb Rce1 promotes proper Ras2p localization.*

Yeast strains that were **A**) wildtype (EG123) or **B-F**) deficient for endogenous yeast *CaaX* proteolytic activity (yWS164) were each co-transformed with a plasmid encoding a GFP-Ras2p reporter (pWS750) and either an empty vector (A and B), or a plasmid encoding yeast Rce1p (C), yeast Ste24p (D), *Tb* Rce1 (E), or *Tb* Ste24 (F). For each condition, a small cluster of cells are shown as imaged after 6 hours of induction of the reporter in SGal-ura media. The *CaaX* proteases were encoded in pSM1107, pSM1314, pWS766, and pWS767; pRS316 was used as the empty vector.

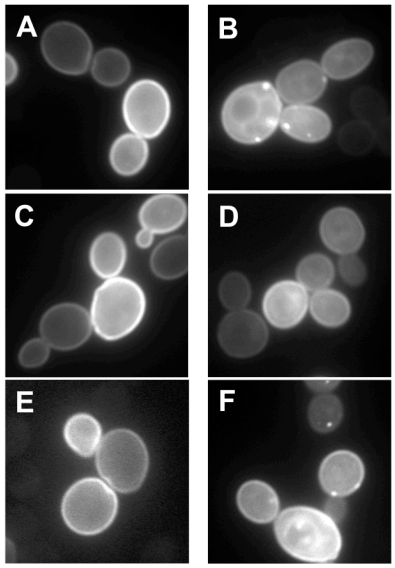
A
B
C
D
E
F

Figure 2.3. *Certain trypanosomal Hsp40 proteins rescue the temperature sensitive phenotype of a Ydj1p-deficient yeast strain*.

A) Inspection of the *T. brucei* genome identifies four trypanosomal Hsp40 proteins (Tbj1, Tbj2, Tbj3, and Tbj4) with homology to the yeast Hsp40 protein Ydj1p. The trypanosomal enzymes were heterologously expressed in *ydj1*Δ yeast (yWS304) and individual strains assessed for growth at the indicated permissive and restrictive temperatures. In the case of Tbj1 alone, it was expressed as a GST fusion. The plasmids used were pWS782, pWS888, pWS889, and pWS890. **B**) Plasmids encoding GST fusions of Ydj1p, Tbj1, and Tbj1(C401S) were transformed into *ydj1*Δ yeast (yWS304), and the transformed strains assessed along with *ydj1*Δ yeast and the isogenic wildtype strain (BY4741) for the ability to grow at the indicated temperatures. The plasmids used were pWS338, pWS782, and pWS783.

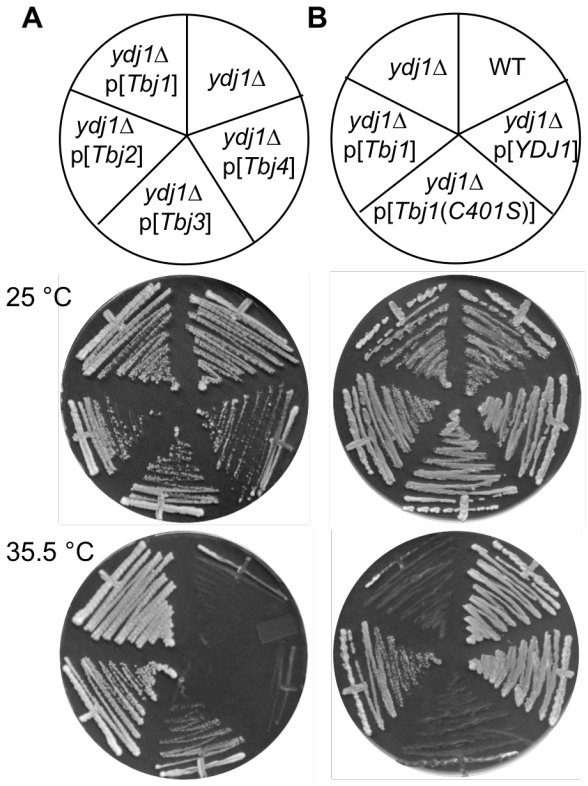
A
ydj1Δ p[Tbj1]
ydj1Δ
ydj1Δ p[Tbj2]
ydj1Δ p[Tbj4]
ydj1Δ p[Tbj3]
B
ydj1Δ
WT
ydj1Δ p[Tbj1]
ydj1Δ p[YDJ1]
ydj1Δ p[Tbj1(C401S)]
25 °C
35.5 °C

Figure 2.4. *Trypanosomal CaaX proteases have similar specificity toward a synthetic K-Ras4B-based substrate*.

Yeast membranes enriched for the indicated trypanosomal (**A**) or yeast (**B**) *CaaX* protease were evaluated for their ability to cleave a farnesylated nonapeptide based on the K-Ras4B C-terminus. The peptide contains an amino benzoic acid fluorophore that intensifies in fluorescence after cleavage of the *CaaX* motif (CVIM), which contains a dinitrophenol quencher that is coupled to a lysine (Q_L) placed at either the a_1, a_2, or *X* position. Activity for each *CaaX* protease is reported relative to the condition where maximal activity was observed. Closed bars represent Rce1 activity, and open bars represent Ste24 activity. The maximal activities were 15.16 and 11.02 RFU/min for trypanosomal Rce1 and Ste24, respectively, and 93.27 and 25.10 RFU/min for yeast Rce1 and Ste24, respectively. All membrane samples were prepared in the SM3614 background. The plasmids used were pSM1282, pWS479, pWS766, and pWS767. RFU – relative fluorescence units.

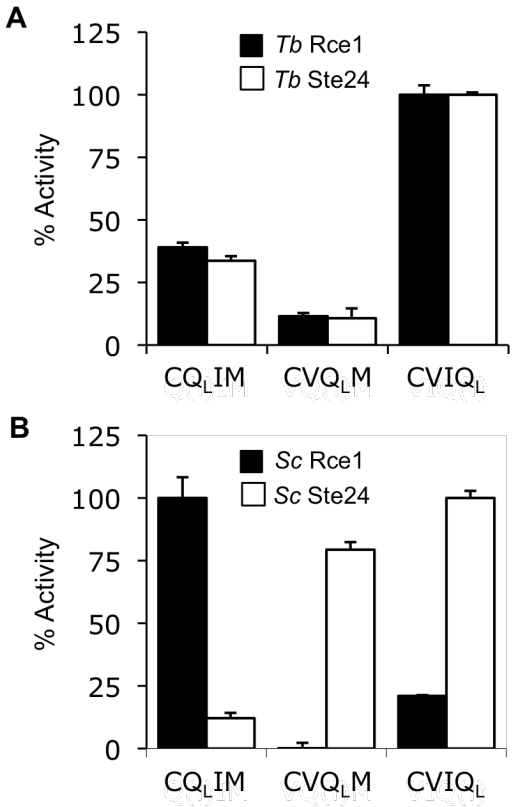
A
125
100
75
50
25
0
% Activity
Tb Rce1
Tb Ste24
CQLIM
CVQLM
CVIQL
B
125
100
75
50
25
0
% Activity
Sc Rce1
Sc Ste24
CQLIM
CVQLM
CVIQL

Figure 2.5. *Chemical agents can disrupt trypanosomal Rce1 activity in vivo.*

A) Effect of chemical agents on *Tb* Rce1 activity. yWS164 yeast expressing a GFP-Ras2p reporter and *Tb* Rce1 were transiently treated for 1 hour with DMSO (D) or the indicated chemical agents prior to induction of GFP-Ras2p expression as described in Figure 2.2. Compounds were used at doses that were largely non-toxic to liquid cultures of yeast (EC_{10}). The EC_{10} doses for compounds **3, 4, 6, 7, 8,** and **9** were 7.89, 6.78, 0.67, 11.1, 10.8, and 3.78 μM, respectively. All others were used at 55.6 μM. The plasmids used were pWS750 and pWS766. **B**) Dose-dependent effects of compounds **7** and **8** on human and trypanosomal Rce1. yWS164 yeast expressing a GFP-Ras2p reporter (pWS750) and either the human (pWS335) or trypanosomal (pWS766) Rce1 ortholog were evaluated for sensitivity to compounds **7** and **8** by the protocol described in panel A using the doses of compounds indicated. The percentage of cells with a delocalized phenotype are reported from a minimum population of 60 cells from at least 3 independent cell fields.

A

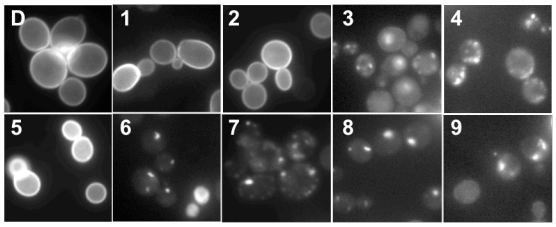

B

		% delocalization observed at indicated dose			
Compound	Enzyme	0 μM	5.3 μM	11.1 μM	25 μM
7	Tb Rce1	0	5.3 ± 3.1	10.4 ± 4.5	17.6 ± 5.1
	Hs Rce1	0	0	5.5 ± 8.2	6.0 ± 4.0
		0 μM	5.1 μM	10.8 μM	25 μM
8	Tb Rce1	0	4.4 ± 1.8	19.8 ± 8.3	24.6 ± 6.9
	Hs Rce1	0	0	0	20.5 ± 6.0

CHAPTER 3

SPECTROSCOPIC CHARACTERIZATION OF THE HEMOGLOBIN BINDING RECEPTOR FROM *NEISSERIA MENINGITIDIS*[1]

[1] David Z. Mokry, Angela-Nadia Albete, Kenton R. Rodgers, Michael K. Johnson, and William N. Lanzilotta. 2010. *Submission to JBC in progress*

ABSTRACT

The hemoglobin receptor (HmbR) is involved in the acquisition of heme from hemoglobin in the pathogen *Neisseria meningitidis*. To aid in elucidating the mechanism of iron transport, we spectroscopically characterized HmbR using electronic absorption, circular dichroism, EPR, and resonance Raman techniques. Through these methods, we determined that HmbR has a predominant β-sheet structure with a heme binding site containing a 5-coordinate high spin ferric heme. We also demonstrate that the heme binding site can accommodate an extra ligand from imidazole, which results in a 6-coordinate low spin ferric species, and that both of these species are susceptible to reduction by sodium hydrosulfite. We further identified four mutants with decreased binding efficiency for heme (H87C, H280A, Y282A, and Y456C), and propose that the heme iron is coordinated by a negatively charged oxygen moiety. In summary, this study provides the first spectroscopic characterization of any heme or iron transporter in *Neisseria meningitidis*, and suggests a coordination environment unlike other currently characterized bacterial outer membrane heme transporters.

INTRODUCTION

Iron is essential for many types of biochemical reactions throughout biology. One obstacle faced by pathogenic organisms is the acquisition of iron from their environment, which is highly regulated by the host and tightly sequestered in heme and iron binding proteins. Gram-negative bacteria have evolved rather sophisticated mechanisms to meet their iron requirements. These are classified into two broad categories, referred to as siderophore and receptor mediated transport [1]. In the former, a low molecular weight compound with a high affinity for iron, referred to as a siderophore, is synthesized and secreted by the bacteria into the extracellular milieu. Upon binding to ferric iron, the siderophore undergoes transport into the cell utilizing a receptor, and the iron is reduced and released [2-4]. The second mechanism involves direct binding to a host protein that contains heme iron by a specific bacterial receptor. The binding interaction hijacks the heme iron from the native protein and transports it into the periplasm of the bacteria [5-7]. Both of these types of receptors require the proton motive force of the TonB accessory protein for proper transport, and thus are referred to as TonB dependent transporters (TBDTs) [8]. Once inside the periplasm, heme is further transported by a periplasmic binding protein to an inner membrane transporter, which shuttles it into the cytoplasm [9]. There it is processed by a heme oxygenase to yield free iron (Fe^{3+}), carbon monoxide, and biliverdin [10].

The bacterial pathogen *Neisseria meningitidis* is one of the leading causes of bacterial meningitis and meningococcal septicemia [11]. The virulence of this pathogen is tightly coupled to the availability of iron in the local environment of the host. To date, the synthesis of siderophores has not been identified in this organism, suggesting that specific receptors for iron containing host proteins are the sole means by which iron requirements are fulfilled [12].

Several of these receptors have been identified in *N. meningitidis*, including a transferrin, lactoferrin, and hemoglobin receptor, and a dual specificity hemoglobin/haptoglobin receptor [7]. As suppression of any one of these transport systems is believed to decrease the degree to which this pathogen can cause disease, many of these receptors are being investigated as possible drug targets. The hemoglobin receptor (HmbR) is one of the more promising targets due to its high prevalence in invasive strains, specificity for human hemoglobin, surface accessibility, and monomeric nature [13, 14]. Additionally, the expression of HmbR significantly increases when hemoglobin is the sole source of iron, suggesting that it is a major iron delivery protein that contributes to the aggressive nature of meningococcal septicemia [15].

Although HmbR is a promising drug target, very little is known about its structure, and how it abstracts and transports heme from hemoglobin. To aid in understanding the heme binding properties of HmbR, we performed a spectroscopic characterization by obtaining electronic absorption, circular dichroism (CD), electron paramagnetic resonance (EPR), and resonance Raman (rR) spectra on the purified protein. We determined that HmbR has a prominently β-sheet fold, consistent with other bacterial outer membrane proteins, and copurifies with a 5-coordinate high spin axial heme moiety, which can adopt a 6-coordinate low spin ferric state with the addition of imidazole, and that both of these species are susceptible to reduction by treatment with sodium hydrosulfite. We also identified residues involved in maintaining proper heme binding properties, and propose that a residue with an oxygen containing a partial negative charge, such as tyrosine, acts as an axial ligand in coordinating the heme, unlike a histidine residue observed in other TBDTs. As a whole, our investigation provides the first spectroscopic characterization of any heme or iron transporter in *Neisseria meningitidis,* and indicates that HmbR may have unique heme binding properties relative to functionally similar transporters.

MATERIALS AND METHODS

Creation of HmbR Mutants – The plasmids used in this study are listed in **Table 1**. Residues selected for mutational analysis were determined in two ways. Mutations H87C, H280A, Y282A, and Y497C were selected from regions on HmbR determined to be important in heme binding from a previous study [16]. Mutations Y456C and Y763C were selected from conserved residues identified from a ClustalW sequence alignment of HmbR with other outer membrane heme and iron transport proteins, specifically, BpR, HemR, HutA, ShuA, and YpR (accession numbers NP_879220, CAA48250, YP_002812154, AAC27809, and Q56989, respectively). Each mutation was engineered using Quickchange site-directed mutagenesis. In brief, complimentary mutagenic oligonucleotide primers were designed to contain the desired mutation flanked by a 15-20 base pair extension on each end homologous to the parent plasmid (DPB1809). Each PCR reaction contained a total volume of 50μL with 4μM of each primer, 200μM of each dNTP, and 10μg of parent DNA, in ThermoPol reaction buffer (20mM Tris-HCl (pH 8.8), 10mM KCl, 10mM $(NH_4)_2SO_4$, 2mM $MgSO_4$, 0.1% Triton X-100). After preheating each condition at 95ºC for 5 minutes, 1.0μL of $Vent_R$® DNA Polymerase (New England Biolabs; #M0254S) was added to each tube, and the PCR reactions were allowed to proceed (annealing: 55-58ºC, 1 minute; extension: 68-72ºC, 20 minutes; denaturing: 95ºC, 1 minute; 18 complete cycles). Following the PCR reaction, 1.0 μL of DpnI (New England Biolabs; #R0176S) was added to each tube and allowed to react at 37ºC for 6 hrs. The suspensions were then transformed into competent DH5α *E. coli*, and identification of plasmids with the desired mutations was performed by subsequent isolation and sequencing of plasmid DNA from candidate colonies.

Purification of HmbR – Wild-type and single amino acid HmbR mutants were purified by identical methods. In general, competent BL21-CodonPlus (DE3)-RIPL *E. coli* (Stratagene) were transformed with the appropriate plasmid, and grown in 1-liter flasks of LB containing 50μg/mL carbenicillin. When the cells reached A_{600} 0.6-0.9, HmbR expression was induced by the addition of 1mM isopropyl β-D-1-thiogalactopyranoside (IPTG) for 2.5 hrs. Approximately 24 liters of cell pellets were utilized for the purification of each HmbR variant. Cell pellets were collected and resuspended in 225mL of 10mM potassium phosphate, pH 6.8 supplemented with 2 complete EDTA-free protease inhibitor tablets (Roche; #04693132001), and approximately 1 mg each of PMSF, trypsin inhibitor, aprotinin, leupeptin, chymostatin, pepstatin, and DNAse. The cell suspension was then subsequently passed once through a French pressure cell, and then spiked with 1mM of $MgSO_4$, and cleared of large cellular debris by spinning at 6,370g for 15 minutes. The resulting supernatant was supplemented with hemin to a final concentration of 2.1μM (using a 4 mM stock concentration containing 10 mM potassium hydroxide prepared in ethanol), and fractionated at 100,000g for 1.25 hours to recover membranes. The isolated membranes were washed once in 150mL of 20mM potassium phosphate, pH 6.8, 2% Triton X-100, recovered at 100,000g for 1.25 hours, and incubated overnight at 4°C in 150mL of 20mM potassium phosphate, pH 7.4, 500mM NaCl, and 1% n-octyl-ß-D-glucopyranoside (OG). The unsolubilized material was recovered at 100,000g for 1.25 hours, and incubated overnight at 4°C in 150mL total volume of 20mM potassium phosphate, pH 7.4, 500mM NaCl, and 1% Anzergent™ 3-14 (Anatrace). Solubilized protein was recovered by centrifugation of the sample at 100,000g for 1.25 hours and then supplemented with 10mM imidazole, and allowed to incubate with 20 mL of a Ni-NTA resin overnight. The suspension was then transferred to a

gravity-flow column, washed with 90 mL of 20mM potassium phosphate, pH 7.4, 500mM NaCl, 10mM imidazole, and 1% Anzergent™ 3-14, followed by elution with 20mM potassium phosphate, pH 7.4, 500mM NaCl, 500mM imidazole, and 0.5% Anzergent™ 3-14. Elution fractions containing the highest protein concentrations were pooled into a centrifugal filter unit with a 50 KDa nominal molecular weight cut-off (NMWC) (Millipore; #4323), and concentrated to an approximate volume of 1.0 mL by 10 minute centrifugation intervals at 1500 g. The imidazole was removed from these samples by two different methods. For hemochromogen assays (described below), 500μL of each protein variant (concentrations ranging from 2-10 mg/mL) were transferred to a Slide-a-Lyzer cassette (Pierce, 7,000 NMWC), and allowed to equilibrate in 1 liter 20mM potassium phosphate, pH 7.4, 500mM NaCl, and 0.5% Anzergent™ 3-14 for 24 hrs. For all other applications, the imidazole was removed from the samples by iterative dilutions and concentrations in an Amicon concentrator (5,000 NMWC) using 20mM potassium phosphate, pH 7.4, 500mM NaCl, and 0.5% Anzergent™ 3-14 until the concentration was less than 5.0 mM. The final imidazole concentration was determined by calculating the dilution factor of the retentate after each spin.

Electronic Absorption Spectrum – Electronic absorption spectra of different HmbR species were recorded both aerobically on a nanodrop (ND-1000) spectrophotometer (35 mg/mL protein, 1.5 μL /sample) and anaerobically on a Shimadzu (UV-1601) spectrophotometer, (5.8 mg/mL, 600μL /sample) at room temperature. Each method evaluated purified HmbR with or without the presence of 500mM imidazole, in both ferric and ferrous states. To record reduced spectra under aerobic conditions, samples were supplemented with 5.0 mM of sodium hydrosulfite and immediately mounted and scanned. To record spectra under anaerobic conditions, samples and

buffers were degassed using a vacuum manifold, and transferred to an anaerobic chamber. A 100 mM stock solution of sodium hydrosulfite was subsequently prepared in the appropriate buffers and titrated into samples at 0, 160, 330, and 500 μM intervals. Electronic absorption spectra were obtained using samples that were anaerobically sealed in quartz cuvettes with a 1 cm pathlength. All plots were generated using Excel graphing software from data electronically extracted from the nanodrop (ND-1000) software program (version 3.3).

Determination of Molar Percent of Heme to HmbR Variants – In order to determine the molar percent of heme present within purified HmbR samples, we performed a pyridine hemochromogen assay as previously described [17]. In general, samples dialyzed using Slide-a-Lyzer cassettes as described above were diluted to 3.33 μM in dialysis buffer (20mM potassium phosphate, pH 7.4, 500mM NaCl, 0.5% Anzergent™ 3-14, and 5 mM imidazole) and further diluted to 2.50 μM by the addition of 250 mM NaOH and 25% pyridine. Half the volume of these samples was removed and reduced with sodium hydrosulfite, and the absorbance difference between the reduced and unreduced samples was determined at 530 nm. Heme concentrations were calculated using a millimolar extinction coefficient of 20.7 cm^{-1} mM^{-1}. These were compared to protein concentrations previously determined through a detergent compatible protein assay (Bio-Rad DC). Each HmbR variant was evaluated by this method three independent times.

Circular Dichroism – A circular dichroism spectrum was recorded for purified HmbR obtained as described above in the ferric state. The sample was diluted to 0.34 mg/mL in 10mM potassium phosphate, pH 7.4, 250mM NaCl, and 0.25% Anzergent™ , and placed in a 0.1 cm

cuvette for data collection. A Jasco J-715 spectropolarimeter obtained measurements from 190 to 240 nm using a 10 nm bandwidth. Following data collection, the Y-axis was converted to molar ellipticity ($\Delta\varepsilon$) and plotted as a function of wavelength utilizing software associated with the instrument.

Electron Paramagnetic Resonance – EPR spectra were recorded on samples containing approximately 200 μM of HmbR in sample buffer (20 mM potassium phosphate, pH 7.4, and Anzergent™ 3-14) with or without the addition of 500 mM imidazole using a Bruker ESP300D spectrometer equipped with an Oxford Instruments ESR-900 helium flow cryostat to maintain the temperature of the samples at 10K. The modulation amplitude was 6.477G with a modulation frequency of 100 kHz. The microwave frequency and power was 9.6 GHz and 5mW, respectively.

Resonance Raman Spectroscopy – Resonance Raman spectra were obtained with a 406.7 nm emission from a Kr^{+} laser using a power of 14mW, and a 135° backscattering geometry. Samples were prepared in .05% Anzergent™ , 300 mM NaCl, and 100 mM buffer (MES, Tris, or CAPS, pH 6.4, 7.8, and 9.7, respectively) and spun at 20 Hz in 5 mM NMR tubes at room temperature to avoid laser induced degradation. The laser bean was calibrated against Raman frequencies of toluene and DMF, and focused to a line on the spinning NMR tubes. No spectral artifacts resulting from these radiation powers were observed.

RESULTS

Absorption Spectra of HmbR – The protocol described above for the purification of HmbR yielded protein of the predicted size (90 KDa) with more than 90% purity as judged by SDS-PAGE analysis using Coomassie stain. The removal of imidazole from purified protein fractions resulted in a characteristic color change from bright red to rust brown. We therefore hypothesized that the imidazole was interacting with the coordination of the heme present in HmbR, and monitored the electronic absorption spectra of samples with and without imidazole present, in both the ferric and ferrous states. The ferric HmbR sample with 500 mM imidazole present showed a Soret maximum at 413 nm that shifted to 426 nm when reduced. Additionally, this sample also had a small peak at 535 nm, which split into α and β peaks at 560 nm and 530 nm, respectively (**Fig. 3.1A**). These spectra are characteristic of a hexacoordinate hemophore [18]. The samples with reduced (< 5 mM) imidazole conveyed slightly different behavior. The ferric sample had a Soret maximum at 400 nm, that shifted to 427 nm when reduced, and is consistent with a pentacoordinate hemophore (**Fig. 3.1B)** [18]. This sample also had small α and β peaks found at 616 nm and 490 nm, which shifted to 566 nm and 533 nm and when reduced. However, the intensity of these bands was significantly depressed relative to the more prominent peaks observed in the presence of imidazole. To rule out the possibility that the observed reduced absorption spectra were not a result of spurious artifacts resulting from the oxidation of the sample during the course of the experiment, we also performed a titration experiment under anaerobic conditions using limiting quantities of sodium hydrosulfite, and acquired electronic absorption spectra in the absence of oxygen. The overall spectra obtained were identical to those observed when measurements were taken aerobically (data not shown).

Certain HmbR Variant Display Different Binding Profiles for Heme – While the absolute stoichiometry of heme to HmbR monomer remains unknown, the intensity of our absorption spectra was less than anticipated assuming a 1:1 ratio. We therefore quantified the molar percent of heme to protein present using an established pyridine hemochromogen assay and determined that approximately 30% of the HmbR present was saturated with heme (**Table 3.2**). In order to obtain protein with an increase in the heme binding ratio for spectroscopic studies, and to determine important residues involved in heme binding, we created a number of point mutations targeting either highly conserved residues (Y456C and Y763C), or ones within regions previously determined to be functionally significant for heme binding (H87C, H280A, Y282A, and Y497C) [16]. Of the six mutants evaluated, four had a statistically significant decrease in the amount of residual heme purified with HmbR relative to wild-type. These were H87C, H280A, Y282A, and Y456C (**Table 3.2**). The remaining two (Y497C and Y763C) had a diminished effect, but not pronounced enough to be considered statistically significant. This investigation did not identify mutants with either enhanced or completely abrogated heme binding

Circular Dichroism of Wild Type HmbR – One possible explanation for the low molar binding ratio of heme to HmbR may be that the protein was being denatured during purification, and therefore losing its affinity for heme. This would have also potentially explained why we were unable to identify mutants with enhanced heme binding. While no crystal structure of HmbR exists, the tertiary structure is predicted to be a 22-stranded β-barrel, consistent with other TBDTs. We therefore obtained a circular dichroism spectrum on the ferric imidazole free

sample in order to establish if the overall native structure was intact. The spectrum obtained is consistent with a protein composed primarily of β-sheets, as would be expected for a β-barrel fold, and very similar to CD spectra obtained on ShuA, which is a functionally related protein with a high-resolution structure available. (**Fig 3.2**) [6, 19]. Additionally, the spectrum does not indicate a significant random coil structure, which would likely be present if the protein was completely denatured.

Electron Paramagentic Resonance of HmbR – The electronic absorption spectra of HmbR indicates a hexacoordinate heme in the presence of imidazole, and a pentacoordinate in the absence of imidazole. To augment these findings, and to elucidate details on the spin states and coordination environment of the heme, we performed EPR on ferric samples with and without the presence of 500 mM imidazole (**Fig. 3.3**). In the absence of imidazole, the EPR spectrum reveals a classic 5-coordinate high spin axial ferric heme signal with a well defined g value at 6.09 (**Fig. 3.3A**). In the presence of imidazole, the EPR spectrum reveals significant g-values at 2.98, 2.26, and 2.06 (**Fig. 3.3B**). This is consistent with a 6-coordinate low spin ferric heme signal [20]. Additionally, in hemoproteins, g-values between 2.9 and 3.6 typically arise from two imidazole rings orientated axially to the plane of the porphyrin ring [21]. Hence, the increase in coordination most likely arises from the ability of imidazole to act as an axial ligand to the heme (bis-imidazole).

Resonance Raman Spectroscopy of HmbR – Our EPR spectra suggest an axial bis-imidazole heme coordination environment in the 6-coordinate low spin species. However, this information may not be accurate due to the interaction imidazole may have on the heme moiety. For

example, the presence of imidazole could lead to a 6-coordinate species in two ways. Either a single imidazole may occupy the vacant iron coordination site, or two molecules of imidazole may coordinate the heme; one in the free coordination site, and the other replacing a ligand in the axial site on the opposite side of the iron. We therefore decided to obtain resonance Raman spectra on the 5-coordinate high spin ferric species to aid in the identification of the unknown axial ligand. Soret-excited resonance Raman spectra of this species at pH 6.4, 7.8, and 9.7 is shown in **Figure 3.4.** The high frequency signature of the heme reveals marker bands ν_2, ν_3, and ν_4 at 1570, 1489, and 1370 cm^{-1}, respectively, which is expected for a five-coordinate high spin ferric heme (**Fig. 3.4A**). The low frequency signature of the heme reveals a prominent marker band at 379, and a small peak at 518 cm^{-1} (**Fig. 3.4B**). When compared to other heme and iron proteins previously evaluated, the peak observed at 518 cm^{-1} suggests that the fifth axial ligand is bound to an oxygen atom with at least a partial negative charge [22-24]. The persistence of this signal at pH 6.4 without a loss in intensity indicates that it is not a hydroxide anion. Therefore, the ligand is most likely an amino acid residue that contains an oxygen than can adopt a negative charge.

DISCUSSION

This study presents the first spectroscopic characterization of any heme or iron transporter in *Neisseria meningitidis.* Electronic absorption, EPR, and resonance Raman data support the presence of a 5-coordinate high spin ferric heme bound to purified HmbR (**Fig. 3.1, 3.3,** and **3.4A**). Additionally, we have several pieces of evidence that suggests this heme moiety is loosely bound within a binding pocket that allows access to the surrounding environment.

First, the heme can be coaxed into a 6-coordinate low spin ferric species through the addition of imidazole, and is susceptible to reduction (**Fig. 3.1** and **3.3**). This behavior is opposite of what would be expected for a tightly bound heme sequestered in a densely folded interior of a protein. Second, the molar ratio of heme to purified protein was only 30% (**Table 3.2**). If a tight binding pocket existed, one would expect this ratio to be much higher. The argument can be made that heterologous expression and/or purification of HmbR interfered with its native structure, thereby reducing its affinity for heme. While at this time we are unable to completely refute this possibility, our circular dichroism results demonstrate that HmbR possesses an overall native β-fold structure after purification, which is consistent with other bacterial outer membrane proteins, and may indicate that we were evaluating the biologically relevant form of the protein (**Fig. 3.2**). Third, we were unable to identify mutants that completely occluded heme binding. This finding suggests that the heme may be bound in a flexible pocket, whereby the loss of one coordinating residue can be compensated by neighboring related residues (**Table 3.2**). Last, our Raman data indicates that a residue with a partial negative charge on an oxygen acts as the fifth ligand in coordinating the heme (**Fig. 3.4B**). This is suggestive of a weak coordinating environment, as a strong interaction would likely include a 6-coordinate species with strong heme iron chelators, such as histidine residues. The hypothesis of a loosely coordinated heme within a relatively open environment is completely consistent with the function of HmbR. The receptor must not only extract heme from hemoglobin, but also transport and release it into the periplasm.

HmbR mediated transport is likely the primary means of iron acquisition during meningococcal septicemia infections, and positively correlated with the virulence of the pathogen [15]. This necessarily requires a source of hemoglobin, which is likely derived from hemolysis resulting from the secretion of specific lytic factors produced by the bacteria [25, 26].

Previous reports have demonstrated that the release of free oxyhemoglobin from intravascular erythrocyte lysis quickly undergoes autoxidation to yield methemoglobin [27]. Furthermore, we have observed a unique electronic absorption peak when HmbR was titrated with as little as 25% molar equivalents of methemoglobin in its tetramer form, and this signature was different from HmbR titrated with hemin, or hemoglobin alone (data not shown). Hence, our identification of a ferric heme in HmbR is consistent with the suggestion that methemoglobin is the biologically relevant substrate. Future investigations evaluating the degree of HmbR specificity for methemoglobin over hemin should be compared with other forms of hemoglobin utilizing more analytically sensitive techniques.

The precise manner in which heme is extracted from hemoglobin and transported to HmbR remains difficult to determine without a high-resolution structure. To date, only one outer membrane receptor for a heme containing protein has been solved. This is the ShuA protein, which serves the same function as HmbR in the pathogen *Shigella dysenteriae* [19]. Despite this functional redundancy, differences between the two proteins imparts difficulties in making direct comparisons. First, they only share 15% sequence homology. Second, the structure of ShuA identifies two histidine residues involved in coordinating the heme, whereas our data indicates one residue with a Raman signature that supports an oxygen ligand. Last, the extracellular regions of ShuA and HmbR, like all TBDTs, are highly variable. Thus, the design of drugs targeting heme transport proteins will likely need to evaluate the differences between receptors of different organisms, even if they have identical substrates. Towards this effect, we are currently undertaking crystallographic studies on HmbR to further identify these important structural details.

ACKNOWLEDGEMENTS

We are grateful to Dr. Donna Perkins-Balding for supplying the parent HmbR expression plasmid used in these studies (DPB1809), and members of the Lanzilotta laboratory for criticaldiscussions and technical assistance. This work was supported in part by an R01 grant from the National Science Foundation (to WNL).

REFERENCES

1 Wandersman, C. and Delepelaire, P. (2004) Bacterial Iron Sources: From Siderophores to Hemophores. Annual Review of Microbiology. **58**, 611-647

2 Wyckoff, E. E., Mey, A. R. and Payne, S. M. (2007) Iron acquisition in Vibrio cholerae. Biometals. **20**, 405-416

3 Fetherston, J. D., Kirillina, O., Bobrov, A. G., Paulley, J. T. and Perry, R. D. (2010) The yersiniabactin transport system is critical for the pathogenesis of bubonic and pneumonic plague. Infection and Immunity. **78**, 2045-2052

4 Poole, K. and McKay, G. A. (2003) Iron acquisition and its control in Pseudomonas aeruginosa: many roads lead to Rome. Frontiers in Bioscience. **1**, d661-d686

5 Schryvers, A. B. and Gray-Owen, S. (1992) Iron acquisition in Haemophilus influenzae: receptors for human transferrin. journal of Infectious Diseases. **165 Supplemental**, S103-S104

6 Burkhard, K., Wilks, A. (2007) Characterization of the Outer Membrane Receptor ShuA from the Heme Uptake System of Shigella dysenteriae The Journal of Biological Chemistry **282**, 15126-15136

7 Perkins-Balding, D., Ratliff-Griffin, M., Stojiljkovic, I. (2004) Iron Transport Systems in Neisseria meningitidis. Microbiology and Molecular Biology Reviews. **68**, 154-171

8 Ferguson, A. D. and Deisenhofer, J. (2002) TonB-dependent receptors-structural perspectives. Biochimica et Biophysica Acta. **1565**, 318-332

9 Krewulak, K. D. and Vogel, H. J. (2008) Structural Biology of bacterial iron uptake. Biochimica et Biophysica Acta. **1778**, 1781-1804

10 Frankenberg-Dinkel, N. (2004) Bacterial heme oxygenases. Antioxidants & Redox Signaling. **6**, 825-834

11 Stephens, D. S. (2009) Biology and pathogenesis of the evolutionarily successful, obligate human bacterium Neisseria meningitidis Vaccine. **27**, B71-B77

12 West, S. E. and Sparling, P. F. (1985) Response of Neisseria gonorrhoeae to iron limitation: alterations in expression of membrane proteins without apparent siderophore production. Infection and Immunity. **47**, 388-394

13 Harrison, O. B., Evans, N. J., Blair, J. M., Grimes, H. S., Tinsley, C. R., Nassif, X., Kriz, P., Ure, R., Gray, S. J., Derrick, J. P., Maiden, M. C. J. and Feavers, I. M. (2009) Epidemiological evidence for the role of the haemoglobin receptor, HmbR, in meningococcal virulence. The Journal of Infectious Diseases. **200**, 94-98

14 Stojiljkovic, I., Larson, J., Hwa, V., Anic, S., So, M. (1996) HmbR Outer Membrane Receptors of Pathogenic Neisseria spp.: Iron-regulated, Hemoglobin-Binding Proteins

with a High Level of Primary Structure Conservation. American Society for Microbiology. **178**, 4670-4678

15 Stojiljkovic, I., Hwa, V., de Saint Martin, L., O'Gaora, P., Nassif, X., Heffron, F. and So, M. (1995) The Neisseria meningitidis haemoglobin receptor: its role in iron utilization and virulence. Molecular Microbiology. **15**, 531-541

16 Perkins-Balding, D., Baer, M., T., Stojiljkovic. (2003) Identification of functionally important regions of a haemoglobin receptor from neisseria meningitidis. Microbiology. **149**, 3423-3435

17 Dailey, H. A. and Fleming, J. E. (1983) Bovine ferrochelatase. Kinetic analysis of inhibition by N-methyprotoporphyrin, manganese, and heme. Journal of Biological Chemistry. **258**, 11453-11459

18 Nygaard, T. K., Liu, M., McClure, M. J. and Lei, B. (2006) Identification and characterization of the heme-binding proteins SeShp and SeHts of Streptococcus equi subspecies equi. BMC Microbiology. **6**

19 Cobessi, D., Meksem, A., Brillet, K. (2009) Structure of the heme/hemoglobin outer membrane receptor ShuA from Shigella dysenteriae: Heme binding by an induced fit mechansim. Proteins. **78**, 286-294

20 Walker, F. A. (1999) Mangentic spectroscopic (EPR, ESEEM, Mössbauer, MCD and NMR) studies of low-spin ferriheme centers and their corresponding heme proteins. Coordination Chemistry Reviews. **185-186**, 471-534

21 Moreira, L. M., Poli, A. L., Costa-Filho, A. J. and Imasato, H. (2006) Pentacoordinate and hexacoordinate ferric hemes in acid medium: EPR, UV-Vis and CD studies of the

giant extracellular hemoglobin of Glossoscolex paulistus. Biophysical Chemistry. **124**, 62-72

22 Eakanunkul, S., Lukat-Rodgers, G. S., Sumithran, S., Ghosh, A., Rodgers, K. R., Dawson, J. H. and Wilks, A. (2005) Characterization of the Periplasmic Heme-Binding Protein ShuT from the Heme Uptake System of Shigella dysenteriae. Biochemistry. **44**, 13179-13191

23 Das, T. K., Coulture, M., Lee, H. C., Peisach, J., Rousseau, D. L., Wittenberg, B. A., Wittenberg, J. B. and Guertin, M. (1999) Identification of the ligands to the ferric heme of Chlamydomonas chloroplast hemoglobin: evidence for the ligation of tyrosine-63 (B10) to the heme. Biochemistry. **38**, 15360-15368

24 Nagai, M., Yoneyama, Y. and Kitagawa, T. (1989) Characteristics in tyrosine coordinations of four hemoglobins M probed by resonance Raman spectroscopy. Biochemistry. **28**, 2418-2422

25 Kamal, N. and Shafer, W. M. (2010) Biologic Activities of the TolC-Like Protein of Neisseria meningitidis as Assessed by Functional Complementation in Escherichia coli Antimicrobial agents and chemotherapy. **54**, 506-508

26 Ulmer, J. B., Burke, C. J., Shi, C., Friedman, A., Donnelly, J. J. and Liu, M. A. (1992) Pore formation and mitogenicity in blood cells by the class 2 protein of Neisseria meningitidis Journal of Biological Chemistry. **267**, 19266-19271

27 Hargrove, M. S., Whitaker, T., Olson, J. S., Vali, R. J. and Mathews, A. J. (1997) Quaternary Structure Regulates Hemin Dissociation from Human Hemoglobin. Journal of Biological Chemistry. **272**, 17385-17389

Table 3.1. Plasmids used in this study

Plasmid	**HmbR Variant**
pDPB1809	Wild-type
pDZM1	H87C
pDZM2	H280A
pDZM3	Y282A
pDZM4	Y456C
pDZM5	Y497C
pDZM6	Y763C

Table 3.2 Molar Percent of Heme to Protein of HmbR variants

HmbR Variant	**Molar Percent of Heme to Protein**	**P-value[1]**
Wt	30.4 ± 0.4	*
H87C	17.6 ± 0.4	.007
H280A	18.2 ± 0.1	.009
Y282A	20.5 ± 0.1	.019
Y456C	17.6 ± 0.2	.009

[1]Relative to wild-type

Figure 3.1. *Electronic Absorption Spectra of HmbR.*

Purified HmbR in sample buffer (20 mM phosphate, pH 7.4, 500 mM NaCl) was subjected to UV-visible absorption scans either **A**) as purified (with 500 mM imidazole) or **B**) after removal of imidazole. Black lines represent the spectra of samples in the ferric state, and gray lines represent the spectra of samples reduced to the ferrous state by the addition of 5 mM sodium hydrodulfite to the sample. Each spectra was obtained using 1.5 μL of protein at approximately 35 mg/mL on a nanodrop (ND-1000) spectrophotometer. Soret, α, and β peaks are indicated by their respective wavelengths within the graphs.

A.

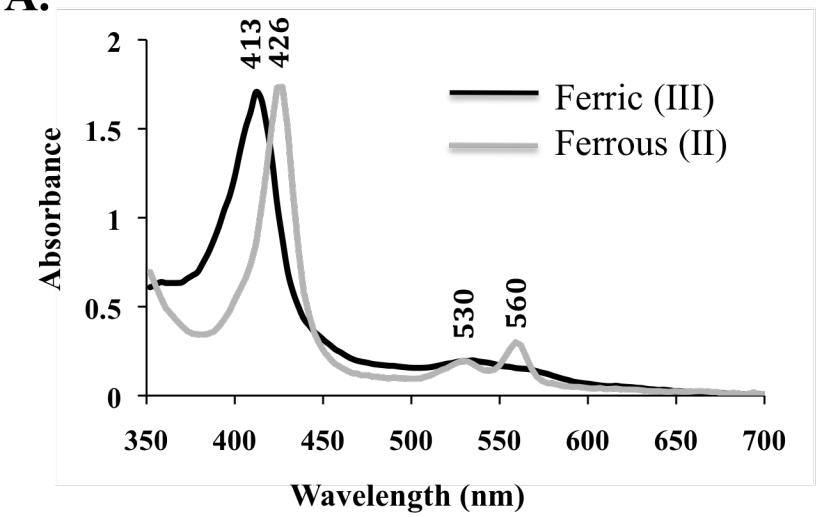
413
426
530
560
Ferric (III)
Ferrous (II)
Absorbance
Wavelength (nm)
0
0.5
1
1.5
2
350
400
450
500
550
600
650
700

B.

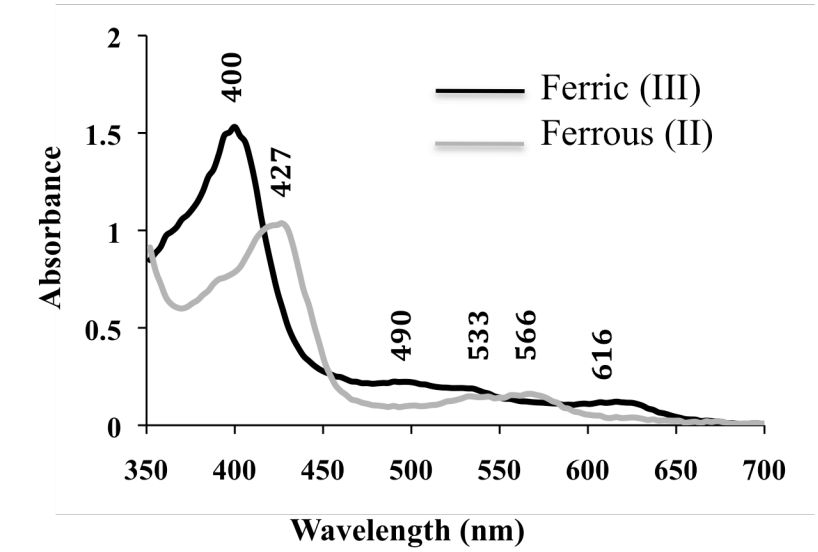
400
427
490
533
566
616
Ferric (III)
Ferrous (II)
Absorbance
Wavelength (nm)
0
0.5
1
1.5
2
350
400
450
500
550
600
650
700

Figure 3.2. *Circular dichroism of HmbR.*

Circular dichroism of ferric HmbR in sample buffer (10mM potassium phosphate, pH 7.4, 250mM NaCl, and 0.25% Anzergent™) at approximately 0.34 mg/mL protein concentration. Data was collected using a Jasco J-715 spectropolarimeter and a 0.1 cm cuvette containing the sample. Measurements were taken from 190 to 250 nm using a 10 nm bandwidth. Data was plotted as a function of molar ellipticity ($\Delta\varepsilon$) utilizing software associated with the instrument.

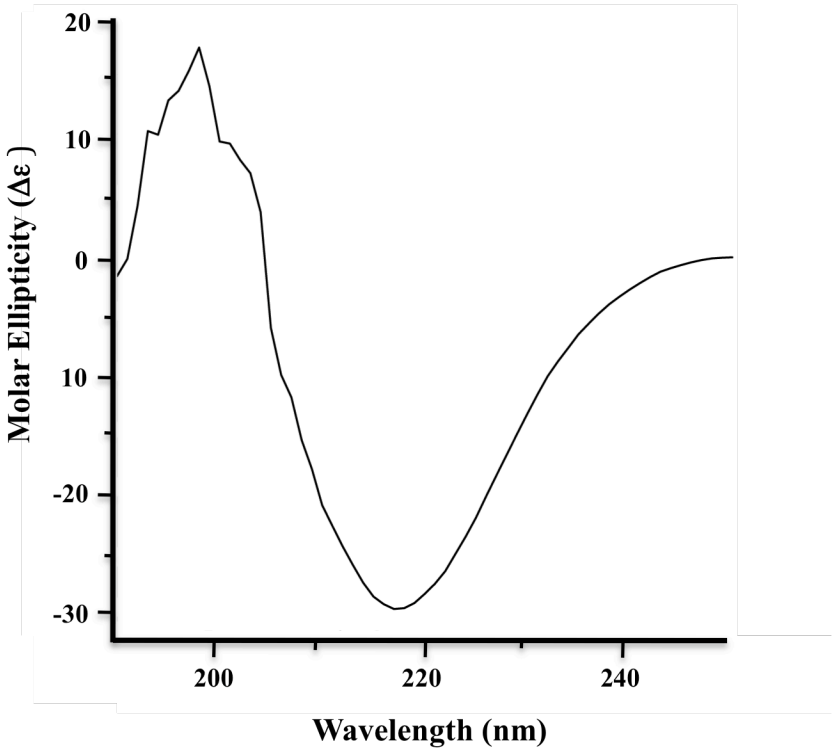
20
10
0
10
-20
-30
Molar Ellipticity (Δε)
200
220
240
Wavelength (nm)

Figure 3.3. *Electron paramagnetic resonance spectra of HmbR.*

EPR spectra were recorded on samples containing approximately 200 μM of HmbR in sample buffer (20 mM phosphate, pH 7.4, and Anzergent™ 3-14) either **A**) without imidazole, or **B**) in the presence of 500 mM imidazole. All data was collected using a Bruker ESP300D spectrometer equipped with an Oxford Instruments ESR-900 helium flow cryostat to maintain the temperature of the samples at 10K. The modulation amplitude was 6.477G with a modulation frequency of 100 kHz. The microwave frequency and power was 9.6 GHz and 5mW, respectively. Significant g-values are indicated in each spectrum.

A.

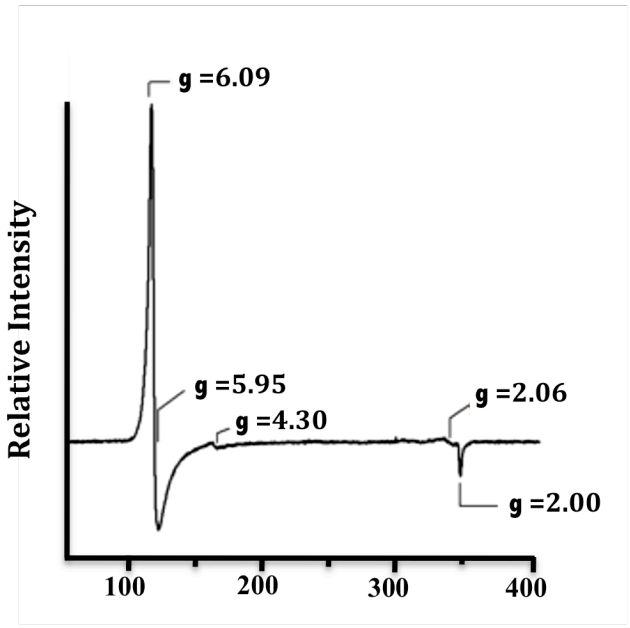
g =6.09
g =5.95
g =4.30
g =2.06
g =2.00
Relative Intensity
100
200
300
400

B.

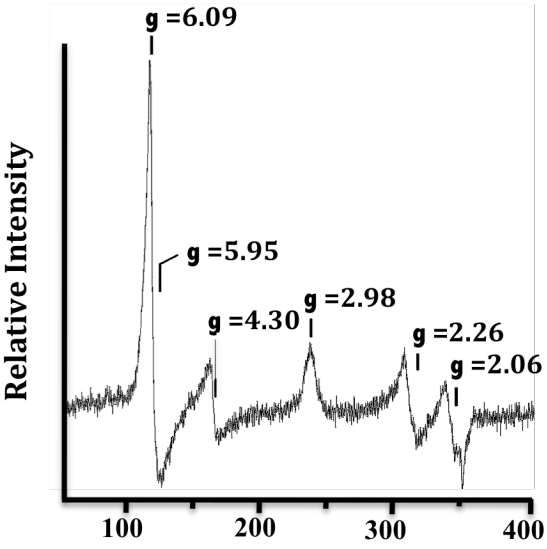
g =6.09
g =5.95
g =4.30
g =2.98
g =2.26
g =2.06
Relative Intensity
100
200
300
400

Figure 3.4. *Resonance Raman spectrum of HmbR.*

Resonance Raman of HmbR showing the **A**) high frequency and **B**) low frequency spectra. Each panel has three spectra (bottom, middle, and top) corresponding to different buffers (MES, Tris, or CAPS) and pH conditions (6.4, 7.8, and 9.7), respectively. Samples were prepared in .05% Anzergent™ , 300 mM NaCl, and 100 mM of the indicated buffer. Data was obtained using a 406.7 nm emission from a Kr^+ laser using a power of 14mW, a 135° backscattering geometry, and spun at 20 Hz in 5 mM NMR tubes at room temperature to avoid laser induced degradation. The laser bean was calibrated against Raman frequencies of toluene and DMF, and focused to a line on the spinning NMR tubes. The identity of certain peaks is indicated in each graph.

A.

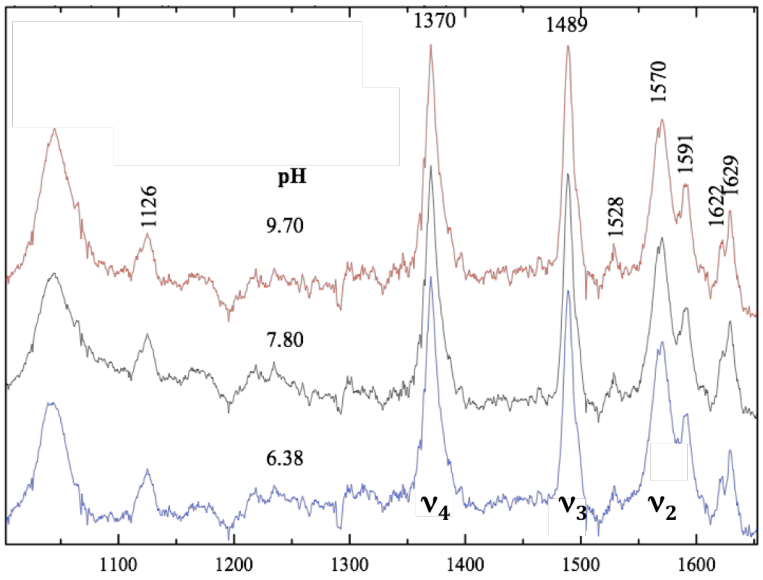
1370
1489
1570
1591
1622
1629
1528
1126
pH
9.70
7.80
6.38
ν_4
ν_3
ν_2
1100
1200
1300
1400
1500
1600
Raman Shift (cm^{-1})

B.

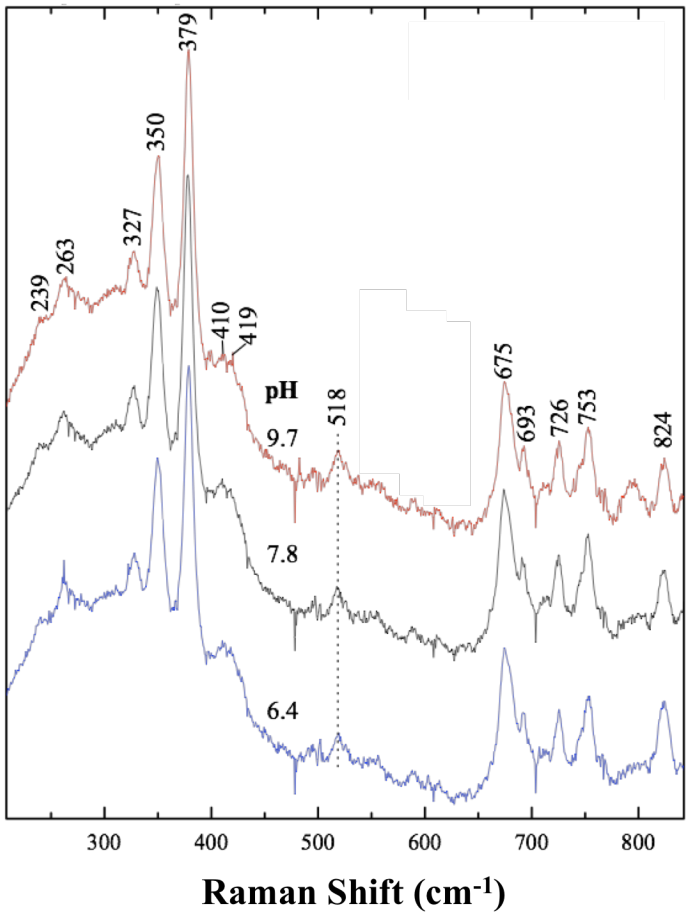
379
350
327
263
239
410
419
518
675
693
726
753
824
pH
9.7
7.8
6.4
300
400
500
600
700
800
Raman Shift (cm^{-1})

CHAPTER 4

DISCUSSION AND CONCLUSIONS: FOUNDATIONS FOR CONTINUING INVESTIGATIONS

As stated in Chapter 1, information on membrane proteins is universally underrepresented in biology, despite their strong biomedical relevance. Any studies on the enzymology, biochemistry, and three-dimensional structure and functions of these proteins aids in advancing the global knowledge of the field. The work presented in Chapters 2 and 3 has utilized and developed techniques to better characterize two distinct types of membrane proteins. The significance of this work, and the foundations for continuing investigations on these proteins is described below.

SCIENTIFIC IMPACT OF THESE STUDIES

Impact on CaaX protease biology

In Chapter 2, we convincingly demonstrated the presence of two *CaaX* proteolytic activities associated with the genes encoding Rce1 and Ste24 othologs in *Trypanosoma brucei*. This finding served to correct a previously published report in the literature that identified *Tb Rce1* as the sole source of proteolytic activity [1]. The identification of a dual *CaaX* proteolytic activity in *Trypanosoma brucei* is consistent with *CaaX* proteases

evaluated from other eukaryotic organisms [2-5]. One possible explanation for the conserved presence of these activities for a seemingly redundant function may be that a single enzyme is unable to process all the *CaaX* proteins within a particular proteome. However, no substrates have been identified that are exclusively processed by Ste24 outside of **a**-factor variants. This raises the issue of whether Ste24 has as broad a substrate profile as Rce1p. Additionally, Ste24 is known to cleave precursors of both **a**-factor and mammalian prelaminA in regions outside of the *CaaX* motif, suggesting it that it may serve a more specialized function other than *CaaX* proteolysis [6, 7].

In Chapter 2, we addressed the above issue by identifying a second substrate processed by Ste24 within the *CaaX* motif namely, an Hsp40 chaperone native to *Trypanosoma brucei*. This expansion of substrates suggests the presence of other proteins that are exclusively or partly processed by Ste24 throughout biology. Importantly, this chaperone was not processed by either protease when appended to **a**-factor, but was processed by both within its native protein context, providing a possible explanation why so few Ste24 substrates have been identified. Future research should be directed at better characterizing the targets of each *CaaX* protease within their most biologically relevant context.

The presence of two *CaaX* protease activities represents a challenge to the development of agents that interfere with *CaaX* proteolysis as a therapeutic strategy. If using an inhibitor specific for a single *CaaX* protease for the treatment of a protozoan infection, certain parasitic proteins, such as Ydj1, may continue to be *CaaX* proteolyzed by the alternate enzyme, and this may contribute to the survivability of the pathogen. Alternately, if using a dual inhibitor for the treatment of cancer, proper processing of Ste24

specific targets may be negatively affected, and may have detrimental effects on essential cellular functions of the patient. Therefore, it is important to identify additional *CaaX* protease targets, and in which manner they are processed.

Impact on HmbR biology

In Chapter 3, we provided the first spectroscopic investigation of any outer membrane heme or iron transporter in *Neisseria meningitidis*. Evidence is presented for a five coordinate high spin heme moiety ligated by an amino acid residue that contains a negatively charged oxygen within its side chain. Specifically, other outer membrane transporters studied only demonstrate a histidine, or a dual histidine and tyrosine coordination environment. Hence, this study expands the variety of ways heme transporters can function to include mechanisms that are completely histidine independent. Considering the emerging role of heme in the regulation of processes including cholesterol biosynthesis, protein translation, and regulation of circadian rhythms, these data may provide clues towards describing "heme sensing" mechanisms through novel coordination environments within these pathways [8-10].

Prior studies on other heme transporters were successful at identifying residues involved in binding and maintaining heme bound [11-13]. Typically, single or double point mutations in highly conserved or functionally important regions impact the ability to bind and/or transport heme. We conducted a similar investigation and identified four mutations that reduced the heme binding efficiency of HmbR. Two of these are histidine mutants (H280A, H87A), while the other two are tyrosine (Y456C, Y282A). We were unable to identify single point mutations that completely abrogated heme binding. The

diminished heme binding efficiencies conferred by histidine mutations do not necessarily conflict with our spectroscopic analysis, considering that the heme must first be removed from hemoglobin, and then transported through HmbR. It is possible that many residues are indirectly involved in either of these processes, and that the loss of a single residue may be functionally compensated by proximal histidine or tyrosine ligands within the local environment. This further suggests that the pore channel is flexible and dynamic in order to accommodate this change in coordination environment, as would be expected for a transmembrane transport protein.

Our study on HmbR contributes to the knowledge of heme and iron transporters in ways that impact future drug design. Specifically, it may be possible to engineer heme analogs that preferentially bind to the coordination environment observed in HmbR over other proteins that utilize an alternative coordination environment. Such analogs, such as metalloporphyrins, are already under investigation as potential therapeutics for a number of diseases [14-16]. Likewise, sideromycins are a class of drugs that take advantage of outer membrane transporters to gain access into the cell, and it might be possible to design an HmbR specific variant [17]. In order to achieve such goals, the finer structural aspects of the heme transport mechanism for HmbR must be obtained. Suggestions on how to proceed, and preliminary results for future investigations, are described below.

FOUNDATIONS FOR FUTURE INVESTIGATIONS

Biophysical characterization of Ste24 and HmbR: Crystallization of HmbR and Ste24

We have isolated yeast Ste24p (from yeast) and HmbR (from *E. coli*) of sufficient purity to permit crystallization trials of each protein (see Chapter 3 and below). Crystal screens of Ste24p were not ultimately performed due to low enzymatic activity and difficulties associated with obtaining adequate concentrations for optimal screening (see below).

HmbR crystal trials were performed using the hanging drop method with the following kits: Wizard I, Wizard II (Emerald Biostructures), Crystal Screen I, and Crystal Screen II (Hampton Research). We also used a crystallization kit for protein complexes (Sigma) with a purified HmbR/hemoglobin complex. None of these screens resulted in any crystals. However, at the time these trials were performed, the conditions in which HmbR was purified were not optimal for the stability of the protein. To identify a condition that could result in a more stable environment for the purified protein, we used dynamic light scattering (DLS) to perform an optimal solubility screen as previously described [18]. The results of this screen are shown in **Table 4.1**. Of the 17 buffers screened, 13 resulted in the formation of a precipitant. The buffers that resulted in the most monodisperse species were those that either had a low pH profile, or were already present within the currently used purification protocol. Since low pH conditions might influence the native structure of the protein, we decided to retain the original buffer and hypothesized that the stability of the protein could be rescued by altering one of the detergents used to purify the protein. When we modified our existing purification protocol by replacing the use of n-octyl β-D-

thioglucopyranoside with 3-(N,N-Dimethylmyristylammonio) propanesulfonate, and omitted the application of a detergent exchange procedure, we observed a significant increase in protein stability. The modified protocol is described in the materials and methods section of Chapter 2. Preliminary crystal screens have been performed using HmbR from the optimized protocol, with emphasis on conditions that were successful for other bacterial membrane heme and iron transporters. We have been successful at obtaining several crystals with a plate morphology (**Figure 4.1**). However, these diffract very poorly. Future efforts should focus on obtaining crystals with enhanced diffraction. This is currently being pursued by Nishi Shah, an undergraduate in Dr. William Lanzilotta's laboratory.

Biophysical characterization of Ste24: Reconstitution of purified Ste24p activity

The mechanistic features of membrane proteins are difficult to elucidate in the absence of high-resolution structural information. Therefore, it is sometimes necessary to employ a variety of techniques in order to gain a holistic understanding of their mechanistic details, and to validate observations. For example, the study described in Chapter 2 evaluated the *Tb CaaX* proteases heterologously expressed in *Saccharomyces cerevisiae*, and compared them to their yeast orthologs. To compliment this study, we also determined the K_m and V_{max} values of the *Saccharomyces cerevisiae CaaX* proteases, using it as the host organism. By use of our fluorescence assay, we were the first to report a K_m for Ste24. The results from this study are further described in Appendix B.

To further our enzymatic studies on Ste24 and Rce1, we also attempted using purified components of each protein. We employed the use of a modified purification

protocol previously described to obtain purified Ste24 (see below) [19]. However, the purification of Rce1 was more challenging, despite the variety of techniques we employed. When Rce1 was engineered as a glutathione S-transferase (GST) fusion protein containing a linker region with a Factor Xa cleavage site, neither glutathione, nor treatment with Factor Xa eluted the protein from the column. A truncated functional variant of the protein also behaved in the same manner. Immobile metal affinity chromatography (IMAC) was slightly more successful, but yields were less than 1%. Hence, we omitted Rce1 from our enzymatic studies requiring purified enzyme, but did include it during a detergent screen, described below.

The enzymatic activities of purified Ste24 compared to enriched membrane fractions had a marked reduction in activity. We therefore investigated a number of ways to reconstitute purified Ste24 activity. We conducted a screen of 72 detergents (Hampton) and monitored the activity and solubilization efficiency of a detergent solubilized lysate (DSL) for both *CaaX* proteases. This information is summarized in **Table 4.2**. For Ste24, we identified six detergents that retained 25% or more of the original enzymatic activity within the DSL. Four of these are nonionic detergents containing a modified disaccharide structure. Of the remaining two, one is nonionic (TritonX-100), and the other is a zwitterionic detergent containing a choline moiety (FOS-Choline 12). For Rce1, we identified five detergents that retained between 4.5% and 16% of the initial enzymatic activity. Three of these are zwitterionic detergents, containing modified choline or cholersterol derivatives. The other two are nonionic and contain modified disaccharide structures (N-Dodecyl-β-D-maltoside and sucrose monolaurate). In general, the most

common class of detergents that retained both Ste24 and Rce1 activities were different nonionic detergents containing disaccharide structures, followed by zwitterionic detergents.

We used the detergents identified from our screen to purify Ste24, but none yielded protein with enhanced activity relative to a negative control. We furthered our investigation to include the presence of lipids (0.1% *E. coli* or liver polar lipids) during the purification procedure, and again observed no enhanced activity relative to an appropriate negative control. The loss of Ste24 activity using these different approaches likely reflects a change in the native structure of the enzyme that cannot be recovered by the variety of amphipathic molecules that were screened. We therefore considered alternative methods to enhance activity of the purified enzyme.

A previous report identified Zn^{+2} and Co^{+2} as cofactors capable of restoring purified Ste24 activity that had been leached of metals using 1,10-orthophenanthroline [19]. The other metals tested in this study included magnesium and copper. Additionally, sequence analysis of Ste24 reveals an HEXXH zinc-binding motif, indicating that it is a zinc dependent metalloprotease. We therefore hypothesized that the catalytic zinc ion of Ste24p was being displaced during purification. This was investigated using X-ray absorption Spectroscopy (XAS) to monitor the zinc-binding site. The absorption spectrum from these studies indicates a significant reduction in the expected zinc concentration within the samples, and confirms the absence of zinc within the catalytic domain of purified Ste24p (**Figure 4.2**). When we directly supplemented zinc into purified fractions, and monitored activity using our established fluorescence assay, we did not observe an enhancement in activity.

To identify additional metals that could reactivate Ste24 activity, and to validate the previous metal screen, we performed our own divalent cation replacement screen on Ste24 enriched membranes leached of metals using 1,10-orthophenanthroline. Included in the screen were the metals previously examined, as well as an additional 6 (Ba^{+2}, Cd^{+2}, Ca^{+2}, Mn^{+2}, Sr^{+2}, and Ni^{+2}). Consistent with the previous report, we identified Zn^{+2} and Co^{+2} as metals capable of restoring Ste24 activity, but also identified Mn^{+2} as a third activator. Each metal reconstituted activity to varying degrees, with Zn^{+2} and Mn^{+2} imparting the strongest effects, and Co^{+2} conferring the weakest. Elevated concentrations of Zn^{+2} and Co^{+2} were observed to have an inhibitory effect on Ste24 activity. The inhibition is consistent with observations of other metalloproteases, and may be due to the formation of zinc or cobalt hydroxide complexes which interfere with the active site of the enzyme [20]. The results of this study are presented in **Figure 4.3**.

Future attempts at reconstituting purified Ste24p activity should be aimed at maintaining or replacing divalent cations that have been shown to reconstitute activity in purified or membrane fractions [19]. It is possible that the addition of molecular crowding agents, such as polyethylene glycols, within the activity assay buffer and/or purification procedure, could enhance zinc retention and should be investigated. Since elevated concentrations of some metals inhibit the activity of Ste24p, a range of concentrations should be tested (see **Figure 4.3**). To quantify and verify the presence of certain metals within samples, XAS or inductively coupled mass spectrometry could be utilized. It may also be useful to maintain the presence of some lipids during protein isolation, although at a lower concentration than attempted in this study. Additionally, a combination of metal and lipid supplementation, coupled to an optimized detergent, could also be investigated.

Biophysical characterization of HmbR: Defining regions essential for proper heme abstraction

The study described in Chapter 3 identified four amino acid residues within HmbR that, when mutated, exhibited a statistically significant lower binding profile for heme. We were not able to identify any residues that completely abrogated heme binding, but this is somewhat expected considering that the binding and transport mechanism may involve multiple sites of interaction for the heme group. In general, the mutations targeted a combination of conserved amino acid residues, and those contained in regions known to be important in heme release from a previous study [21]. This analysis could be broadened to include more mutations. Two examples include H382A and Y744A, due to the highly conserved nature of these residues. Additionally, during the course of this study, we identified a 42 nucleotide insertion in the HmbR expression construct that is not present in the annotated sequence. Within this region is a tandem extension of six polyhistidine residues. This insertion may arise from the specific type of HmbR isoform used for cloning, or it may be an unanticipated artifact of incorporating a histidine tag on the protein (the expression plasmid used was obtained from Donna Perkins-Balding at Macon State University). In either case, the effect of deleting this insertion should be evaluated.

Mutational analysis on hemoglobin can also be used to probe its interaction with HmbR. A previous study demonstrated that HmbR could discriminate between different hemoglobin orthologs. Whereas human hemoglobin supported the most robust cell growth, no proliferation was observed using snake hemoglobin [22]. This suggests that sequence variations between different isoforms of hemoglobin are important for interactions with

HmbR. A ClustalW2 sequence alignment of eight hemoglobin isoforms in both the α and β chains is shown in **Figure 4.4**. Although most regions are homologous with each other, there are 10 regions where dissimilarity is observed. Areas that vary between orthologs by 3 or more amino acids for 2 or more adjacent residues are shaded gray. These regions should be considered for mutagenesis in future investigations involving hemoglobin binding by HmbR.

MATERIALS AND METHODS

Optimum Solubility Screen on HmbR – An optimum solubility screen using the buffers indicated in **Table 4.1** was performed on HmbR as modeled after Jancaric et al. [18]. In general, HmbR isolated as described in Chapter 2 was further purified using a HiLoad 16/60 Superdex 200 gel filtration column. Protein was loaded on the column equilibrated with 10 mM Phosphate buffer, pH 7.4 and 500 mM NaCl, and eluted with 10 mM Phosphate buffer, pH 7.4, 500 mM NaCl, and 0.8% n-octyl β-D-thioglucopyranoside at a flow rate of 1.1 mL/minute using an Äkta program to monitor the procedure. Relevant protein samples were then pooled and concentrated to 2.5 mg/mL in a 50 KDa nominal molecular weight cut-off (NMWC) concentrator (Millipore, product #4323). Each buffer to be tested was prepared at a concentration of 100 mM and filter sterilized prior to use. The protein was then diluted at a ratio of 1:14 in each buffer condition in a sterile dust-free Eppendorf tube, and centrifuged at 16,000g for 20 minutes at room temperature, after which point a precipitant, if present, was observed by eye. Samples were loaded in a quartz cuvette for dynamic light scattering analysis at 25 ºC using a DynaPro99 molecular sizing instrument (Protein Solutions, Piscataway, NJ) at 15% laser power and a total acquisition

time of 100 seconds. Data was analyzed using DYNAMICS version 6.0 software assuming a globular shape in PBS buffer.

Isolation of Yeast Membranes – Yeast membranes were isolated using a modified procedure as described in Porter, et al. [23]. In general, yeast strains transformed with the appropriate plasmid were grown in SC-Ura liquid media at 30ºC to 1.0 A_{600} units, harvested (3,000 g for 10 minutes), and subsequently treated with 10 mM NaN_3 and 100 mM Tris, pH 9.4, 10 mM dithiothreitol for 10 minutes at 10 A_{600}/mL. The recovered cells were resuspended in oxalyticase buffer (50 mM potassium phosphate, pH 7.5, 1.4 M sorbitol, and 10 mM NaN_3) to 25 A_{600}/mL containing either oxalyticase (1µg/OD_{600}) or zymolyase (4 µg/OD_{600}) and incubated at 30ºC for 30 minutes, followed by 10 minutes on ice. The resulting spheroplasts were washed with oxalyticase buffer and resuspended in lysis buffer (50 mM Tris, pH 7.5, 0.2 M sorbitol, and 1 mM EDTA) containing protease inhibitors (1 mM phenylmethylsulfonyl fluoride, 2 µg/ml aprotinin, 1 µg/ml leupeptin, 2 µg/ml chymotrypsin, and 1µg/ml pepstatin at 500 A_{600}/mL). Speroplasts were lysed using silica beads (4 x 4 minute pulses at 4ºC with 2 minute intervals on ice), and membranes recovered using differential centrifugation with intermediate washes of lysis buffer (2X at 500 g and 2X at 16,000 g).

Purification of Ste24 from Yeast and XAS sample preparation – Purification of Ste24 was carried out using a modification of an existing protocol [19]. Ste24 enriched membranes isolated by the above procedure were treated with solubilization buffer (2% triton X-100, 20 mM Tris, pH 7.4, 10% glycerol, 50 mM NaCl, 5 mM imidazole) at 40

A_{600}/mL for 1.5 hours on ice, clarified (14,000 g for 30 minutes), and incubated with a nickel-nitrilotriacetic acid (Ni-NTA)-agarose resin (80 µl of resin/mL of lysate) overnight. The slurry was packed into a gravity-flow column and washed with three column volumes of solubilization buffer substituting 1% n-octyl β-D-thioglucopyranoside (OG) for Triton X-100, and protein eluted using the same buffer, but containing 500 mM imidazole. Relevant elution fractions were pooled and concentrated in a 30 KDa nominal molecular weight cut-off (NMWC) concentrator (Millipore, product #4322). Where alternative detergents were analyzed, a concentration at twice the critical micelle concentration was used during the solubilization, wash, and elution procedures in place of other detergents. Where lipids were evaluated, 0.1% of either liver polar lipids or *E. coli* lipids (Avanti) were supplemented in the wash and elution procedures. Samples prepared for X-ray absorption spectroscopy were further prepared by dialyzing protein fractions against wash buffer devoid of imidazole, and subsequently concentrated in a 30 KDa nominal molecular weight cut-off (NMWC) concentrator (Millipore, product #4322). The resulting retentate, and any precipitant that formed during dialysis or concentration was loaded into cryovial cuvettes secured with Mylar™ or Kapton™ tape, and immediately flash frozen in liquid nitrogen. All XAS data was performed in collaboration with Robert A. Scott (University of Georgia) using the Stanford Synchrotron Radiation Lightsource.

Detergent Screens of Rce1 and Ste24 – Detergent screens to optimize recovery of solubilized Ste24 and Rce1 activity were performed using 50 µg of membranes derived from a yeast strain transformed with the appropriate plasmid using the membrane isolation protocol described above. The strains used were SM3614 transformed with either SM1282

(Ste24), pWS479 (Rce1), or SM174 (negative control). Membranes were resuspended in 70 µL resuspension buffer (20 mM Hepes, pH 7.4, 1 mM $MgCl_2$, 10% glycerol, 50 mM NaCl) containing 2X the critical micelle concentration of the detergent to be tested, and incubated for one hour at 4 ºC at 1050 rpm in a Eppendorf Thermomixer. The resulting lysate was clarified (16,000 g for 15 minutes), and 50 µL of the detergent solubilized lysate was directly added to a microtiter plate for activity analysis using an established fluorescence assay as previously described [23, 24]. The percent activity in each condition was calculated relative to 50µg of untreated membranes.

Divalent Cation Replacement Screen of Ste24 – Divalent cation replacement screens were carried out to determine which metals reconstituted Ste24 activity *in vitro* using a modification of an existing halo assay [19, 23]. In brief, membranes were recovered using the above protocol for membrane fractionation on SM3614 transformed with SM1282 and resuspended to 1 mg protein/mL in lysis buffer (50 mM Tris, pH 7.5, 0.2 M sorbitol, and 1 mM EDTA). Upon treatment with 1 mM 1,10 phenanthroline, membranes were incubated on ice for 10 minutes, followed by an incubation with 0.5-2.0 mM of the appropriate divalent cation for an additional 10 minutes. The resulting activity was monitored using 1-2 µL of the divalent cation treated membranes in the halo assay. For all conditions, Ste24 membranes were incubated with a synthetic **a**-factor substrate for 10 minutes at 30ºC, followed by heat inactivation at 95ºC for 1 minute, and 1 hour incubation with Ste14 membranes at 30ºC. The Ste14 membranes were derived from SM3614 transformed with SM1317 using the membrane fractionation procedure described above. A portion of each reaction (2 µl) was spotted on a lawn of *sst2-1* yeast that are hypersensitive to the presence

of mature **a**-factor. Membranes not treated with 1,10 phenanthroline, or treated and not reconstituted with any metal, served as positive and negative controls, respectively. The metals tested were derived from a Hampton additive screen (HR2-428) and included 10 divalent cations: Ba^{+2}, Cd^{+2}, Ca^{+2}, Co^{+2}, Cu^{+2}, Mg^{+2}, Mn^{+2}, Sr^{+2}, Zn^{+2}, and Ni^{+2}.

REFERENCES

1 Gillespie, J. R., Yokoyama, K., Lu, K., Eastman, R. T., Bollinger, J. G., Van Voorhis, W. C., Gelb, M. H. and Buckner, F. S. (2007) C-terminal proteolysis of prenylated proteins in trypanosomatids and RNA interference of enzymes required for the post-translational processing pathway of farnesylated proteins. Mol Biochem Parasitol. **153(2)**, 115-124

2 Plummer, L. J., Hildebrandt, E. R., Porter, S. B., Rogers, V. A., McCracken, J. and Schmidt, W. K. (2006) Mutational analysis of the ras converting enzyme reveals a requirement for glutamate and histidine residues. J Biol Chem. **281**, 4596-4605

3 Bracha, K., Lavy, M. and Yalovsky, S. (2002) The Arabidopsis AtSTE24 is a CAAX protease with broad substrate specificity. J Biol Chem. **277**, 29856-29864

4 Cadiñanos, J., Schmidt, W. K., Fueyo, A., Varela, I., Lopez-Otin, C. and Freije, J. M. (2003) Identification, functional expression and enzymic analysis of two distinct CaaX proteases from *Caenorhabditis elegans*. Biochem J. **370**, 1047-1054

5 Cadiñanos, J., Varela, I., Mandel, D., Schmidt, W. K., Díaz-Perales, A., López-Otín, C. and JMP, F. (2003) AtFACE-2, a prenylated-protein protease from

Arabidopsis thaliana related to Ras converting enzymes. Journal of Biological Chemistry. **278**, 42091-42097

6 Fujimura-Kamada, K., Nouvet, F. J. and Michaelis, S. (1997) A novel membrane-associated metalloprotease, Ste24p, is required for the first step of NH_2-terminal processing of the yeast **a**-factor precursor. JCB. **136**, 271-285

7 Kilic, F., Dalton, M. B., Burrell, S. K., Mayer, J. P., Patterson, S. D. and Sinensky, M. (1997) *In vitro* assay and characterization of the farnesylation-dependent prelamin A endoprotease. J Biol Chem. **272**, 5298-5304

8 Hughes, A. L., Powell, D. W., Bard, M., Eckstein, J., Barbuch, R., Link, A. J. and Espenshade, P. J. (2007) Dap1/PGRMC1 binds and regulates cytochrome P450 enzymes. Cell Metabolism. **5**, 143-149

9 Furuyama, K., Kaneko, K. and Vargas V., P. D. (2007) Heme as a Magnificent Molecule with Multiple Missions: Heme Determines Its Own Fate and Governs Cellular Homeostasis The Tohoku journal of Experimental Medicine. **213**, 1-16

10 Mackiewicz, M., Naidoo, N., Zimmerman, J. E. and Pack, A. L. (2008) Molecular mechanisms of sleep and wakefulness. Annuals of the New York Academy of Sciences. **1129**, 335-349

11 Burkhard, K., Wilks, A. (2007) Characterization of the Outer Membrane Receptor ShuA from the Heme Uptake System of Shigella dysenteriae The Journal of Biological Chemistry **282**, 15126-15136

12 Eakanunkul, S., Lukat-Rodgers, G. S., Sumithran, S., Ghosh, A., Rodgers, K. R., Dawson, J. H. and Wilks, A. (2005) Characterization of the Periplasmic Heme-

Binding Protein ShuT from the Heme Uptake System of Shigella dysenteriae. Biochemistry. **44**, 13179-13191

13 Izadi-Pruneyre, N., Huche, F., Lukat-Rodgers, G. S., Lecroisey, A., Gilli, R., Rodgers, K. R., Wandersman, C. and Delepelaire, P. (2006) The Heme Transfer from the Soluble HasA Hemophore to its Membrane-bound Receptor HasR is Driven by Protein-Protein Interaction from a High to a Lower Affinity Binding Site. The Journal of Biological Chemistry. **281**, 25541-25550

14 Begum, K., Kim, H., Kumar, V., Stojiljkovic, I. and Wataya, Y. (2003) In vitro antimalarial activity of metalloporphyrins against Plasmodium falciparum. Parasitology Research. **90**, 221-224

15 Rabkin, S. and Klassen, S. (2008) Metalloporphyrins as a therapeutic drug class against peroxynitrite in cardiovascular diseases involving ischemic reperfusion injury. European Journal of Pharmacology. **586**, 1-8

16 Chen, P., Li, A., Zhang, M., He, M., Chen, Z., Wu, X., Zhao, C., Wang, S. and Liang, L. (2008) Protective effects of a new metalloporphyrin on paraquat-induced oxidative stress and apoptosis in N27 cells. Biochimica et Biophysica Acta. **40**, 125-132

17 Braun, V. and Braun, M. (2002) Active Transport of iron and siderophore antibiotics. Current Opinion in Microbiology. **5**, 194-201

18 Jancarik, J., Pufan, R., Hong, C., Kim, S., Kim, R. (2004) Optimum solubility (OS) screening: an efficient method to optimize buffer conditions for homogeneity and crystallization of proteins. Acta Crystallographica **D60**, 1670-1673

19 Tam, A., Schmidt, W. K. and Michaelis, S. (2001) The multispanning membrane protein Ste24p catalyzes CAAX proteolysis and NH2-terminal processing of the yeast a-factor precursor. J Biol Chem. **276**, 46798-46806

20 Larson, K. S. and Auld, D. S. (1989) Carboxypeptidase A: Mechanism of zinc inhibition. Biochemistry. **28**, 9620-9625

21 Perkins-Balding, D., Baer, M., T., Stojiljkovic. (2003) Identification of functionally important regions of a haemoglobin receptor from neisseria meningitidis. Microbiology. **149**, 3423-3435

22 Stojiljkovic, I., Larson, J., Hwa, V., Anic, S., So, M. (1996) HmbR Outer Membrane Receptors of Pathogenic Neisseria spp.: Iron-regulated, Hemoglobin-Binding Proteins with a High Level of Primary Structure Conservation. American Society for Microbiology. **178**, 4670-4678

23 Porter, S. B., Hildebrandt, E. R., Breevoort, S. R., Mokry, D. Z., Dore, T. M. and Schmidt, W. K. (2007) Inhibition of the CaaX proteases Rce1p and Ste24p by peptidyl (acyloxy)methyl ketones. Biochim Biophys Acta. **1773**, 853-862

24 Manandhar, S. P., Hildebrandt, E. R. and Schmidt, W. K. (2007) Small-molecule inhibitors of the Rce1p CaaX protease. J Biomol Screen. **12**, 983-993

Table 4.1 Dynamic light scattering of HmbR in different buffer conditions

Buffer	pH	Number of major species [1]	R(nm)[2] of major species	Percent of Mass at indicated R(nm)
Glycine	3.0	1	9.8-40.0	95%
Citric acid	3.2	1	13-40 nm	95%
Citric acid*	4.0	1	0.06-0.08 nm	96%
Sodium acetate*	4.5	1	.06-.08 nm	99%
Sodium citrate*	5.5	2	17-53 nm 2,650-3500 nm	89% 11%
Potassium phosphate*	5.0	2	17-53 nm 2,000-3500 nm	76% 23%
Potassium phosphate*	6.0	2	17-53 nm 2,000-3500 nm	81% 17%
Potassium phosphate	7.0	1	.06 nm	99%
MES*[3]	6.2	1	.06 nm	99%
ADA*[4]	6.5	1	.06 nm	99%
Cacodylic acid*	6.5	1	.06 nm	96%
Ammonium acetate*	7.0	1	.08-.11 nm	99%
MOPS*[5]	7.0	1	.06 nm	97%
HEPES*[6]	7.5	1	9.8-40.0 nm	98%
Imidazole*	8.0	1	17.2-40.0 nm	97%
Tris*	7.5	2	9.8-40.0 nm 2,000-3500 nm	94% 5%
Tris	8.5	1	.06 nm	99%

[1]Signals with less than 5% mass intensity not considered
[2]R(nm) is average hydrodynamic radius in nanometers
[3]MES is 2-(N-morpholino)ethanesulfonic acid
[4]ADA is N-(2-Acetamido)iminodiacetic Acid
[5]MOPS is 3-(N-morpholino)propanesulfonic acid
[6]HEPES is 4-(2-hydroxyethyl)-1-piperazineethanesulfonic acid
*Designates formation of a precipitate

Table 4.2 Activities of the *CaaX* proteases after detergent solubilization[1\]

Enzyme	**Detergent**	**Activity[2]**
Ste24	FOS-Choline-12	25%
	Triton X-100	33%
	N-Decyl-β-D-maltoside	34%
	N-Decanoylsucrose	39%
	CYMAL-6	44%
	N-Undecyl-β-D-maltoside	50%
Rce1	FOS-Choline-8	4.5%
	N-Dodecyl-β-D-maltoside	7.4%
	CYPFOS-3	8.8%
	CHAPSO	13%
	Sucrose Monolaurate	16%

[1]Solubilization monitored by Western analysis (data not shown)
[2]Calculated as activity of detergent solubilized lysate relative to initial activity

Figure 4.1 *Crystals of HmbR*

Representative crystals of HmbR obtained using a peg/ion hanging drop crystal screen. The most successful conditions maintained the presence of 12- 20% w/v polyethylene glycol 3,350 with a number of additives. The specific conditions associated with this image was 0.2M Potassium Iodide, and 20% w/v polyethylene glycol 3,350. The drop was composed of approximately 2 μL of protein at 10 mg/mL and 2 μL of test solution and allowed to incubate at 18°C for 10-14 days. The image was captured using a Moitcam 2000 camera mounted on an Olympus SZ61 light microscope.

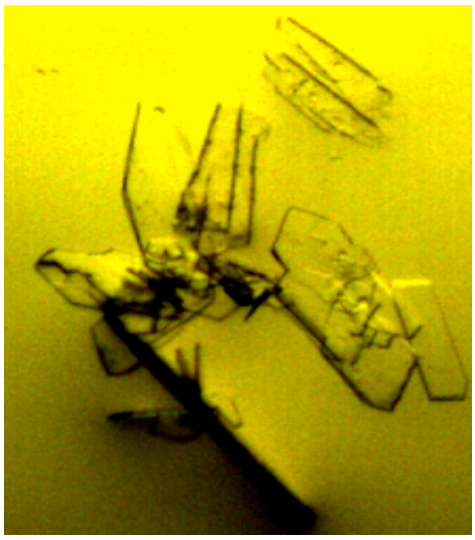

Figure 4.2 *X-ray absorption spectroscopy of purified Ste24*

Graphs of zinc energy absorption versus total energy input. The solid line denotes a 2 mM zinc standard, and the dotted line denotes purified Ste24. The Y-axis on the left corresponds to the zinc standard, whereas the Y-axis on the right is a 100X magnification of the left axis, and corresponds to the signal observed for Ste24. All data was collected at the Stanford Synchrotron Radiation Lightsource in collaboration with Robert A. Scott (University of Georgia).

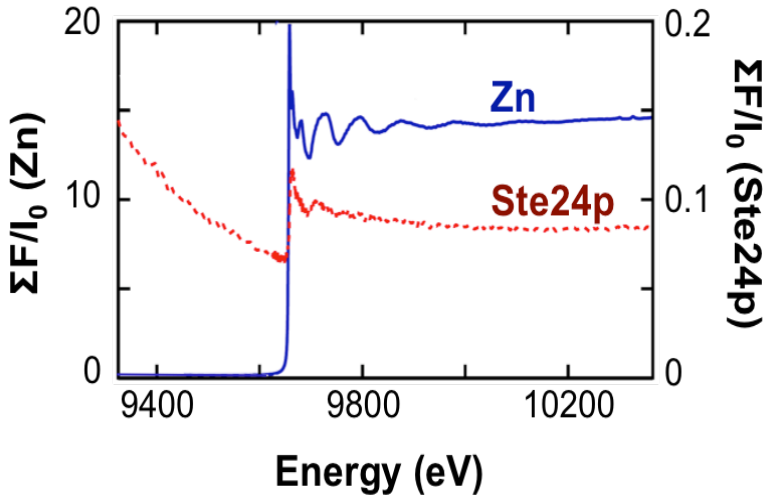
20
10
0
0.2
0.1
0
9400
9800
10200
Energy (eV)
ΣF/I0 (Zn)
ΣF/I0 (Ste24p)
Zn
Ste24p

Figure 4.3 *Certain divalent cations can reconstitute Ste24 activity*

The rescue effect of cobalt, manganese, and zinc on 1,10 phenanthroline treated Ste24 enriched membranes. The concentrations tested were 0.5 mM and 2.0 mM. Higher concentrations of all metals were deemed to confer an inhibitory effect at higher concentrations, although the effect was more pronounced with cobalt and zinc. Membranes not treated with 1,10 phenanthroline, or treated and not reconstituted with any metal, served as positive and negative controls, respectively

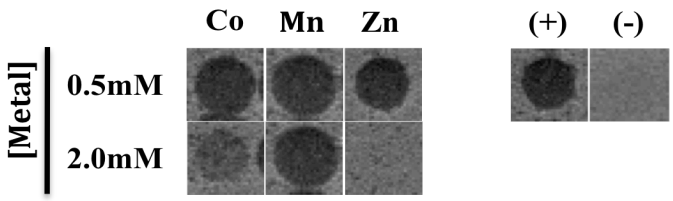
Co
Mn
Zn
(+)
(-)
[Metal]
0.5mM
2.0mM

Figure 4.4 *Sequence alignment of hemoglobin isoforms from different organisms*

Hemoglobin sequence alignment in the alpha and beta chains from human, horse, goat, rat, mouse, dog, turkey, and snake. Areas that vary between orthologs by 3 or more amino acids for 2 or more adjacent residues are shaded gray. Dissimilar regions within 10 amino acids of the initiator methionine were ignored, and variable regions within 3 amino acid residues of each other were grouped. The alignment was generated using ClustalW2 software.

Alpha

```
Human   MVLSPADKTNVKAAWGKVGAHAGEYGAEALERMFLSFPTTKTYFPHFDLSHGSAQVKGHGKKVADALTNAVAHVDDMPNALSALSDLHAHKLRVDPVNFKLL
Horse   MVLSAADKTNVKAAWSKVGGHAGEYGAEALERMFLGFPTTKTYFPHFDLSHGSAQVKAHGKKVGDALTLAVGHLDDLPGALSNLSDLHAHKLRVDPVNFKLL
Goat    MVLSAADKSNVKAAWGKVGGHAGAYGAEALERMFLSFPTTKTYFPHFDLSHGSAQVKGHGEKVAAALTKAVGHLDDLPGTLSDLSDLHAHKLRVDPVNFKLL
Rat     MVLSADDKTNIKNCWGKIGGHGGEYGEEALQRMFAAFPTTKTYFSHIDVSPGSAQVKAHGKKVADALAKAADHVEDLPGALSTLSDLHAHKLRVDPVNFKFL
mouse   MVLSGEDKSNIKAAWGKIGGHGAEYGAEALERMFASFPTTKTYFPHFDVSHGSAQVKGHGKKVADALASAAGHLDDLPGALSALSDLHAHKLRVDPVNFKLL
dog     -VLSPADKTNIKSTWDKIGGHAGDYGGEALDRTFQSFPTTKTYFPHFDLSPGSAQVKAHGKKVADALTTAVAHLDDLPGALSALSDLHAYKLRVDPVNFKLL
turkey  -VLSAADKNNVKGIFTKIAGHAEEYGAETLERMFITYPPTKTYFPHFDLSHGSAQIKGHGKKVVAALIEAANHIDDIAGTLSKLSDLHAHKLRVDPVNFKLL
snake   -VLTEEDKARVRVAWVPVSKNAELYGAETLTRLFAAHPTTKTYFPHFDLSPGSNDLKVHGKKVIDALTEAVNNLDDVAGALSKLSDLHAQKLRVDPDNFQFL

Human   SHCLLVTLAAHLPAEFTPAVHASLDKFLASVSTVLTSKYR
Horse   SHCLLSTLAVHLPNDFTPAVHASLDKFLSSVSTVLTSKYR
Goat    SHSLLVTLACHLPNDFTPAVHASLDKFLANVSTVLTSKYR
rat     SHCLLVTLACHHPQDFTPAMHASLDKFLASVSTVLTSKYR
Mouse   SHCLLVTLASHHPADFTPAVHASLDKFLASVSTVLTSKYR
Dog     SHCLLVTLACHHPTEFTPAVHASLDKFFAAVSTVLTSKYR
Turkey  GQCFLVVVAIHHPAALTPEVHASLDKFLCAVGTVLTAKYR
Snake   GLCLEVTIAAHSGGPLKPEVLLSVDKFLGQISKVLASRYR
```

Beta

```
Human  MVHLTPEEKSAVTALWGKVNVDEVGGEALGRLLVVYPWTQRFFESFGDLSTPDAVMGNPKVKAHGKKVLGAFSDGLAHLDNLKGTFATLSELHCDKLHVDP
Horse  VQLSGEEKAAVLALWDKVNEEEVGGEALGRLLVVYPWTQRFFDSFGDLSNPGAVMGNPKVKAHGKKVLHSFGEGVHHLDNLKGTFAALSELHCDKLHVDP
Goat   -----MPNKALITGFWSKVKVDEVGAEALGRLLVVYPWTQRFFEHFGDLSSADAVLGNAKVKAHGKKVLDSFSNGVQHLDDLKGTFAELSELHCDKLHVDP
Rat    MVHLTDAEKAAVNGLWGKVNPDDVGGEALGRLLVVYPWTQRYFDSFGDLSSASAIMGNPKVKAHGKKVINAFNDGLKHLDNLKGTFAHLSELHCDKLHVDP
Mouse  MVHLTDAEKAAVSGLWGKVNADEVGGEALGRLLVVYPWTQRYFDSFGDLSSASAIMGNAKVKAHGKKVITAFNDGLNHLDSLKGTFASLSELHCDKLHVDP
Dog    -VHLTAEEKSLVSGLWGKVNVDEVGGEALGRLLIVYPWTQRFFDSFGDLSTPDAVMSNAKVKAHGKKVLNSFSDGLKNLDNLKGTFAKLSELHCDKLHVDP
Turkey -VHWSAEEKQLITGLWGKVNVADCGAEALARLLIVYPWTQRFFASFGNLSSPTAILGNPMVRAHGKKVLTSFGDAVKNLDNIKNTFSQLSELHCDKLHVDP
Snake  VHWSAEEKQLITGLWGKVDVAEVGGATLGKLLVVFPWTQRFFAHFGNLSSANAIICNPVVKAHGKKVLTSFGEAIKHLDSIKETFAKLSELHCEKLHVDP

Human   ENFRLLGNVLVCVLAHHFGKEFTPPVQAAYQKVVAGVANALAHKYH
Horse   ENFRLLGNVLVVVLARHFGKDFTPELQASYQKVVAGVANALAHKYH
Goat    ENFRLLGNVLVIVLARHFGKEFTPELQAEFQKVVAGVASALAHRYH
Rat     ENFRLLGNMIVIVLGHHLGKEFTPCAQAAFQKVVAGVASALAHKYH
Mouse   ENFRLLGNMIVIVLGHHLGKDFTPAAQAAFQKVVAGVAAALAHKYH
Dog     ENFKLLGNVLVCVLAHHFGKEFTPQVQAAYQKVVAGVANALAHKYH
Turkey  ENFRLLGDILIIVLAAHFSKDFTPECQAAWQKLVRVVAHALARKYH
Snake   ENFRLLGNILIIVLAGHHGKEFTPSTHAAFQKLVRAVAHSLARVYH
```

APPENDIX A

Pertinent studies related to this thesis and not presented elsewhere within this document are described below. The rationale for conducting each of these studies is also described.

Identification of additional Ste24 and Rce1 substrates: Ydj1 as a candidate

The *CaaX* tetrapeptide motif is found on 2-5% of all eukaryotic proteins, yet the processing of only a handful of these potential substrates have been characterized. *CaaX* protease substrates that have been characterized with some detail include Ras and Rho GTPases, prelaminA, and the **a**-factor fungal mating pheromone [1-4]. Identification of additional *CaaX* protease substrates continues to be an important goal (see Chapter 1 and Chapter 4). However, this task is challenging due to a number of factors, including the combination of motifs possible, the tripartite nature of the *CaaX* processing pathway, obtaining appropriate substrates, subtle phenotypes, and correctly determining specific from nonspecific *CaaX* proteolysis.

This study adds to the list by providing the first evidence for processing of an Hsp40 chaperone native to *Trypanosoma brucei* by both *CaaX* proteases (see Chapter 2). In support of the yeast ortholog of the chaperone (Ydj1p) being isoprenylated, we have taken advantage of the observation that genetic complementation of a ydj1Δ strain with wild-type Ydj1p, as well as orthologs from other organisms, namely human and trypanosomes, rescues the temperature sensitive phenotype of the null (**Figure A.1A**, and Chapter 2). Complementation with the *Trypanosoma brucei* Ydj1p ortholog harboring a cysteine to serine mutation within the *CaaX*

motif does not rescue the temperature sensitivity (see Chapter 2, **Figure 2.3**). These observations suggest that isoprenylation is essential for proper functioning of Ydj1p, and alludes that it may also be *CaaX* proteolyzed. However, if *CaaX* processing does occur, and is essential for Ydj1p activity, one would expect that a strain devoid of any *CaaX* proteases would also convey temperature sensitivity, and this is not the case (**Figure A.1B**.). However, two observations suggest that Ydj1p is processed in some manner by Ste24p. First, Ydj1p possesses a CaaX motif (CASQ) that is solely recognized by Ste24p when in context of **a**-factor [5]. Second, suppression of a yeast prion phenotype is supported by independent overexpression of Ste24 and Ydj1p, but not Rce1 (**Figure A.2**). However, the suppression phenotypes may also arise from the independent effects of each protein. Ste24p may directly suppress the prion phenotype, or process a protein other than Ydj1p that mediates suppression. Future studies involving the post translational processing of Ydj1p, and how this may effect prion suppression should be performed in order to elucidate any involvement of Ste24.

Evaluating the effect of arresting Rce1 and Ste24 activity in Trypanosoma brucei

The study described in Chapter 2 demonstrated a dual *CaaX* proteolytic activity associated with the Rce1 and Ste24 othologs encoded in the *Trypanosoma brucei* genome. A previous report detected an activity associated with only Rce1 and was likely due to an inappropriate reporter used to determine Ste24 activity [6]. The same study further demonstrated a lethal phenotype in bloodstream form trypanosomes when the isoprenyl transferase, Rce1, or Icmt expression was silenced using RNAi. Ste24 was not included in this RNAi study. We performed our own RNAi silencing of the *Trypanosoma brucei CaaX* proteases in part to reproduce the original findings and to expand the focus to Ste24. Surprisingly, neither Rce1 nor

Ste24 RNAi-mediate silencing had any effect on growth relative to controls. The discordant observations between our RNAi study and that published may be due to transcription of a suboptimal region of the Rce1 and Ste24 genes in our RNAi transcripts, or overall poor RNAi transcription. Future RNAi studies should be performed using longer target extensions of the Rce1 and Ste24 genes, and transcription should be verified by northern blot analysis.

The effect of arresting Rce1 and Ste24 activity in *Trypanosoma brucei* could be further evaluated by other methods. For example, inhibitors of the enzymes, such as the compounds we identified in Chapter 2, could be used in a dose lethality screen of the parasites. One caveat to this approach is the potential for promiscuous specificity of the compounds. This complication may be mitigated by identifying more potent inhibitors. Chemical alteration of the compounds we identified, or a large-scale library screening could aid the selection process. Towards this effect, a system capable of performing high-throughput screening, such as our established fluorescence assay, should be considered, as well as the use of membrane extracts derived directly from *Trypanosoma brucei* to provide more biologically relevant kinetic information.

Structure determination of ShuS

The study described in Chapter 3 spectroscopically characterized the heme transport protein native to *Neisseria meningitidis*, HmbR. As detailed in Chapter 1, heme and iron transport systems also exist in other pathogenic bacteria, and many details of these systems are unknown. For example, the heme transport operon in *Shigella dysenteriae* involves eight different proteins, four of which are poorly characterized [7, 8]. One of these is ShuS, which has been suggested to serve a variety of functions, including heme degradation, preventing heme toxicity, and enhancing heme utilization [8].

To better characterize the function of ShuS, we performed hanging drop crystal screens to obtain diffraction quality crystals for structure determination. Our initial screen yielded ShuS crystals in a solution containing 30% PEG 8K, and 100 mM Tris pH 8.5. Crystals grown in this condition were mounted and tested for diffraction using a diffractometer. Representative crystals used and the resulting diffraction pattern are shown in **Figure A.3**. To enhance the resolution, we performed an optimization screen on the crystallization conditions using additive screens I and II (Hampton), and varying the PEG 8K concentration. We identified six conditions that yielded ShuS crystals. These are summarized in **Table A.1**. Additional crystallographic studies on ShuS should utilize these conditions to obtain crystals for diffraction and structure determination at an appropriate synchrotron facility.

MATERIALS AND METHODS

Construction of Plasmids encoding Ydj1 Orthologs – Yeast expression plasmids were created by PCR-directed recombination-mediated plasmid construction [9]. In brief, the open reading frames (ORFs) of Xdj1, JJJ2, and DnaJA2 (accession numbers CAA97651, P46997, and NM005880, respectively) were inserted behind the phosphoglucokinase driven promoter contained in pWS28. For Xdj1 and JJJ2, the ORFs were amplified by PCR from *Saccharomyces cerevisiae* genomic DNA using yWS198 and yWS829, respectively, while DnaJA2 was amplified from cDNA derived from human liver. The PCR products were co-transformed into yeast with pWS28 that had been linearized with XmaI. To facilitate recombination, the PCR products were engineered to contain 39 basepair extensions homologous to sequences immediately 5′ and 3′ of the yeast ORFs encoded in pWS479 and pWS154. The transformed

yeast were plated on selective media (SC-ura) to allow for growth of cells that had formed a circularized plasmid; a linearized plasmid is inefficiently propagated and does not support colony growth on selective media. Independent plasmids were isolated from yeast colonies, reamplified in *E. coli*, and subjected to restriction digest analysis and sequencing to verify the presence and sequences of the Xdj1, JJJ2, and DnaJA2 ORFs.

Determination of Prion Suppression –Prion suppression experiments utilized yeast strains containing a PSI^+ PIN^+ genetic background that confers a predisposition to form prions (gifted to us from the laboratory of Yury Chernoff at Georgia Tech). For determination of Ydj1p prion suppression, GT81-1C was transformed with an empty vector (SM640) or plasmids encoding the known prion suppressor Hsp104 (pWS701), or Ydj1 (pWS882) and allowed to grow at 30 ºC on either SC-Ura, or synthetic complete containing 2% galactose and 2% raffinose, but lacking uracil and adenine (SC-Gal/Raff-Ura/Ade). Prion suppression was determined by growth on SC-Ura, but not SC-Gal/Raff-Ura/Ade.

Ste24 prion suppression was determined by transforming OT55 with either Rce1(pWS716), Ste24(pWS723), an inactive Ste24 mutant (pWS753), or relevant controls (pWS701 and SM334). Transformant colonies were selected and allowed to grow in SC-Gal/Raff-Ura for 3 days, upon which they were serially diluted and plated onto SC-Gal/Raff-Ura/Ade solid media.

REFERENCES

1 Boyartchuk, V., Trueblood, C., Vik, A. and Rine, J. (1997) Roles of CAAX proteases in **a**-factor and Ras maturation. In Yeast Cell Biology (Davis, T., Rose, M. and Stevens, T.), Cold Spring Harbor, NY

2 Leung, K. F., Baron, R., Ali, B. R., Magee, A. I. and Seabra, M. C. (2007) Rab GTPases containing a CAAX motif are processed post-geranylgeranylation by proteolysis and methylation. Journal of Biological Chemistry. **282**, 1487-1497

3 Roberts, P. J., Mitin, N., Keller, P. J., Chenette, E. J., Madigan, J. P., Currin, R. O., Cox, A. D., Wilson, O., Kirschmeier, P. and Der, C. J. (2008) Rho Family GTPase modification and dependence on CAAX motif-signaled posttranslational modification. J Biol Chem. **283**, 25150-25163

4 Sinensky, M., Fantle, K., Trujillo, M., McLain, T., Kupfer, A., Dalton, M. (1994) The processing pathway of prelamin A. J Cell Sci. **107**, 61-67

5 Plummer, L. J., Hildebrandt, E. R., Porter, S. B., Rogers, V. A., McCracken, J. and Schmidt, W. K. (2006) Mutational analysis of the ras converting enzyme reveals a requirement for glutamate and histidine residues. J Biol Chem. **281**, 4596-4605

6 Gillespie, J. R., Yokoyama, K., Lu, K., Eastman, R. T., Bollinger, J. G., Van Voorhis, W. C., Gelb, M. H. and Buckner, F. S. (2007) C-terminal proteolysis of prenylated proteins in trypanosomatids and RNA interference of enzymes required for the post-translational processing pathway of farnesylated proteins. Mol Biochem Parasitol. **153(2)**, 115-124

7 Wyckoff, E. E., Duncan, D., Torres, A. G., Mills, M., Maase, K. and Payne, S. M. (1998) Structure of the Shigella dysenteriae haem transport locus and its phylogenetic distribution in enteric bacteria. Molecular Microbiology. **28**, 1139-1152

8 Wyckoff, E. E., Lopreato, G. F., Tipton, K. A. and Payne, S. M. (2005) Shigella dysenteriae ShuS promotes utilization of heme as an iron source and protects against heme toxicity. Journal of Bacteriology. **187**, 5658-5664

9 Oldenburg, K. R., Vo, K. T., Michaelis, S. and Paddon, C. (1997) Recombination-mediated PCR-directed plasmid construction in vivo in yeast. Nucleic Acids Res. **25**, 451-452

Table A.1 Optimized crystallization conditions of ShuS

[Tris], pH 8.5	[PEG 8K]	Additive	Protein: Solution ratio[1]
100mM	10%	11.1 mM MgCl	1:1
100mM	10%	16.5 mM MgCl	3:1
100mM	20%	12.9 mM Spermine tetra-HCl	3:1
100mM	20%	12.9 mM StCl	3:1
100mM	20%	13.8 mM CaCl	3:1
100mM	20%	10.5 mM BaCl	3:5

[1] 4μL final volume

Figure A.1 *Temperature sensitivity evaluations of Ydj1 and CaaX protease deleted constructs.* **A**) Plasmids encoding DnaJA2 (pWS940), JJJ2 (pWS931), or Xdj1 (pWS935) were transformed into a *ydj1*Δ temperature sensitive yeast strain (yWS304) and assessed for growth after 3 days at 34.5º. DnaJA2, a human ortholog, has a strong rescuing effect, while JJJ2 and Xdj1, yeast chaperones related to Ydj1, have an intermittent effect to no effect, respectively. **B**) Yeast strains devoid of Rce1 (SM3689), Ste24 (SM3375), or both *CaaX* proteases (yDM1) are not temperature sensitive when grown at 37.0º. The positive and negative controls were BY4741 (wt) and yWS304 (*ydj1*Δ), respectively.

A.

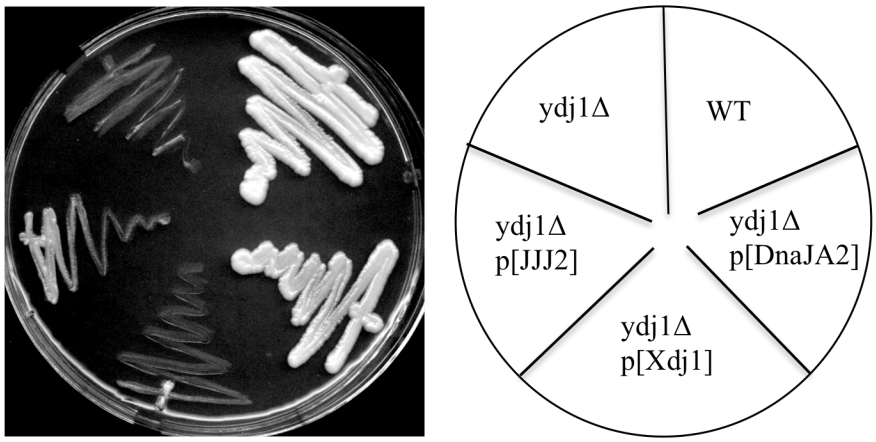
ydj1Δ
WT
ydj1Δ
p[JJJ2]
ydj1Δ
p[DnaJA2]
ydj1Δ
p[Xdj1]

B.

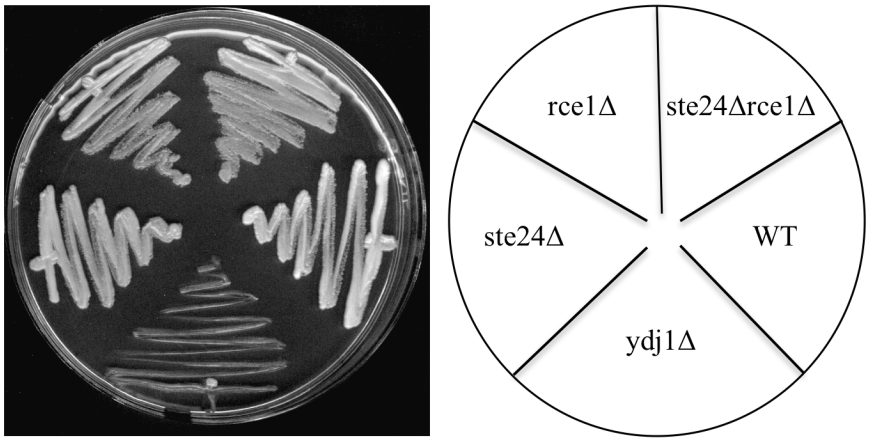
rce1Δ
ste24Δrce1Δ
ste24Δ
WT
ydj1Δ

Figure A.2 *Prion suppression conferred by independent expression of Ydj1and Ste24.* **A**) GT81-1C was transformed with Ydj1 (pWS882) and plated onto synthetic complete solid media containing 2% galactose and 2% raffinose, but lacking uracil and adenine (Sc-Gal/Raff-Ura/Ade). The SC-Ura plates serve as internal standards to compare transformation efficiencies between different plasmids. **B**) Ste24 expression suppresses a prion phenotype. The yeast strain OT55 was transformed with Rce1 (pWS716), Ste24(pWS723), and an inactive Ste24 mutant, Ste24H297A (pWS753), grown in liquid media (SC-Gal/Raf/Ura) for 3 days and serially diluted and plated onto Sc-Gal/Raff-Ura/Ade solid media. For both A and B, an empty vector (SM640 and SM334, respectively) and the strong prion suppressor Hsp104 (pWS701) served as negative and positive controls, respectively. Prion suppression is indicated if no colonies grow on SC-Gal/Raff-Ura/Ade. Panel B was provided by Emily Hildebrandt, University of Georgia.

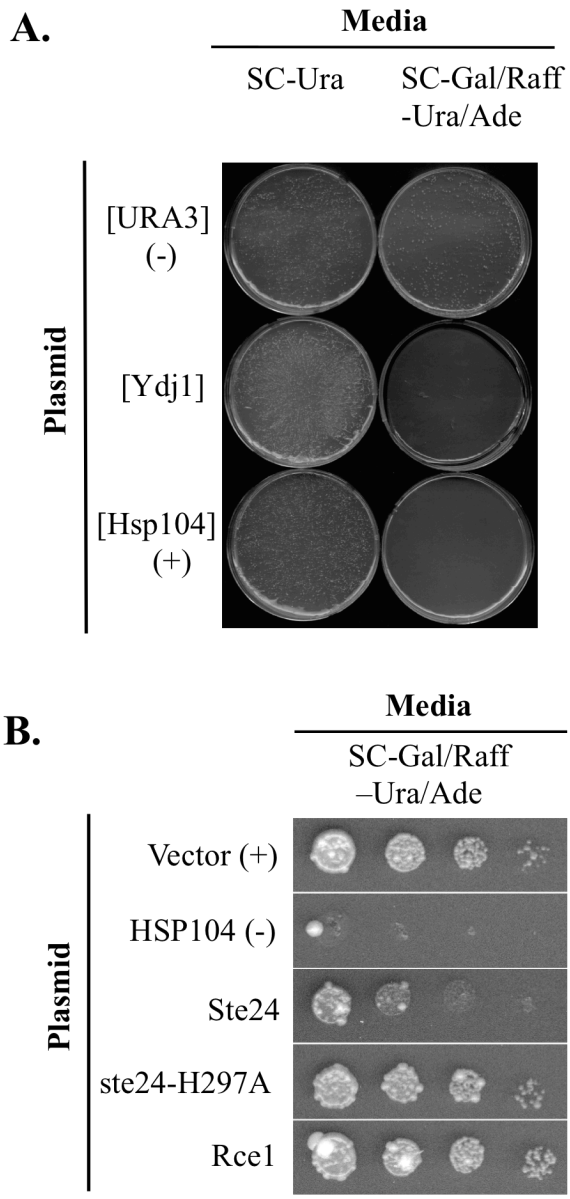
A.
Media
SC-Ura
SC-Gal/Raff
-Ura/Ade
Plasmid
[URA3]
(-)
[Ydj1]
[Hsp104]
(+)
B.
Media
SC-Gal/Raff
–Ura/Ade
Plasmid
Vector (+)
HSP104 (-)
Ste24
ste24-H297A
Rce1

Figure A.3 *Crystals and diffraction of ShuS*

A) Representative crystals of ShuS derived from the conditions described in Table A.1. B) Diffraction to approximately 4Å of ShuS crystals. Data was collected from a RU 200 diffractometer at the University of Georgia and displayed using MOSFLM software.

A.

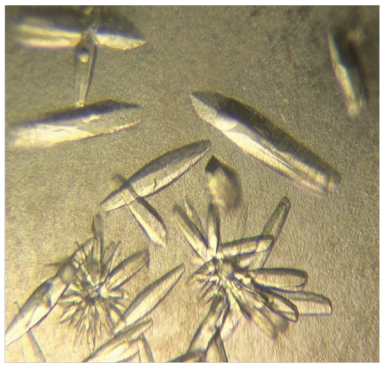

B.

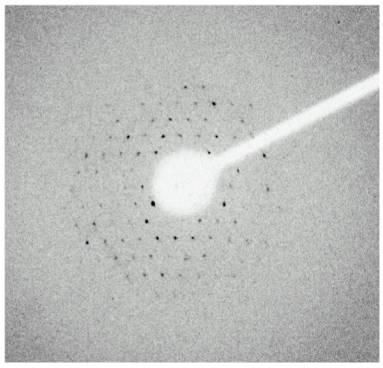

APPENDIX B

INHIBITION OF THE CAAX PROTEASES RCE1P AND STE24P BY PEPTIDYL (ACYLOXY)METHYL KETONES[1]

[1] Stephen B. Porter, Emily R. Hildebrandt, Sarah R. Breevoort, David Z. Mokry, Timothy M. Dore, and Walter K. Schmidt. 2007. *Biochimica et Biophysica Acta*. 1773(6) 853-862

Reprinted here with permission of publisher

The Ste24p K_m value reported here was contributed by David Z. Mokry

ABSTRACT

The CaaX proteases Rce1p and Ste24p can independently promote a proteolytic step required for the maturation of certain isoprenylated proteins. Although functionally related, Rce1p and Ste24p are unrelated in primary sequence. They have distinct enzymatic properties, which are reflected in part by their distinct inhibitor profiles. Moreover, Rce1p has an undefined catalytic mechanism, whereas Ste24p is an established zinc-dependent metalloprotease. This study demonstrates that both enzymes are inhibited by peptidyl (acyloxy)methyl ketones (AOMKs), making these compounds the first documented dual specificity inhibitors of the CaaX proteases. Further investigation of AOMK-mediated inhibition reveals that varying the peptidyl moiety can significantly alter the inhibitory properties of AOMKs toward Rce1p and Ste24p and that these enzymes display subtle differences in sensitivity to AOMKs. This observation suggests that this compound class could potentially be engineered to be selective for either of the CaaX proteases. We also demonstrate that the reported sensitivity of Rce1p to TPCK is substrate-dependent, which significantly alters the interpretation of certain reports having used TPCK sensitivity for mechanistic classification of Rce1p. Finally, we show that an AOMK inhibits the isoprenylcysteine carboxyl methyltransferase Ste14p. In sum, our observations raise important considerations regarding the specificity of agents targeting enzymes involved in the maturation of isoprenylated proteins, some of which are being developed as anti-cancer therapeutic agents.

INTRODUCTION

Rce1p and Ste24p[2] are proteases that mediate the maturation of certain lipid-modified proteins, specifically those whose precursors have a C-terminal tetrapeptide CaaX motif (C-cysteine; a-aliphatic; X-one of several amino acids) [1, 2]. Their substrates (*i.e.,* CaaX proteins) typically undergo three ordered post-translational modifications: covalent attachment of an isoprenoid lipid to the cysteine, proteolytic removal of the aaX tripeptide, and carboxyl methyl esterification of the exposed isoprenylated cysteine [2, 3]. While the proteases share a common function and are both ER-localized integral membrane proteins that possess multiple transmembrane spans, they are otherwise unrelated by primary sequence [4].

Several substrates of Rce1p have been described. Many but not all Rce1p substrates are involved in signal transduction. Some have key roles in cellular transformation (*e.g.* Ras, RhoB). Thus, agents that inhibit the maturation of CaaX proteins are hypothesized to have chemotherapeutic potential [3, 5]. The testing of this hypothesis has led to the development of farnesyltransferase inhibitors that are being examined for their ability to moderate tumor growth [6-9]. The inhibition of Rce1p holds similar anti-cancer potential [3, 10, 11]. By contrast, few substrates have been described for Ste24p. One specific target is the lamin A precursor. Defects in lamin A maturation are associated with abnormal musculo-skeletal development, varied laminopathies, and progeroid syndromes [12-14]. The only other known target of Ste24p is the precursor of the yeast **a**-factor mating pheromone, which is also a target of Rce1p [1, 15]. For both of its targets, Ste24p appears to catalyze not only CaaX cleavage but also a second cleavage

[2] There are various name designations for the Ras converting enzyme and the Sterile 24 protein - Rce1p and Ste24p/Afc1p (*S. cerevisiae*), Rce1/FACE-2 and Zmpste24/FACE-1 (human), AtRce1/AtFACE-2 and AtSte24 (*A. thaliana*), CeRce1p/CeFACE-2 and CeSte24p/CeFACE-1 (*C. elegans*), and the Type I (Ste24p) and Type II (Rce1p) CaaX proteases. In order to clearly convey the ortholog being described, and with apologies to others who study these enzymes, we have opted to use a standard naming convention for these enzymes – a species identifier followed by Rce1p or Ste24p.

distal to the farnesylated cysteine [16, 17]. Other targets of Ste24p likely exist but have not yet been identified. The yeast **a**-factor precursor is thus far unique as a CaaX protein in being a substrate of both Ste24p and Rce1p [1]. Once processed by either Rce1p or Ste24p, CaaX proteins are obligatory substrates of the isoprenylcysteine carboxyl methyltransferase (ICMT) [18]. The minimum recognition determinant for this ER-localized membrane protein is a farnesyl cysteine [19, 20]. Both proteolysis and carboxyl methylation can significantly alter the function, localization, and other properties of CaaX proteins [1, 10, 21].

The modern classification system for proteases designates four categories of proteolytic mechanisms: serine/threonine, cysteine, aspartic, and metal-dependent. Ste24p is a zinc-dependent metalloprotease. As expected, Ste24p possesses a consensus zinc metalloprotease motif that is essential for its activity, requires zinc for optimal activity, and is inhibited by zinc chelating compounds such as 1,10-phenanthroline [16, 22]. By contrast, the mechanistic classification of Rce1p has eluded definition, primarily because it lacks a readily identifiable protease motif. Rce1p has also been refractory to purification, which has hindered detailed biochemical and structural analysis of this integral membrane protein.

Rce1p is reportedly sensitive to certain serine/cysteine protease inhibitors (*e.g.* TPCK), and this sensitivity has been used in part to support a proposed cysteine protease classification for Rce1p [23-26]. Nevertheless, TPCK-sensitivity should be viewed cautiously when used as an indicator of protease classification because TPCK covalently modifies the active site histidine residues of both serine and cysteine proteases (*e.g.* chymotrypsin and papain, respectively), and possibly other catalytic types. Moreover, Rce1p is insensitive to thiol-modifying agents such as NEM and iodoacetamide, which further counters a cysteine protease classification for this enzyme [24, 27]. Certain mutational studies are also inconsistent with a cysteine protease

classification for Rce1p [28]. Supporting a proposed metalloprotease classification for Rce1p are the observations that it requires certain glutamate and histidine residues for activity and its inhibition by 1,10-phenanthroline [24, 28]. Nevertheless, the partial sensitivity of Rce1p to a non-chelating form of phenanthroline (*i.e.,* 4,7-phenanthroline) suggests that the inhibition by this compound class may be unrelated to chelating effects. It is also formally possible that Rce1p utilizes a novel proteolytic mechanism. The recent identification of a carboxyl peptidase requiring a Glu-Gln catalytic dyad reveals that additional proteolytic mechanisms may yet be discovered [29].

Several inhibitors of Rce1p in addition to those discussed above have been described [23-27, 30-35]. These fall into two classes: general non-specific inhibitors and substrate mimetics. The first class includes chloromethyl ketones, organomercurials (*e.g.* MSA, PHMB, and PHMS), and certain metal ions (*i.e.,* Cu^{2+} and Zn^{2+}). Rce1p is reportedly insensitive to many broad-spectrum inhibitors, such as EDTA, EGTA, antipain, chymostatin, pepstatin A, leupeptin, E64, and is partially sensitive to MMTS. It should be noted that the sensitivity of Rce1p to the serine protease inhibitors PMSF and DFP and the alkylating agent NEM has been inconsistently reported [24, 27, 30, 31]. The second class of Rce1p inhibitors is represented by substrates with non-cleavable peptide bonds, isoprenoid-like compounds, and bisubstrate analogues (*i.e.,* compounds containing both a farnesylmimetic and peptidomimetic). These compounds typically act competitively to inhibit Rce1p, and some have IC_{50} values in the nM range [27, 32, 34-36]. Despite the various studies probing the enzymology and inhibitor profile of Rce1p, the mechanistic classification of Rce1p remains undefined, with cysteine and metalloprotease categories having been independently proposed [24, 37].

In this study, we have compared the inhibitor profiles of Rce1p and Ste24p orthologs using

two primary agents, chloromethyl ketones and peptidyl (acyloxy)methyl ketones (AOMKs). AOMKs were included in our analysis because a pilot screen of about 20 compounds yielded an AOMK as a candidate yeast Rce1p inhibitor. Compounds of this class reportedly inhibit the cysteine protease cathepsin B [38-41], but the impact of AOMKs on Rce1p activity had not previously been reported. We evaluated three distinct orthologs of each enzyme to assess whether enzymatic profiles are evolutionarily conserved within each group and investigated the inhibitor profiles of these enzymes using two distinct assays to independently confirm our observations. The orthologs were all expressed using the yeast system to aid comparative evaluations. We present evidence that the inhibition of Rce1p and Ste24p by cholоromethyl ketones is substrate-specific, and we report for the first time that AOMKs can inhibit both of the CaaX proteases as well as the yeast ICMT Ste14p. Additionally, we demonstrate that the peptidyl portion of AOMKs can modulate the inhibitory properties of this class of agent. Besides providing a new reagent that may be useful for probing the enzymology of CaaX modifying enzymes, this study underscores the caution that must be taken when evaluating the inhibitor profiles of these enzymes.

MATERIALS AND METHODS

Yeast Strains and Plasmids – The yeast strains used in this study were SM3614 (*MAT***a** *trp1 leu2 ura3 his4 can1 ste24*Δ*::LEU2 rce1*Δ*::TRP1*) and RC757 (*MAT*α *sst2-1*) [15, 42]. Plasmid-bearing versions of SM3614 were generated by transformation with the indicated plasmids according to published methods [43]. Transformed strains were routinely grown at 30 °C on synthetic complete dropout (SC-) media, as previously described [44]. The Rce1p, Ste24p, and Ste14p-encoding plasmids used in this study have previously been described and are listed in **Table B.1**.

Substrate Reagents – The peptide substrates used in this study were made synthetically. The fluorogenic substrates ABZ-KSKTKC(farnesyl)Q_LIM, ABZ-KSKTKC(farnesyl)VQ_LM, and ABZ-KSKTKC(farnesyl)VIQ_L were initially obtained from Wyeth Research (Pearl River, NY) and subsequently purchased from AnaSpec (San Jose, CA). ABZ is aminobenzoic acid, and Q_L is lysine ε-dinitrophenyl. The **a**-factor-based substrate YIIKGVFWDPAC(farnesyl)VIA was purchased from California Peptide (Napa, CA).

Peptidyl (acyloxy)methyl ketones and other compounds – Several distinct AOMKs were evaluated in this study (**Figure B.1**). Z-Phe-Lys-2,4,6-trimethylbenzoyloxymethyl ketone (FKBK$(CH_3)_3$) was purchased from Bachem (Torrance, CA). A Phe-Ala derivative (FABK$(CH_3)_3$) was a gift from Dr. Jan Potempa (Jagiellonian University, Poland), and was subsequently synthesized in house according to standard chemical methods that will be described elsewhere (Porter, Deshert, Breevoort, Hembree, Dore and Schmidt, in preparation). Phe-Arg (FRBK$(CH_3)_2$), Phe-Gly (FGBK$(CH_3)_2$), AcTyr-Phe-Arg (YFRBK$(CH_3)_2$), and AcTyr-Phe-Gly (YFGBK$(CH_3)_2$) derivatives were obtained from Dr. Matthew Bogyo (Stanford University). Additional amounts of FRBK$(CH_3)_2$ and FGBK$(CH_3)_2$ were synthesized in house according to standard chemical methods that will be described elsewhere (Porter, Dechert, Breevoort, Hembree, Dore and Schmidt, in preparation). All inhibitors were dissolved in DMSO, with the exception of TLCK, which was dissolved in H_2O. Other chemical reagents were purchased from Sigma-Aldrich.

In vitro fluorescence-based CaaX proteolysis assay - An established fluorescence-based assay was used to monitor Rce1p-dependent cleavage of a quenched fluorogenic peptide substrate [36]. By using a slightly different substrate, this assay was adapted to monitor Ste24p activity. In brief, the assay involves mixing an appropriate fluorogenic substrate with membranes derived

from yeast over-expressing the appropriate CaaX protease. The membranes used as the source of activity were isolated as 1 mg/ml total protein stocks in Lysis Buffer (50 mM Tris, pH 7.5, 0.2 M sorbitol, 1 mM EDTA, 0.2% NaN_3, protease inhibitors CLP, aprotinin, PMSF) according to our reported methods [22, 28]. Prior to use, the membranes were diluted to 0.5 mg/ml with Assay Buffer (100 mM HEPES, pH 7.5, 5 mM $MgCl_2$) and preincubated with DMSO or inhibitors for 10 min at 30 °C, unless otherwise indicated. The substrate was typically diluted with Assay Buffer to 40 μM from a 1 mM stock; a range of concentration (0-200 μM) was used in instances where kinetic parameters were sought. Assays were initiated by mixing equal volumes (50 μl) of the membrane and substrate dilutions in a 96-well plate suitable for use in a microtiter plate fluorometer. The fluorescence in the samples was measured at 420 nm every 30 sec over a 35-60 min time course at 30 °C using either a SpectraMax Gemini EM fluorometer (Molecular Devices) or a Bio-Tek Synergy fluorometer equipped with a 320/420 nm excitation/emission filter set. The collected data were graphed and initial linear slopes determined using Microsoft Excel. These values were used to calculate % activities relative to the DMSO-treated enzyme, which was always included as a control in each reaction set.

Kinetic Analyses - Kinetic parameters were typically determined using nonlinear regression methods (Prism 4.0 GraphPad Software Inc.). The Kitz-Wilson approach was used to compare the time-dependent interactions of TPCK and $FKBK(CH_3)_3$ with Rce1p [Kitz, 1962 #2761]. According to the associated theory, an irreversible active-site directed inhibitor of an enzyme should show a linear decrease in $\ln[E_t/E_0]$ with time of incubation, where E_t is the activity at time t and E_0 is the activity of the uninhibited enzyme at time zero; the slope of this line is defined as the apparent inactivation rate K_{app}. TPCK was previously shown to be an irreversible active-site inhibitor of bovine Rce1p by this analysis [Chen, 1996 #2290].

In vitro a-factor-based CaaX proteolysis assay – An established assay was used for the *in vitro* production of bioactive **a**-factor from the farnesylated pentadecapeptide precursor YIIKGVFWDPAC(farnesyl)VIA [16]. In brief, the assay involves mixing membranes derived from yeast over-expressing the appropriate CaaX protease with the farnesylated substrate. The membranes were isolated and diluted for the assay as described above. The substrate was diluted from a 100 μM stock to 40 μM using Assay Buffer (see above). Assays were initiated by mixing equal volumes (10 μl each) of the substrate and membrane components in a 96-well plate suitable for use in a PCR thermocycler. After an 8 min incubation at 30 °C, the samples were heated to 95 °C for 1 min to inactivate enzymatic activity, cooled, and supplemented with S-adenosylmethionine (1.7 mM final) and yeast membranes containing the Ste14p ICMT (0.33 mg/ml final) to initiate carboxyl methylation of cleaved products. For reactions with limited S-adenosylmethionine and Ste14p, the concentrations were 160 μM and 0.1 mg/ml respectively. The Ste14p-membranes were derived from a CaaX protease-deficient strain as previously described [16]. After 60 min of incubation at 30 °C, the samples were supplemented with copper sulfate (1.2 mM final) to stop the methylation reaction. The **a**-factor activity in each sample was determined using a biological response assay in which yeast supersensitive to the **a**-factor mating pheromone (RC757) undergo growth arrest in the presence of 7 nM or greater concentrations of pheromone [45]. The activity observed for a two-fold dilution series of a sample was compared to that of other samples for an assessment of relative activity measurements.

Inhibitor and Chaotropic Agent Treatments - To assess the inhibition by the compounds described in this study, the above assay protocols were modified such that diluted membrane samples were pretreated with the appropriate compound or control (DMSO or H_2O) for 10 min at 30 °C prior to use. The pre-treated sample was split into two portions for use in each assay when

evaluating substrate-specific effects. For reversibility experiments, pre-treated membranes were recovered by centrifugation at 16,000g for 15 min, washed twice with 2-fold excess of Wash Buffer (a 1:1 ratio of Lysis Buffer and Assay Buffer) containing varying amounts of NaCl (0-1.5 M) or urea (0-0.125 M), and finally resuspended to the original input volume with Wash Buffer lacking added salt or urea. The resuspended membranes were used directly in the fluorescence-based assay along with an unprocessed control to confirm that inefficient membrane recovery was not the reason for observed decreases in activity.

RESULTS

Peptidyl (acyloxy)methyl ketones inhibit Rce1p

The enzymes evaluated in this study were isolated from CaaX protease deficient yeast (*MAT***a** *rce1*Δ *ste24*Δ) engineered to over-express the human, plant (*A. thaliana*), or native yeast Rce1p enzyme. Because the yeast CaaX proteases localize to the endoplasmic reticulum (ER) compartment in yeast, enriched ER membranes were used as the source of enzyme activity for our experiments [4]. Using a previously described fluorescence-based activity assay designed for human Rce1p, we observed Rce1p dependent activity for all three orthologs. Despite the common expression system and activity assay, the specific activities for the isolated membranes were quite distinct, with yeast Rce1p-containing membranes having the highest value (3.48 nmol/min/mg of total membrane protein), which was followed by plant and human Rce1p-containing membranes (0.89 and 0.10 nmol/min/mg, respectively). The activity observed was dependent on Rce1p since membranes derived from yeast deficient in CaaX proteases had inconsequential activity in this assay (0.0014 nmol/min/mg). The reason for the varied specific activities is unknown but could be attributable to differential enzymatic properties, expression, localization, and/or substrate specificity. For example, the specific activity of plant Rce1p is

two-fold higher at pH 6.0 than at pH 7.5 (the pH used in this study) while yeast Rce1p has optimal activity at pH 7.5 and 35% less activity at pH 6.0.

Using the fluorescence assay, we evaluated the inhibitor profile of the three Rce1p orthologs. To facilitate cross-species comparisons, the observed activities for each ortholog were normalized to an appropriate mock treated control. Our analysis revealed that the orthologs were all inhibited by TPCK and, to a lesser extent, by TLCK (**Figure B.2**). Variations in sensitivity were observed. For example, yeast Rce1p appeared least sensitive to chloromethyl ketones by comparison to the other enzymes, while human Rce1p had an increased sensitivity to TLCK by comparison. When AOMKs were evaluated, we observed that FKBK$(CH_3)_3$ inhibited all three Rce1p orthologs. Variations in sensitivity to FKBK$(CH_3)_3$ were also observed. For example, the human enzyme was relatively more sensitive than either the yeast or plant enzyme. The related compound FABK$(CH_3)_3$ inhibited the three Rce1p orthologs to a much lesser degree, even at concentrations as high at 1 mM (86%, 87% and 74% activity for *Sc*, *At* and *Hs* Rce1p respectively). This suggests that the dipeptidyl portion of this class of compound impacts inhibitor specificity by some manner. Generally, the three Rce1p enzymes were found to be sensitive to TPCK and FKBK$(CH_3)_3$ and relatively less sensitive to TLCK and FABK$(CH_3)_3$.

Because of the observed inhibition of Rce1p by FKBK$(CH_3)_3$, we evaluated additional AOMKs using the Ras-based fluorescence assay. The dipeptidyl AOMK FRBK$(CH_3)_2$ and tripeptidyl AOMK YFRBK$(CH_3)_2$ are similar to FKBK$(CH_3)_3$ in that they have a charged amino acid in the last position of the peptidyl portion of the compound (**Figure B.1**); they mainly differ in having distinct peptidyl moieties and two rather than three methyl substitutions on the benzoyl group. FRBK$(CH_3)_2$ inhibited Rce1p and was the most potent Rce1p inhibitor of the AOMKs evaluated, whereas YFRBK$(CH_3)_2$ was the least inhibitory (**Table B.2**). The dipeptidyl AOMK

FGBK$(CH_3)_2$ and tripeptidyl YFGBK$(CH_3)_2$ are similar to FABK$(CH_3)_3$ in that they have a small uncharged amino acid in the last position of the peptidyl portion. None of these compounds inhibited Rce1p activity. Our results suggest that a positively charged amino acid in the last position of the dipeptidyl moiety of the AOMK is required for the ability of this compound class to inhibit Rce1p.

The inhibition of yeast Rce1p by TPCK is substrate-specific

To independently confirm the inhibitory effects of TPCK and certain AOMKs, we evaluated these compounds using a coupled CaaX proteolysis-methylation assay that generates the bioactive **a**-factor mating pheromone [16]. This assay utilizes a distinct substrate and readout that essentially eliminates any interference arising from unanticipated autofluorescing or quenching properties associated with compounds being evaluated. Using the coupled assay, we surprisingly observed that TPCK did not significantly inhibit **a**-factor production (**Figure B.3**). An aliquot of the same TPCK-treated sample demonstrated reduced Rce1p activity when evaluated using the fluorescence assay (**Figure B.3B**, lower panel). Except for the nature of the substrate, the reaction conditions for the proteolytic step in both assays were identical (*i.e.,* the same buffer and concentrations of substrate and membrane). The activity observed in the presence of TPCK in the **a**-factor assay cannot be attributed to an unaccounted **a**-factor-specific proteolytic activity because membranes lacking Rce1p and Ste24p have insignificant activity in this assay [16]. Unlike TPCK, FKBK$(CH_3)_3$ inhibited regardless of the assay used. Consistent with our previous observations, neither TLCK nor FABK$(CH_3)_3$ inhibited Rce1p to any significant extent when evaluated using the **a**-factor assay.

Inhibition of Rce1p by FKBK$(CH_3)_3$ is not readily reversible

As a first step toward investigating the nature of interaction between AOMKs and Rce1p, we

evaluated whether FKBK$(CH_3)_3$-mediated inhibition was readily reversible by washing inhibitor-treated membranes with buffers containing salt (0-1.5 M NaCl) or urea (0-0.125 M). The washes themselves did not significantly affect the activity of untreated Rce1p by comparison to an unwashed sample (data not shown). Using this approach, we observed that FKBK$(CH_3)_3$-treated Rce1p could not be reactivated by any of the wash conditions employed (**Table B.3**).

To further resolve the inhibitory mechanism of FKBK$(CH_3)_3$, we examined the kinetics of enzyme inhibition. This analysis revealed that FKBK$(CH_3)_3$ reduced the V_{max} of Rce1p in a dose-dependent manner (**Figure B.4A and B**). TPCK-treatment at the same concentration also reduced the V_{max} of Rce1p, but to a lesser extent. The observed K_m values were essentially unchanged relative to the untreated control. Linear transformations of the kinetic data (*e.g.*, Lineweaver-Burke analysis) revealed that inhibition by FKBK$(CH_3)_3$ could be attributable to either a reversible noncompetitive or irreversible mechanism. By point of comparison, TPCK is reportedly an irreversible active-site inhibitor of Rce1p [23]. One characteristic of this type of inhibitor is that the extent of inhibition depends on time of exposure. We found that FKBK$(CH_3)_3$ did not inhibit Rce1p in a time-dependent manner (**Figure B.4C**) [23]. We should also note a complicating issue regarding our analysis of kinetic parameters. During the course of our investigations, we determined that FKBK$(CH_3)_3$ partitions onto yeast membranes in a non-selective manner (**Figure B.4D**). This observation suggests that the amount of free inhibitor in solution is actually less than predicted in our assays. This property would necessarily lead to an overestimation of IC_{50} and could alter the kinetic parameters observed in the presence of this compound.

<u>Ste24p can be inhibited by AOMKs</u>

In order to further understand the specificity of chloromethyl ketones and AOMKs, we

sought to determine the inhibitor profile of Ste24p in relationship to these agents. For this study, we developed a fluorescence-based assay to monitor Ste24p activity. Initially, we evaluated the Rce1p substrate (CQ_LIM) for its ability to be cleaved by yeast Ste24p and determined that it was a poor substrate (**Figure B.5**); similar results were obtained for plant and human Ste24p (Porter and Schmidt, unpublished observation). We next evaluated isoprenylated substrates that differed only in the placement of the quenching group. This analysis revealed that yeast Ste24p had a marked preference for the quencher at either the a_2 (CVQ_LM) or X position ($CVIQ_L$) of the CaaX motif relative to the a_1 position (CQ_LIM), while yeast Rce1p had a marked preference for the quencher at the a_1 position. Using the $CVIQ_L$ fluorogenic substrate, we determined the specific activities of several Ste24p orthologs. These values varied as had been observed for the Rce1p orthologs. Yeast Ste24p had the highest specific activity, followed by the human and plant enzymes (9.41 nmol/min/mg, 1.43 nmol/min/mg, 1.01 nmol/min/mg of total membrane protein, respectively). To our knowledge, this is the first assay described that is amenable for kinetic analyses of Ste24p activity. Accordingly, we have determined that yeast Ste24p has a K_M of 10.9 μM using the $CVIQ_L$ fluorogenic substrate and nonlinear regression methods.

Using the fluorescence-based assay, we evaluated the inhibitor profile of three Ste24p orthologs (*Sc* Ste24p, *At* Ste24p, and *Hs* Ste24p). $FKBK(CH_3)_3$ consistently inhibited these enzymes (**Figure B.6**). $FABK(CH_3)_3$ was a weak inhibitor at best, with human Ste24p appearing to be the most sensitive of the group. Neither TPCK nor TLCK had significant inhibitory activity. Yeast Ste24p was also determined to be inhibited by $FRBK(CH_3)_2$, but not by $FGBK(CH_3)_2$ or tripeptidyl AOMKs (**Table B.2**). To investigate whether the observed inhibition profile of Ste24p was substrate-specific, we evaluated the effects of these compounds using the **a**-factor based assay. Paralleling our results with Rce1p, we observed that TPCK did not inhibit

yeast Ste24p, whereas FKBK$(CH_3)_3$ remained a potent inhibitor by comparison (**Figure B.7**). Like Rce1p, we also observed that the inhibition of Ste24p by FKBK$(CH_3)_3$ was not readily reversible (**Table B.3**).

FKBK$(CH_3)_3$ inhibits the Ste14p ICMT

The ability of FKBK$(CH_3)_3$ to inhibit both Rce1p and Ste24p prompted us to examine whether the isoprenylcysteine carboxyl methyltransferase (ICMT) was a target of this compound. The integral membrane protein Ste14p is the yeast ICMT [20]. To investigate this issue, we took advantage of the fact that **a**-factor production relies on a coupled assay having distinct proteolytic and methylation steps (Steps 1 and 2, respectively). Thus, the inhibition of Ste14p can be evaluated by simply adding the agent after proteolysis has been completed and the protease heat-inactivated (Step 1). Under standard reaction conditions where Ste14p activity was added in excess, FKBK$(CH_3)_3$ had only a modest inhibitory effect on **a**-factor production when added during Step 2 (**Figure B.8A**). The inhibition was less than that observed when added during Step 1, suggesting that FKBK$(CH_3)_3$ does indeed inhibit the CaaX proteases and that the loss of activity observed in the **a**-factor assay with this compound is due to synergistic inhibition of the CaaX protease and ICMT. The inhibitory effect of FKBK$(CH_3)_3$ was exaggerated when limiting amounts of Ste14p were present in the reaction (**Figure B.8B**), demonstrating that the ICMT is indeed inhibited by FKBK$(CH_3)_3$.

DISCUSSION

This study reports several new findings. First, we document using a single expression system that Rce1p orthologs have a similar inhibitor profile to certain agents (**Figure B.2**). This observation, when combined with the observation that Rce1p orthologs have conserved substrate specificity, strengthens the assertion that enzymatic studies of yeast Rce1p and other non-human

orthologs will ultimately lead to a better understanding of the human enzyme, which is of biomedical importance [28]. Second, our study demonstrates that TPCK is an unreliable diagnostic inhibitor of Rce1p (**Table B.2** and **Figure B.3**). This finding suggests the use of caution when interpreting previous studies where TPCK was used in efforts to define the mechanistic class of the enzyme [24, 27]. Lastly, we describe peptidyl AOMKs as novel agents that inhibit both Rce1p and Ste24p (**Table B.2**), and in doing so we developed a new *in vitro* assay for monitoring Ste24p activity (**Figure B.5** and **Figure B.6**). The AOMKs themselves represent new and potentially useful tools for investigating Rce1p and Ste24p enzymology that can perhaps serve as the basis for developing more potent inhibitors of these enzymes. This latter point is supported by the observation that varying the peptidyl moiety of AOMKs can yield an improved Rce1p inhibitor (*i.e.* FRBK$(CH_3)_2$). While no single AOMK evaluated in this study was absolutely specific for either Rce1p or Ste24p, our observation that Rce1p and Ste24p display differential sensitivity to certain AOMKs suggests that Rce1p or Ste24p specific inhibitors might be extractable from this class of compounds (**Table B.2**).

Our observation that substrate context impacts the effectiveness of Rce1p inhibitors could explain the inconsistent effect of serine protease inhibitors and alkylating agents on Rce1p activity [24, 27, 30, 31]. We thus suggest that evaluating inhibitors of Rce1p in the context of multiple substrates is the best way to fully ascertain the inhibitory properties of a particular compound for this multi-substrate enzyme. Rce1p mutants should be similarly evaluated since we have observed that the activities of certain Rce1p mutants are substrate dependent [28]. We suspect that substrate context may also explain why yeast Rce1p C251A is reported to be both active and inactive [24, 28]. While we do not observe activity defects for Rce1p C251A when using any of our *in vitro* or *in vivo* assays, it remains a formal possibility that the initial report on

this particular mutant utilized an enzyme/substrate combination that uncovers sensitivities that our combinations did not. The fact that most studies of Rce1p have been performed using a single enzyme/substrate combination certainly raises important concerns regarding the interpretation of reported data. We fully expect to continue evaluating Rce1p in the context of multiple substrates because of this issue.

Despite AOMKs being described as cysteine protease-specific inhibitors that are proposed to mediate their effects through covalent modification of an active site cysteine residue, it is unlikely that this mechanism applies in the context of Rce1p. First, we have observed that yeast Rce1p C251A is fully functional [28]; C251 is the only cysteine found among Rce1p orthologs that is invariably conserved. Moreover, we have observed that FKBK$(CH_3)_3$ inhibits Rce1p C251A to the same extent as the wildtype enzyme. Second, the fact that Ste24p and Ste14p, two enzymes reportedly lacking active site cysteine residues, are inhibited by FKBK$(CH_3)_3$ argues against a cysteine-directed modification. Lastly, mutational and bioinformatic analyses do not support Rce1p being a cysteine protease.

All together, our kinetic data suggest that FKBK$(CH_3)_3$ is a tightly bound but otherwise reversible noncompetitive inhibitor of Rce1p. We do not believe that FKBK$(CH_3)_3$ acts as an irreversible inhibitor FKBK$(CH_3)_3$ because it lacks time dependent behavior, but we cannot formally exclude that FKBK$(CH_3)_3$ acts faster than we can measure with our existing assays. Another caveat that must be considered is the propensity of FKBK$(CH_3)_3$ to partition with yeast membranes. This property necessarily alters the amount of free inhibitor available for interacting with Rce1p and could markedly alter our reported IC_{50} values and kinetic parameters. Whether other reported Rce1p inhibitors have the same property has not been addressed, but should be considered given our observations. Despite the above caveats, it is clear that FKBK$(CH_3)_3$

inhibits three distinct enzymes involved in CaaX protein maturation. Among several possible explanations for this observation, we suggest that FKBK$(CH_3)_3$ might be an allosteric inhibitor that binds to a common structural feature that is possessed by Rce1p, Ste24p, and Ste14p. Alternatively, FKBK$(CH_3)_3$ may perturb some aspect of membrane association or metal ion coordination, the latter being proposed as a shared property of these enzymes [Anderson, 2005 #2828; Schmidt, 2000 #2227; Pei, 2001 #2567; Tam, 2001 #2519].

As for TPCK, our data are consistent with it being an irreversible inhibitor of yeast Rce1p, which is the reported mechanism described for this agent in the context of bovine Rce1p [Chen, 1996 #2290]. It is challenging to explain, however, the apparent substrate-specific inhibitory properties of TPCK. Among several possibilities, we suggest that the presence of TPCK at the active site interferes with the binding of low-affinity substrates (i.e. the highly charged K-Ras4b based fluorescent peptide) more so than high affinity substrates (i.e. the highly hydrophobic **a**-factor based peptide). It is also plausible that TPCK might bind Rce1p in a way that induces allosteric effects that alter substrate binding in a similar manner. Of note, TPCK is not the only substrate-specific inhibitor of Rce1p. In a recent screen aimed at identifying small molecule *in vitro* inhibitors of Rce1p, over 80% of hits found to inhibit cleavage of the fluorogenic K-Ras4b substrate were determined to be ineffective at preventing Rce1p-dependent **a**-factor production [49]. Clearly, determining the structure of Rce1p in complex with TPCK, an inhibitory AOMK, or any inhibitor is likely to resolve the mode of inhibition for these agents, but this is a daunting task given that Rce1p is an integral membrane protein possessing multiple membrane spans.

This study has provided new insight into the complex enzymology of Rce1p and new tools for future studies of the CaaX proteases. For example, our observation that dipeptidyl AOMKs can inhibit two presumably distinct proteases suggests that the mechanisms and/or active sites of

the CaaX proteases Rce1p and Ste24p are more similar than previously perceived. Our findings also suggest that AOMKs could be modified into more potent and potentially specific inhibitors of either or both of the CaaX proteases. Finally, this study highlights the important need to evaluate enzyme inhibitors in the context of multiple substrates.

ACKNOWLEDGMENTS

We are grateful to Drs. Claiborne Glover, Kelley Moremen, Jim Travis (all of the University of Georgia), and Jan Potempa (Jagiellonian University, Poland) for technical advice, critical discussions, and access to equipment, Wyeth Pharmaceuticals for providing initial samples of the fluorogenic K-Ras peptide substrates, Dr. Matthew Bogyo (Stanford University) for providing FR, YFR, FG, and YFG based AOMKs, and Andrea Lapham-Cardenas and Victoria Rogers for expert technical assistance. This work was supported by a Georgia Cancer Coalition Distinguished Cancer Clinician/Scientist Scholar award, a grant from the National Institutes of Health (to WKS), and an NIH research grant supplement to Promote Diversity in Health-Related Research (for SBP).

REFERENCES

[1] V.L. Boyartchuk, M.N. Ashby and J. Rine, Science 275 (1997) 1796-800.
[2] S.G. Young, P. Ambroziak, E. Kim and S. Clarke. in (Tamanoi, F. and Sigman, D.S., eds.) The Enzymes, Academic Press, New York, NY 2001, pp. 155-213.
[3] A.M. Winter-Vann and P.J. Casey, Nat Rev Cancer 5 (2005) 405-12.
[4] W.K. Schmidt, A. Tam, K. Fujimura-Kamada and S. Michaelis, Proc Natl Acad Sci USA 95 (1998) 11175-80.
[5] J. Gibbs, Cell 65 (1991) 1-4.
[6] A. Cox and C. Der, Current Opinion in Pharmacology 2 (2002) 388-393.
[7] C. Baum and P. Kirschmeier, Curr Oncol Rep 5 (2003) 99-107.
[8] M.A. Morgan, A. Ganser and C.W. Reuter, Leukemia 17 (2003) 1482-98.
[9] K. Zhu, A.D. Hamilton and S.M. Sebti, Curr Opin Investig Drugs 4 (2003) 1428-35.
[10] E. Kim, P. Ambroziak, J.C. Otto, B. Taylor, M. Ashby, K. Shannon, P.J. Casey and S.G. Young, J. Biol. Chem. 274 (1999) 8383-8390.
[11] M.O. Bergo, P. Ambroziak, C. Gregory, A. George, J.C. Otto, E. Kim, H. Nagase, P.J. Casey, A. Balmain and S.G. Young, Mol Cell Biol 22 (2002) 171-81.
[12] M.O. Bergo, B. Gavino, J. Ross, W.K. Schmidt, C. Hong, L.V. Kendall, A. Mohr, M. Meta, H. Genant, Y. Jiang, E.R. Wisner, N. Van Bruggen, R.A. Carano, S. Michaelis, S.M. Griffey and S.G. Young, Proc Natl Acad Sci U S A 99 (2002) 13049-54.
[13] A.K. Agarwal, J.P. Fryns, R.J. Auchus and A. Garg, Hum Mol Genet 12 (2003) 1995-2001.
[14] S.G. Young, L.G. Fong and S. Michaelis, J Lipid Res 46 (2005) 2531-58.
[15] A. Tam, F. Nouvet, K. Fujimura-Kamada, H. Slunt, S.S. Sisodia and S. Michaelis, J. Cell Biol. 142 (1998) 635-49.
[16] A. Tam, W.K. Schmidt and S. Michaelis, J Biol Chem 276 (2001) 46798-806.
[17] D.P. Corrigan, D. Kuszczak, A.E. Rusinol, D.P. Thewke, C.A. Hrycyna, S. Michaelis and M.S. Sinensky, Biochem J 387 (2005) 129-38.
[18] L. Farh, D. Mitchell and R. Deschenes, Archives of Biochemistry and Biophysics 318 (1995) 113-121.
[19] Q. Dai, E. Choy, V. Chiu, J. Romano, S.R. Slivka, S.A. Steitz, S. Michaelis and M.R. Philips, J. Biol. Chem. 273 (1998) 15030-15034.
[20] J.D. Romano, W.K. Schmidt and S. Michaelis, Mol. Biol. Cell 9 (1998) 2231-47.
[21] M.O. Bergo, G.K. Leung, P. Ambroziak, J.C. Otto, P.J. Casey and S.G. Young, J. Biol. Chem. 275 (2000) 17605-10.
[22] W.K. Schmidt, A. Tam and S. Michaelis, J. Biol. Chem. 275 (2000) 6227-33.
[23] Y. Chen, Y.T. Ma and R.R. Rando, Biochemistry 35 (1996) 3227-37.
[24] J.M. Dolence, L.E. Steward, E.K. Dolence, D.H. Wong and C.D. Poulter, Biochemistry 39 (2000) 4096-104.
[25] J. Cadiñanos, W.K. Schmidt, A. Fueyo, I. Varela, C. Lopez-Otin and J.M. Freije, Biochem J 370 (2003) 1047-54.
[26] J. Cadiñanos, I. Varela, D. Mandel, W.K. Schmidt, A. Díaz-Perales, C. López-Otín and F. JMP, Journal of Biological Chemistry 278 (2003) 42091-7.
[27] Y.-T. Ma, B. Gilbert and R. Rando, Biochemistry 32 (1993) 2386-2393.
[28] L.J. Plummer, E.R. Hildebrandt, S.B. Porter, V.A. Rogers, J. McCracken and W.K. Schmidt, J Biol Chem 281 (2006) 4596-605.

[29] M. Fujinaga, M.M. Cherney, H. Oyama, K. Oda and M.N. James, Proc Natl Acad Sci U S A 101 (2004) 3364-9.
[30] T.N. Akopyan, Y. Couedel, A. Beaumont, M.C. Fournie-Zaluski and B.P. Roques, Biochem Biophys Res Commun 187 (1992) 1336-42.
[31] N.H. Georgopapadakou, C.C. Hall, T. Lambros, W. Liu and J.D. Watkins, Anal Biochem 218 (1994) 273-7.
[32] C.C. Hall, J.D. Watkins, S.B. Ferguson, L.H. Foley and N.H. Georgopapadakou, Biochem Biophys Res Commun 217 (1995) 728-32.
[33] E.K. Dolence, J.M. Dolence and C.D. Poulter, J Comb Chem 2 (2000) 522-36.
[34] M. Schlitzer, A. Winter-Vann and P.J. Casey, Bioorg Med Chem Lett 11 (2001) 425-7.
[35] K.S. Craig, D.E. Williams, I. Hollander, E. Frommer, R. Mallon, K. Collins, D. Wojciechowicz, A. Tahir, R. van Soest and R.J. Andersen, Tetrahedron Letters 43 (2002) 4801-4804.
[36] I. Hollander, E. Frommer and R. Mallon, Anal Biochem 286 (2000) 129-37.
[37] J. Pei and N.V. Grishin, Trends Biochem Sci 26 (2001) 275-7.
[38] D. Bromme, B. Bartels, H. Kirschke and S. Fittkau, J Enzyme Inhib 3 (1989) 13-21.
[39] A. Krantz, L.J. Copp, P.J. Coles, R.A. Smith and S.B. Heard, Biochemistry 30 (1991) 4678-87.
[40] B.M. Wagner, R.A. Smith, P.J. Coles, L.J. Copp, M.J. Ernest and A. Krantz, J Med Chem 37 (1994) 1833-40.
[41] D. Kato, K.M. Boatright, A.B. Berger, T. Nazif, G. Blum, C. Ryan, K.A. Chehade, G.S. Salvesen and M. Bogyo, Nat Chem Biol 1 (2005) 33-8.
[42] S. Powers, S. Michaelis, D. Broek, S. Santa Anna, J. Field, I. Herskowitz and M. Wigler, Cell 47 (1986) 413-22.
[43] R. Elble, BioTechniques 13 (1992) 18-20.
[44] S. Michaelis and I. Herskowitz, Mol. Cell. Biol. 8 (1988) 1309-18.
[45] S. Marcus, G.A. Caldwell, D. Miller, C.-B. Xue, F. Naider and J.M. Becker, Mol. Cell. Biol. 11 (1991) 3603-12.
[46] i.E.K.a.M. Silverman RB (1995) Mechanism-based enzyme inactivators, Part D: Developments in Enzyme Dynamics (Purich DL ed), p 240, Academic Press, London.
[47] I. Segel, Enzyme Kinetics - Behavior and Analysis of Rapid Equilibrium and Steady-State Enzyme Systems, John Wiley and Sons 1975.
[48] M.N. Hall, L. Hereford and I. Herskowitz, Cell 36 (1984) 1057-65.
[49] S.P. Manandhar and W.K. Schmidt, Biochemical Journal (submitted).
[50] R.S. Sikorski and P. Hieter, Genetics 122 (1989) 19-27.

Table B.1. Plasmids used in this study.

Plasmid	Genotype	Reference
pRS426	*2μ URA3*	[50]
pSM1282	*2μ URA3* P_{PGK}*-His::HA::STE24*	[16]
pSM1317	*2μ URA3 STE14*	[20]
pWS182	*2μ URA3 HA::HsZmpSte24*	[28]
pWS335	*2μ URA3* P_{PGK}*-His::HA::HsRce1Δ22*	[28]
pWS402	*2μ URA3* P_{PGK}*-AtRCE1::HA*	[26]
pWS450	*2μ URA3 AtSTE24::HA*	[26]
pWS479	*2μ URA3* P_{PGK}*-RCE1::HA*	[28]

Table B.2. Effect of chloromethyl ketones and peptidyl (acyloxy)methyl ketones on the *in vitro* activity of yeast Rce1p and Ste24p.

	% Activity Remaining[a]	
Compound	Rce1p	Ste24p
$FKBK(CH_3)_3$	51.3 ± 6.0	29.4 ± 1.0
$FABK(CH_3)_3$	95.3 ± 2.5	95.1 ± 2.4
$FRBK(CH_3)_2$	41.0 ± 4.4	58.6 ± 0.3
$FGBK(CH_3)_2$	99.0 ± 3.2	112.7 ± 2.1
$YFRBK(CH_3)_2$	80.2 ± 0.9	96.4 ± 4.6
$YFGBK(CH_3)_2$	97.7 ± 1.6	99.4 ± 2.7
TPCK	77.4 ± 1.3	92.3 ± 3.4
TLCK	101.0 ± 0.0	94.7 ± 0.5

[a]Values are averages (n ≥ 3 replicates) of percent activity remaining from studies using 100 μM of the indicated compound relative to a DMSO-treated control.

Table B.3. The effect of salt and urea washes on the *in vitro* activity of inhibitor-treated yeast Rce1p and Ste24p.

	% Activity Remaining[a]			
	Rce1p		Ste24p	
Wash	DMSO[a]	$FKBK(CH_3)_3$	DMSO	$FKBK(CH_3)_3$
0 mM NaCl	100.0 ± 0.5	27.3 ± 1.0	100.0 ± 0.7	30.3 ± 3.5
125 mM NaCl	92.3 ± 0.9	28.9 ± 1.1	97.4 ± 8.7	35.7 ± 2.2
1500 mM NaCl	99.0 ± 2.5	31.6 ± 0.2	113.4 ± 1.3	30.3 ± 1.5
0 mM urea	100.0 ± 0.6	37.9 ± 0.4	100.0 ± 5.5	20.4 ± 10.7
62.5 mM urea	94.9 ± 0.4	37.1 ± 6.0	100.6 ± 2.4	20.0 ± 1.7
125 mM urea	92.6 ± 2.1	39.3 ± 0.6	96.2 ± 3.5	19.4 ± 0.5

[a]Values are averages (n ≥ 2 replicates) of percent activity remaining after treatment under the indicated condition. Values for DMSO-treated samples are relative to the 0 mM wash condition while values for $FKBK(CH_3)_3$ -treated samples are relative to the appropriate washed DMSO-treated sample.

[b]Membranes were pretreated with DMSO or 250 μM of $FKBK(CH_3)_3$ for 10 min at 30 ºC before being washed.

Fig. B.1. *Chemical structures of peptidyl (acyloxy)methyl ketones.*

The general chemical structure of an AOMK is shown (top). The names of the compounds used in this study are listed along with the substitutions specific to the indicated compound.

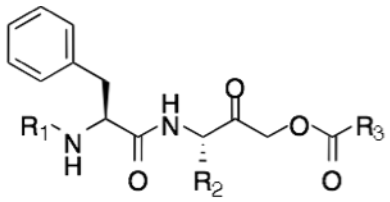

Compound	R_1	R_2	R_3
Z-FKBK$(CH_3)_3$	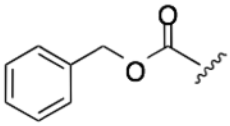	$(CH_2)_4NH_2$	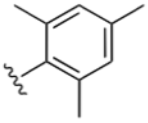
Z-FABK$(CH_3)_3$	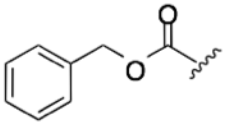	CH_3	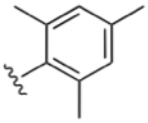
Z-FRBK$(CH_3)_2$	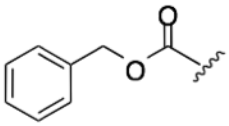	$(CH_2)_3NHCH(NH)NH_2$	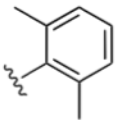
Z-FGBK$(CH_3)_2$	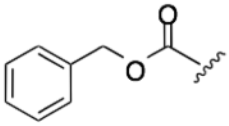	H	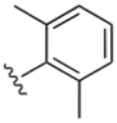
YFRBK$(CH_3)_2$	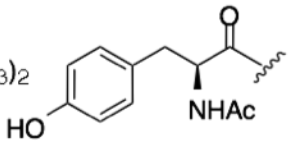	$(CH_2)_3NHCH(NH)NH_2$	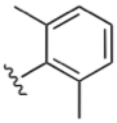
YFGBK$(CH_3)_2$	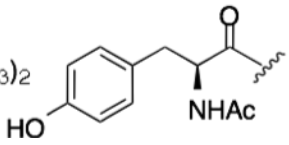	H	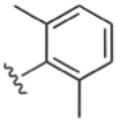

Fig. B.2. *Rce1p orthologs have sensitivity to FKBK(CH_3)$_3$ and TPCK as measured using a fluorescence assay.*

The inhibitory effect of various compounds on the activity of *S. cerevisiae* (Sc), *A. thaliana* (At), and human (Hs) Rce1p (A-C, respectively) was evaluated using a fluorescence-based assay. The assay monitors cleavage of a quenched fluorogenic farnesylated peptide that is based on the C-terminal sequence of the K-Ras4b precursor (ABZ-KSKTKC(farnesyl)Q_LIM). The indicated Rce1p enzyme was over-expressed using a plasmid-based system in yeast lacking the chromosomal copies of *RCE1* and *STE24*. Membranes enriched for Rce1p were isolated and used as the source of enzymatic activity. The compounds evaluated were FKBK(CH_3)$_3$ (FKBK), FABK(CH_3)$_3$ (FABK), TPCK, TLCK, and DMSO as a control. All compounds were used at 250 μM to pretreat the yeast-derived membranes used as the source of enzymatic activity. The DMSO-treated sample was defined as having 100% activity for each membrane set to facilitate cross-species comparative analyses. Each value represents the average activity of three independent reactions with the positive standard deviation of the measurements shown.

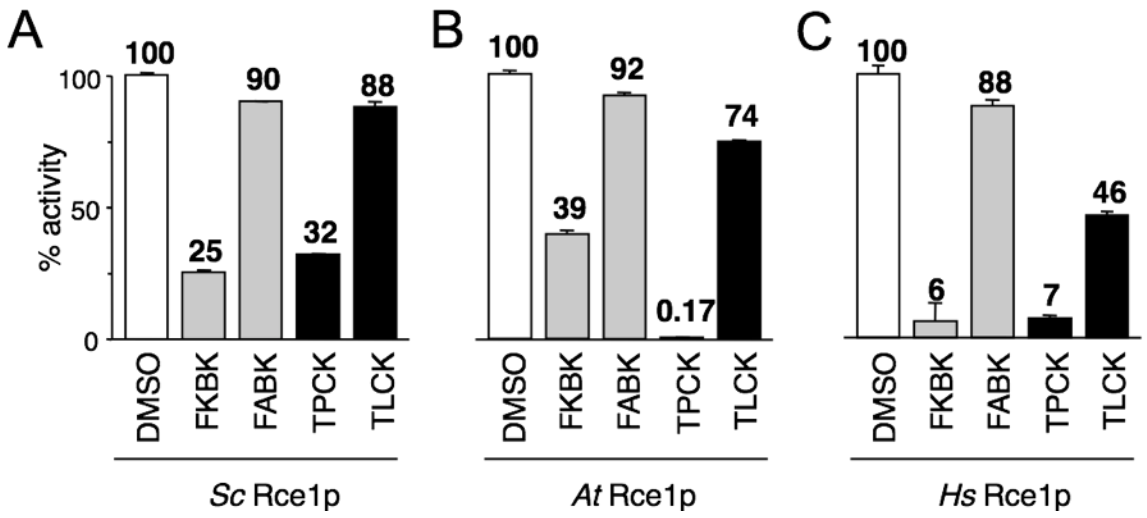
A
B
C
% activity
100
50
0
100
25
90
32
88
100
39
92
0.17
74
100
6
88
7
46
DMSO
FKBK
FABK
TPCK
TLCK
Sc Rce1p
At Rce1p
Hs Rce1p

Fig. B.3. *The sensitivity of yeast Rce1p to TPCK is substrate-specific*.

A) The inhibitory effect of various compounds on the activity of yeast Rce1p was evaluated using an assay that monitors *in vitro* formation of the bioactive **a**-factor mating pheromone. The reaction conditions were similar to those described for Figure B.2, except that the compounds were used at 400 μM to pretreat membranes and the initial proteolysis step of the reaction was followed by an *in vitro* methylation step. A portion of the final sample and two-fold serial dilutions were spotted onto a lawn of *MAT*α *sst2-1* cells that had been spread as a thin lawn on a YEPD plate. This *MAT*α background is supersensitive to the **a**-factor mating pheromone and undergoes a strong growth arrest in its presence, as indicated by a zone of no growth (spot) in the lawn after incubation of the plate at 30 °C for 24 hrs. Each experiment was performed multiple times, and one representative replicate is shown. **B**) Graphical representation of data from trials using the **a**-factor assay (top) or the fluorescence assay (bottom) with the values at the top of each bar representing the average amount of activity observed. The sample order in the two panels is identical.

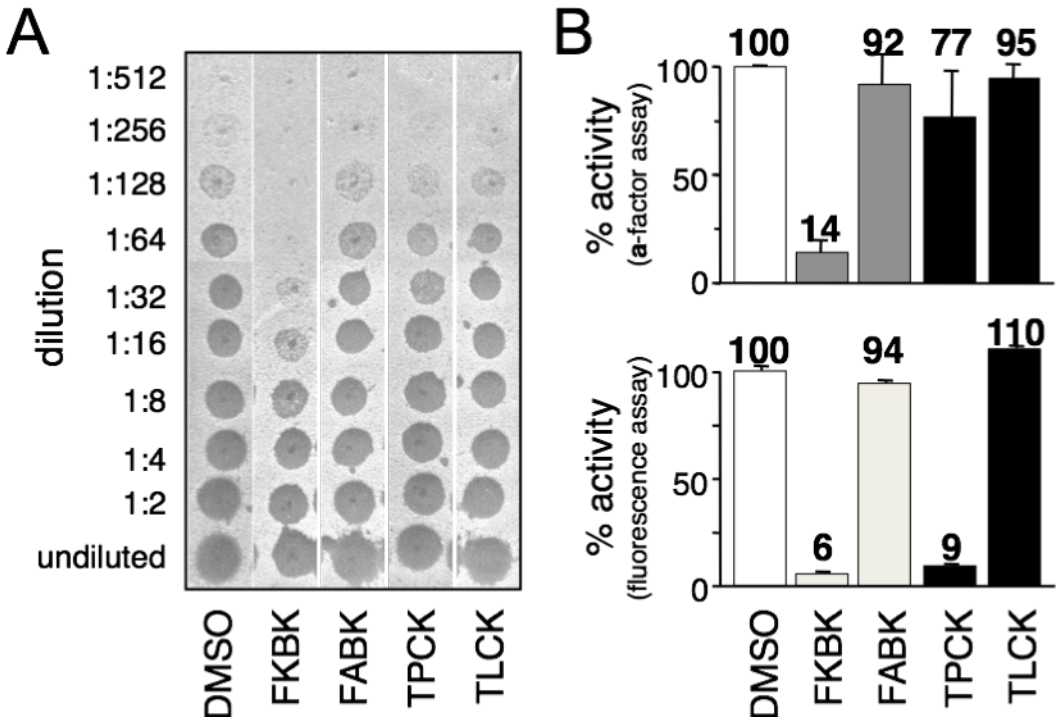
A
1:512
1:256
1:128
1:64
1:32
1:16
1:8
1:4
1:2
undiluted
dilution
DMSO
FKBK
FABK
TPCK
TLCK
B
% activity
(a-factor assay)
100
14
92
77
95
% activity
(fluorescence assay)
100
6
94
9
110
DMSO
FKBK
FABK
TPCK
TLCK

Fig. B.4. *Kinetic analysis of FKBK(CH_3)$_3$ and TPCK mediated inhibition of Rce1p.*

A) FKBK(CH_3)$_3$ and TPCK both reduce the V_{max} of Rce1p. Initial reaction rates were determined after pretreatment with DMSO, 100 μM FKBK(CH_3)$_3$ or 100 μM TPCK using the fluorescence–based assay described in Figure B.2. Data points were plotted and a best-fit curve determined by non-linear regression analysis using Prism 4.0. **B**) Summary of kinetic parameters observed after pretreatment with inhibitors. K_m and V_{max} were determined by non-linear regression analysis. **C**) FKBK(CH_3)$_3$ is a fast-acting inhibitor of Rce1p. FKBK(CH_3)$_3$ and TPCK were each used at 250 μM to pretreat Rce1p for the indicated times. Initial reaction rates were determined at various timepoints (E_t) and used to calculate enzyme activity relative to the reaction rate for a DMSO-treated control at t = 0 min (E_0); the t = 0 timepoint was defined as the time at which inhibitor and substrate were added simultaneously to the enzyme. The natural log of the resultant E_t/E_0 values were plotted vs. time and a best-fit line determined for each dataset. **D**) FKBK(CH_3)$_3$ partitions with yeast membranes. Samples containing buffer alone (buffer) or yeast membranes devoid of CaaX protease activity (membranes) were incubated with DMSO or 100 μM FKBK(CH_3)$_3$ for 10 min at 30 °C. The samples were centrifuged to clear membrane material and the clarified supernatants were used to resuspend Rce1p-containing membrane pellets that were prepared in parallel. The inhibitor activity associated with each preconditioned sample was determined using the assay described in Figure B.2. Values reported for FKBK(CH_3)$_3$ are relative to the DMSO control for each condition.

A

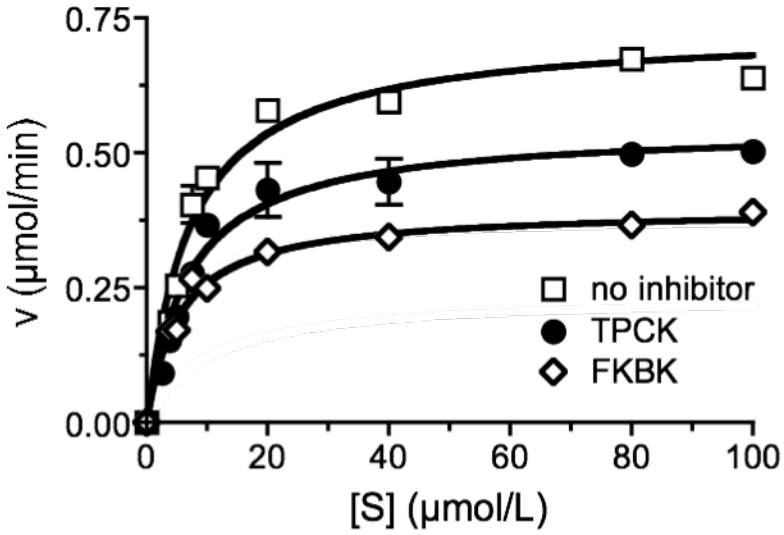

B

Inhibitor	K_m (µM)	V_{max} (µmol/min)	K_m / V_{max}
DMSO	7.20 ± 0.73	0.731 ± 0.022	9.8
TPCK 100 µM	6.94 ± 1.38	0.548 ± 0.030	12.7
TPCK 200 µM	4.34 ± 1.09	0.387 ± 0.020	11.2
FKBK 100 µM	5.34 ± 0.49	0.398 ± 0.009	13.4
FKBK 200 µM	9.70 ± 0.67	0.239 ± 0.005	40.6

C

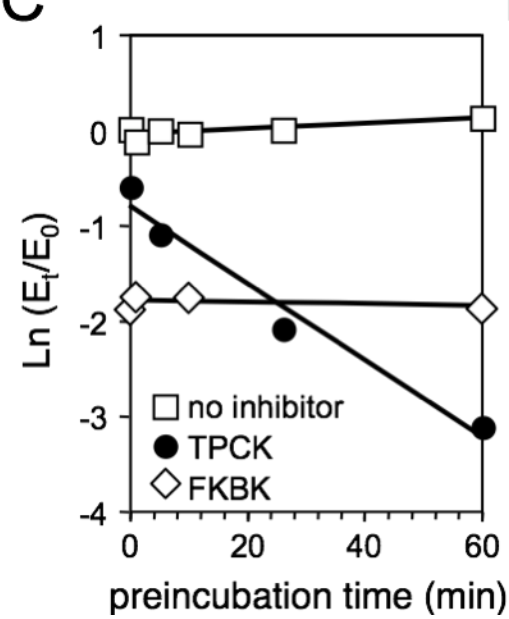

D

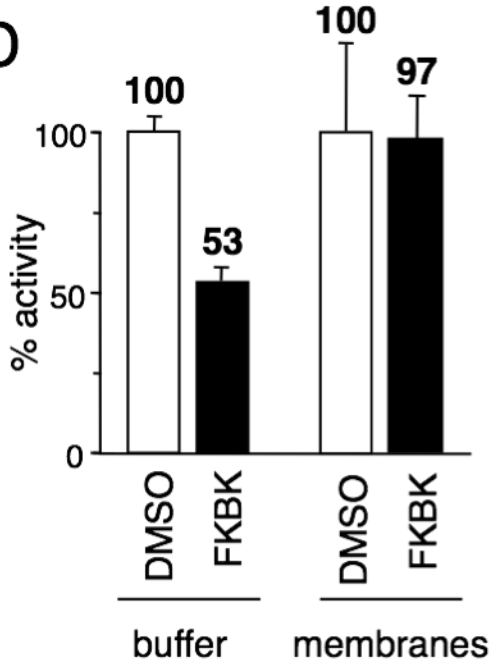

Fig. B.5. *Quencher position impacts the specificity of Rce1p and Ste24p.*

The cleavage of quenched fluorogenic peptides derived from K-Ras4b were evaluated using yeast membrane extracts containing either yeast Rce1p or Ste24p and the assay described in Figure B.2. The substrates vary in the position of the quenching group, which is at either the a_1 (CQ_LIM), a_2 (CVQ_LM), or *X* position ($CVIQ_L$) of the CaaX motif. Otherwise, the samples are identical to the substrate described in Figure B.2. Incorporation of the quenching group at the a_2 or *X* position converts this substrate into a Ste24p reporter. The closed and open bars represent the activities of Rce1p and Ste24p, respectively.

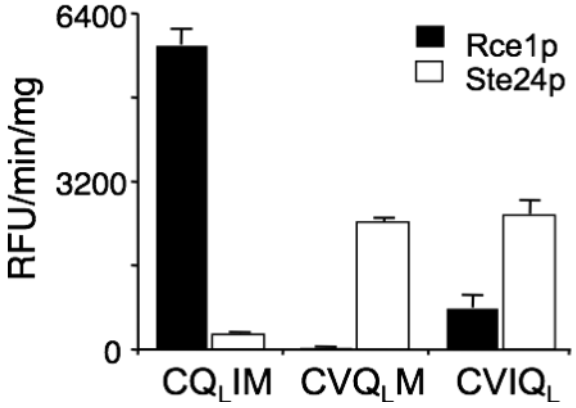
6400
3200
0
RFU/min/mg
Rce1p
Ste24p
CQ$_L$IM
CVQ$_L$M
CVIQ$_L$

Fig. B.6. *Ste24p orthologs have comparable inhibitor profiles as measured using a fluorescence assay*.

The inhibitory effect of the indicated compounds on the activity of *S. cerevisiae* (Sc), *A. thaliana* (At), and human (Hs) Ste24p (A-C, respectively) was evaluated as described in Figure B.2, except that a different substrate ($CVIQ_L$) was used. All compounds were used at 250 μM to pretreat the yeast-derived membranes used as the source of enzymatic activity. The DMSO-treated sample was defined as having 100% activity for each membrane set to facilitate cross-species comparative analyses.

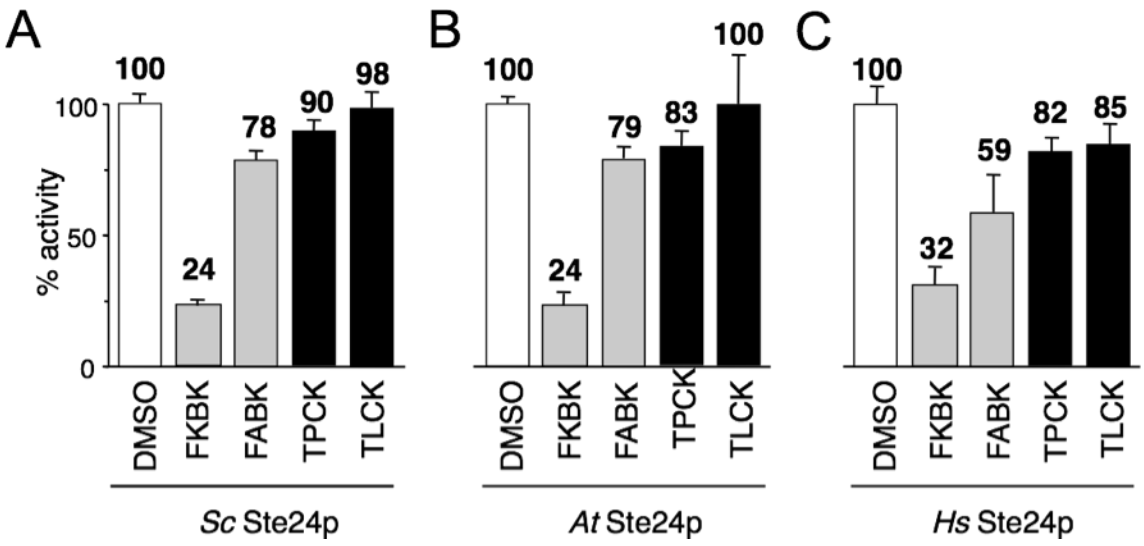
A
B
C
% activity
100
50
0
100
24
78
90
98
100
24
79
83
100
100
32
59
82
85
DMSO
FKBK
FABK
TPCK
TLCK
Sc Ste24p
At Ste24p
Hs Ste24p

Fig. B.7. *The sensitivity of Ste24p to select inhibitors is not substrate-specific.*

A) The inhibitory effect of various compounds on the activity of yeast Ste24p was evaluated using the **a**-factor assay and conditions described in Figure B.3. **B**) Graphical representation of the data from all the trials (n > 3) with the values at the top of each bar representing the average amount of activity observed.

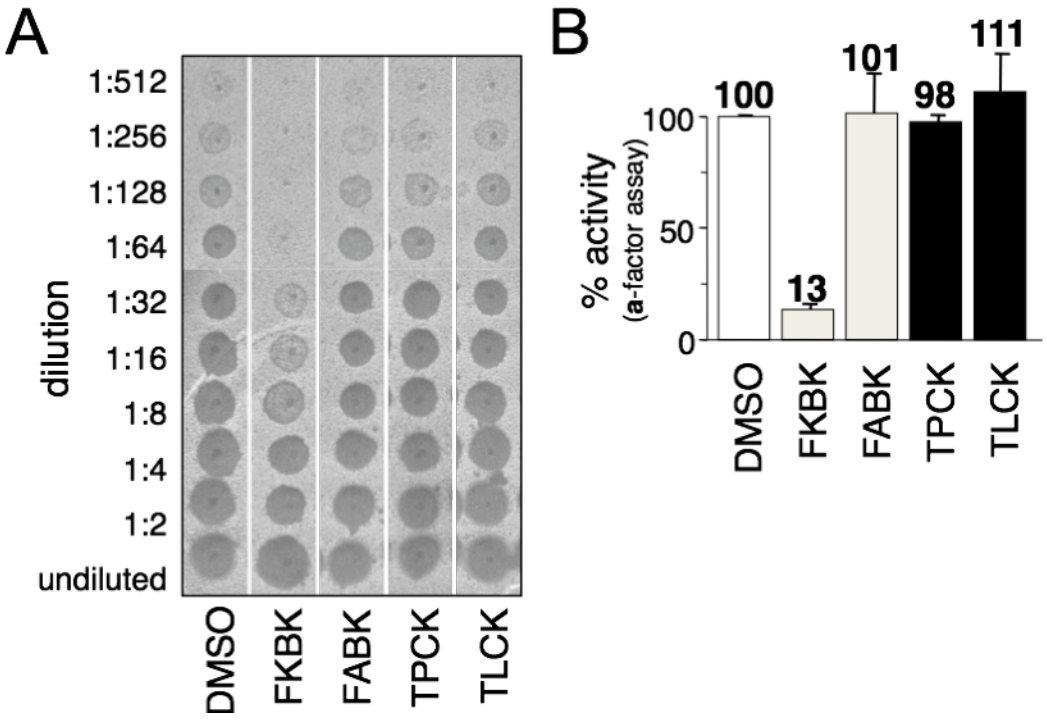
A
1:512
1:256
1:128
1:64
1:32
1:16
1:8
1:4
1:2
undiluted
dilution
DMSO
FKBK
FABK
TPCK
TLCK
B
% activity
(a-factor assay)
100
50
0
100
13
101
98
111
DMSO
FKBK
FABK
TPCK
TLCK

Fig. B.8. *The Ste14p isoprenylcysteine carboxyl methyltransferase is inhibited by FKBK(CH_3)$_3$.* The **a**-factor assay was used to test for inhibition of the Ste14p ICMT. **A**) FKBK(CH_3)$_3$ was added immediately prior to the Rce1p mediated proteolysis step (Step 1) or the Ste14p mediated carboxyl methylation step (Step 2) but otherwise using the conditions described in Figure B.3. A representative replicate data set (top panel) and a graph summarizing the results of the experiment (bottom panel) are shown. **B**) FKBK(CH_3)$_3$ was added to Step 1 or Step 2 as described in A, but in the presence of a limiting amount of Ste14p.

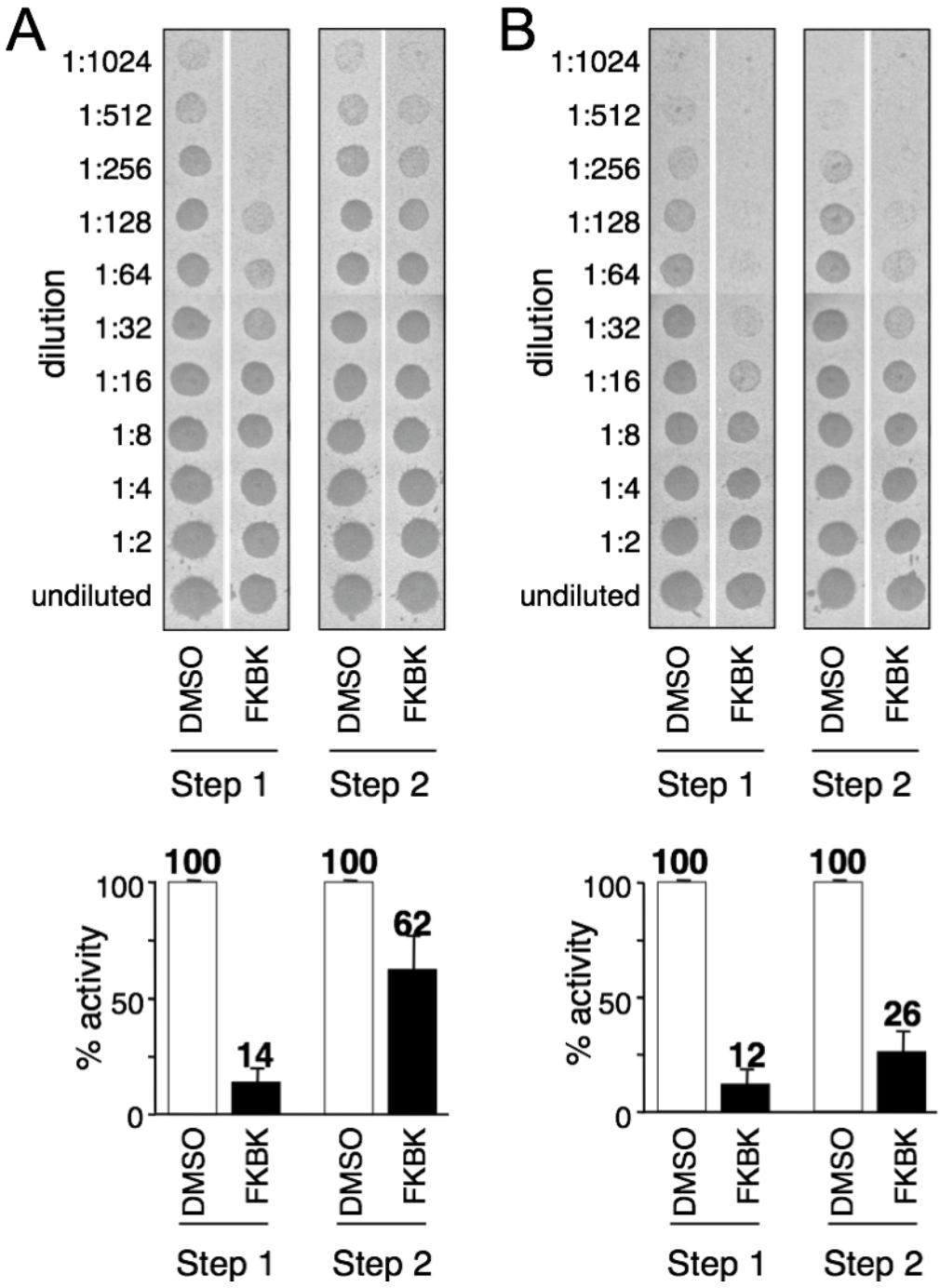
A
B
1:1024
1:512
1:256
1:128
1:64
1:32
1:16
1:8
1:4
1:2
undiluted
dilution
DMSO
FKBK
Step 1
Step 2
% activity
100
14
62
12
26
0
50